UNIVERSITY OF NAPLES FEDERICO II

Department of Civil, Building and Environmental Engineering

PhD in

CIVIL SYSTEMS ENGINEERING

XXXV CYCLE

MECHANICAL BEHAVIOUR AND DURABILITY STUDY OF CEMENTED SOILS LIGHTENED BY FOAM

Filomena Sabatino

A thesis submitted for the degree of Doctor of Philosophy

PhD Coordinator:
Prof. Andrea Papola

Tutor:
Prof. Marco Valerio Nicotera
Co-tutor:
Prof. Giacomo Russo

2023

Acknowledgements

At the end of this long journey, I feel the need to express my gratitude to all the people who stood by me, helped me and supported me so that the achievement of this goal was possible.

First of all, I would like to thank my tutors, Prof. Marco Valerio Nicotera and Prof. Giacomo Russo, for guiding me during these years of my PhD. All my gratitude goes to them for always having tried to transmit the passion for research, and for having stimulated and spurred me to always give my best during these years. Thank you for your help in carrying out the experimental activities, in the subsequent interpretation of the results obtained, and for all the opportunities for confrontation we have had over the years.

My special thanks go to Dr. Enza Vitale, for her constant availability that she always showed me from the beginning to the end of my PhD. Thanks for the valuable suggestions and advice I received during this course and for all the moral support she always offered me, especially in the final period of writing my thesis.

I would like to thank Dr. Raffaele Papa for his help during the experimental activities, for providing me with materials for the research and for his availability whenever his presence was needed to solve a "problem".

Special thanks go to the technicians Alfredo Ponzo and Antonio Cammarota of the "Geotechnical Engineering Laboratory -University of Naples Federico II". Thank you for your fundamental help and support in the experimental activities and for all the playful moments that made less heavy the days spent in the laboratory.

Similarly, I feel the need to thank the entire "LEMTA-Université de Lorraine" team who hosted me during my time abroad and for the opportunity I had to know another scientific reality. My gratitude also goes to the technician Jacques Tisot, for the unfailing availability and patience he always showed me during the laboratory activities.

A huge thank you to my family: my mother, father and sister, for always being by my side during these years and making me feel all their support, especially in the hardest moments.

Thank you for always pushing me to do my best, for encouraging my choices and not giving up in the face of difficulties.

Thank you Luca: partner, friend and colleague. For the Love, comprehension and esteem you have always shown me during this journey. Thank you for standing by me when it was most difficult and for rejoicing together in every little satisfaction that the PhD has given us both.

Special thanks to Gabriella and Marialaura, whom we met at the beginning of this journey and with whom an increasingly strong friendship was forged over time. Thank you for all the advice and support we have exchanged over these years and for all the moments we have experienced together, which have enriched these years spent in Naples.

Thank you to all the colleagues I have met during this course. Each of you has contributed to making the days spent in the Department more pleasant. In particular to Francesco, with whom I shared my PhD from start to finish, for his sincere friendship and sympathy that I have always been able to experience over these years.

Thank you Alice, Zeina and Nicolas for welcoming me in Nancy and always trying to make me feel at home even miles away. Your friendship and closeness were fundamental during my stay in France.

Filomena Sabatino

Ringraziamenti

Al termine di questo lungo percorso, sento la necessità di esprimere la mia gratitudine a tutte le persone che mi sono state accanto, mi hanno aiutata e supportata affinché il raggiungimento di questo obiettivo fosse possibile.

Prima di tutti ringrazio i miei tutor, il Prof. Marco Valerio Nicotera e il Prof. Giacomo Russo, per avermi guidata durante questi anni del dottorato. A loro va tutta la mia riconoscenza per aver sempre cercato di trasmettermi la passione per la ricerca, avermi stimolata e spronata a dare sempre il massimo durante questi anni. Grazie per l'aiuto fornitomi nello svolgimento delle attività sperimentali, nella successiva interpretazione dei risultati ottenuti e per tutte le occasioni di confronto avute nel corso di questi anni.

Un ringraziamento particolare va alla Dott.ssa Enza Vitale, per la sua costante disponibilità che mi ha sempre dimostrato dall'inizio alla fine del dottorato. Grazie per i preziosi suggerimenti e consigli ricevuti durante questo percorso e per tutto il supporto morale che mi ha sempre offerto, soprattutto nel periodo finale di scrittura della tesi.

Ringrazio il Dott. Raffaele Papa, per l'aiuto ricevuto durante le attività sperimentali, per avermi fornito i materiali per la ricerca e per tutta la disponibilità ogniqualvolta la sua presenza fosse stata necessaria alla risoluzione di un "problema".

Un ringraziamento speciale va ai tecnici Alfredo Ponzo e Antonio Cammarota del Laboratorio di Ingegneria Geotecnica dell'Università degli Studi di Napoli Federico II. Grazie per il vostro fondamentale aiuto e supporto nelle attività sperimentali e per tutti i momenti più scherzosi che hanno reso meno pesanti le giornate trascorse in laboratorio.

Allo stesso modo, sento il dovere di ringraziare tutto il gruppo del "LEMTA-Université de Lorraine" che mi ha ospitato durante il mio periodo all'estero e per la possibilità avuta di confrontarmi con un'altra realtà scientifica. La mia gratitudine va anche al tecnico Jacques Tisot, per l'immancabile disponibilità e pazienza che mi ha sempre dimostrato durante lo svolgimento delle attività di laboratorio.

Un immenso grazie alla mia famiglia: mia madre, mio padre e mia sorella, per essermi sempre stati accanto durante questi anni e avermi fatto sentire tutto il loro appoggio, soprattutto nei momenti più duri. Grazie per avermi sempre spronata a dare il massimo, per aver incoraggiato le mie scelte e a non mollare di fronte alle difficoltà.

Grazie Luca: compagno, amico e collega. Per l'Amore, la comprensione e la stima che mi hai sempre dimostrato durante questo percorso. Grazie per essermi stato accanto quando era più difficile e aver gioito insieme di ogni piccola soddisfazione che il dottorato ha regalato ad entrambi.

Un grazie particolare a Gabriella e Marialaura, conosciute all'inizio di questo percorso e con le quali si è creato, nel corso del tempo, un rapporto di amicizia sempre più forte. Grazie per tutti i consigli e il supporto che ci siamo scambiate nel corso di questi anni e per tutti i momenti vissuti insieme, che hanno arricchito di spensieratezza questi anni trascorsi a Napoli.

Grazie a tutti i colleghi che ho conosciuto durante questo percorso. Ognuno di voi ha contribuito a rendere più piacevoli le giornate trascorse in Dipartimento. In particolare a Francesco, con il quale ho condiviso il dottorato dall'inizio alla fine, per la sua amicizia sincera e la sua simpatia che ho sempre potuto riscontrare in questi anni.

Grazie Alice, Zeina e Nicolas per avermi accolta a Nancy e aver sempre cercato di farmi sentire a casa anche a chilometri di distanza da essa. La vostra amicizia e vicinanza sono state fondamentali durante la mia permanenza in Francia.

Filomena Sabatino

TABLE OF CONTENTS

LIST OF FIGURES

LIST OF TABLES

1. INTRODUCTION

The management of debris from the excavation operations necessary for the construction of numerous civil engineering works is one of the most important issues related to the planning of such works and has significant environmental and economic consequences. Excavated rocks and soils are very often characterised by mechanical properties that make them unsuitable for reuse in civil works in their natural condition. In some cases, in order to reuse poor excavated materials, preliminary treatments are used to modify their physical and mechanical properties (e.g., treatments with lime, cement or other binders).

Among the possible treatments, procedures aimed at obtaining so-called *Lightweight Cemented Soils (LWCS)* appear to be of particular technical and economic interest. Generally, these are materials obtained by mixing in fixed quantities soils (both coarse-grained and clayey soils), hydraulic binders and foaming agents. Thus the mixture produced immediately after preparation is fluid, but over time, through the chemical reactions associated with the activation of the binder, results in a material with significant strength and high lightness and porosity.

These characteristics make LWCS suitable for:

- Earthworks construction (i.e., embankments) in presence of highly compressible soil
- Embankments construction on landslide sites where overloads must be limited in order not to aggravate the general stability conditions
- Filling the underground cavities
- Backfills construction behind retaining structures, as these give rise to reduced thrusts while ensuring adequate stiffness.

The reduction of the environmental impact and the economic advantages are considerable: in fact, it is possible to reintroduce the material into the production cycle, reducing the costs related to the purchase and transport of quarry material and, at the same time, those related to the disposal of excavated soil.

The literature on treatment of soils shows a variety of solutions that can be utilized in engineering practices. In the field of soil improvement techniques it is possible to find deep mixing, jet grouting, etc and lime stabilization by means of binding agents (i.e., cement and lime) with the aim to improve the mechanical properties of soils. Marzano (2017) indicates that deep mixing and jet grouting belong to *soil mixing* category, in which soil is shattered and mixed with binding agents with the aid of rotating utensils to realize a new geomaterial with improved mechanical properties on construction site.

On the other hand, lime stabilization technique is based on the reuse of soil by mixing it with binding agents to improve their initial poor mechanical properties and to use it as construction material. Cement or lime are the most commonly used agents, but also fly ash, silica fume and geopolymers can be used for the same aim (Kaniraj and Havanagi, 1999; Wild et al., 1998; Zhang et al., 2013). LWCS method falls into this category with the application of cement as binding agent.

The use of lightweight cemented soil (LWCS) is especially widespread in Japan in coastal constructions, backfilling of underground works (Tsuchida and Egashira, 2004) and lightened embankments (Horpibulsuk et al., 2012). In 1992 in Japan, this type of construction material was first used as backfill material for the quay at the port of Fushiki-Toyama to reduce the pressure of the soil behind the quay. One year after construction, analyses of the soil samples showed that the density and strength met the design criteria, proving the applicability of the method. Then, in 1996, the lightened soil was used in the recovery of Kobe harbour after the Hyogoken-Nambu earthquake of 1995, being used to reduce the pressure behind the docks and to ensure greater stability in a future seismic event. It was the first major job ever, with around 20000 m^3 of treated soil used. The following year, it was used for work at the Kyoto International Airport.

The preparation of a LWCS specimens generally takes place in four distinct phases. In the first phase, the soil is mixed with water in order to obtain the slurry. In the second phase, the grout is prepared by mixing anhydrous cement with water. In the third phase, the grout is added to the soil slurry and mixed with it until a homogenous mixture is obtained. The fourth stage involves preparing the foam and adding it to the previously produced soil-cement-water mixture. The foam is prepared by blowing pressurised air into a solution of water and surfactant. The addition of a suitable amount of foam allows the porosity to be adjusted and a very light material to be obtained. The setting and hardening of the cement ensure that the air bubbles are fixed in the structure of the material and then result as additional voids.

The treatment parameters to be adjusted for the production of these materials are the amount of water to be used for the preparation of the soil slurry, which is commonly indicated by means of gravimetric water content (w_{slurry}), the value of which in the most frequent applications varies in the range between 1.5 and 3 times the liquid limit w_L of the soil to be used; the cement/soil weight ratio (c/s); the water/cement ratio (w_c/c) for the production of the grout; the volume fraction of foam (n_f), equal to the ratio between the volume of foam and the total volume of the mixture. A diagram that represents the distinct preparation phases is reported in Figure 1-1.

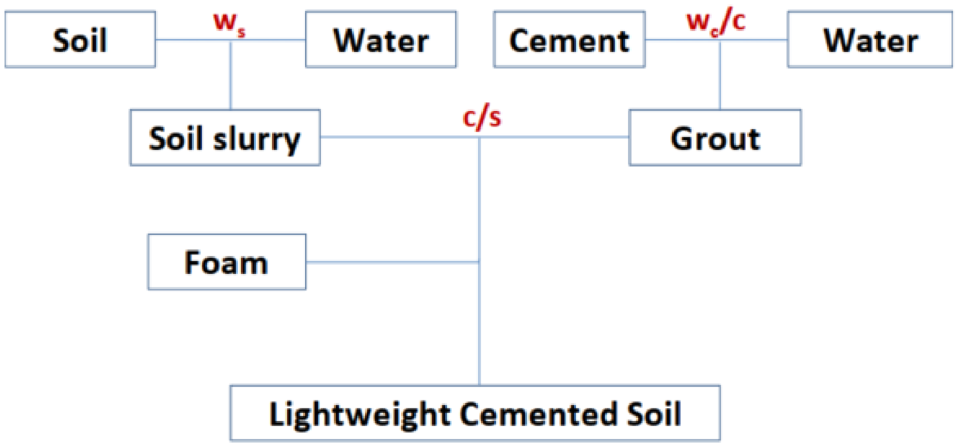

Figure 1-1. Diagram of LWCS preparation phases (De Sarno, 2019).

This experimental study on lightweight cemented soil is in continuity with the earlier works of De Sarno et al., (2019) and Vitale et al., (2020). The authors deeply investigated the chemo-physical and microstructural characteristics with some aspects of the mechanical behaviour of certain LWCS. In particular, the effects of cement and foam addition, together with the curing time, were examined via microstructural and mechanical tests on the soil.

This research work is characterized by two main parts. In the first one, it is proposed a further insight into the chemo-physical and mechanical characterization of the LWCS. In particular, traditional mechanical tests and the adoption of non-destructive testing methods (i.e., ultrasonic tests and electrical resistivity measurements) made possible to find some correlation relationship in order to assess the properties of the LWCS and to estimate geotechnical parameters, starting from measured quantities. Moreover, these techniques offer the possibility of a quick and non-invasive quality control of the treatment (LWCS method) executed on the soils.

The second part deals with the durability issue under environmental loads. Application of wetting-drying cycles, suction measurements and performance of mechanical tests (i.e., unconfined compression tests and triaxial tests) allowed the study of the evolution, and eventual degradation, of the mechanical response of LWCS. Effects of different environmental conditions and the role of suction have been investigated.

In the 2nd chapter a literature review on the main topics of this research work is presented. It is organized in sections. Section I deals with the mechanical aspects of the cemented and lightweight cemented soils behaviour. In section II a literature review of non-destructive testing methods (i.e., ultrasonic testing and electrical resistivity measurements) is reported. Section III is dedicated to the durability of treated soils.

In the 3rd chapter a description of soil, cement and foam is given. Clay and water interaction behaviour, with rheological properties and features of soil slurry, are explained. Moreover, cement and its hydration reactions, structure of hardened paste and rheology of fresh cement paste are examined. Finally, foam, the effects of surfactants within and its bulk properties are described.

In the 4th chapter materials and methods used in this experimental work are presented and explained.

The 5th chapter is dedicated to the results of the first part of this experimental study. Unconfined compression test and torsional shear test results are discussed, together with the results of P-waves velocity and electrical resistivity measurements.

In the 6th chapter the experimental results (i.e., unconfined compression tests, triaxial tests) of durability part are presented.

Finally, in 7th chapter conclusions are drawn and possible further developments are proposed.

References

De Sarno, D., Vitale, E., Deneele, D., Nicotera, M.V., Papa, R., Russo, G., Urciuoli, G., 2019. Effects of cement and foam addition on chemo-mechanical behaviour of lightweight cemented soil (LWCS). E3S Web Conf., 92. https://doi.org/10.1051/e3sconf/20199211006.

Horpibulsuk, S., Suddeepong, A., Chinkulkijniwat, A., Liu, M.D., 2012. Strength and compressibility of lightweight cemented clays. Appl. Clay Sci. 69, 11–21. https://doi.org/10.1016/j.clay.2012.08.006.

Kaniraj, S.R., Havanagi, V.G., 1999. Compressive strength of cement stabilized fly ash-soil mixtures. Cem. Concr. Res. 29, 673–677. https://doi.org/10.1016/S0008-8846(99)00018-6.

Marzano, I.P., 2017. Soil Mixing. Tecnologie esecutive, applicazioni, progetto e controlli, Argomenti di ingegneria geotecnica. Hevelius.

Tsuchida, T., Egashira, K., 2004. The Lightweight Treated Soil Method: New Geomaterials for Soft Ground Engineering in Coastal Areas. CRC Press - Taylor & Francis Group, London.

Vitale, E., Deneele, D., Russo, G., De Sarno, D., Nicotera, M. V., Papa, R., Urciuoli, G. 2020.Chemo-mechanical behaviour of lightweight cemented soils. Acta Geotech. 15, 933–945. https://doi.org/10.1007/s11440-019-00797-8.

Wild, S., Kinuthia, J.M., Jones, G.I., Higgins, D.D., 1998. Effects of partial substitution of lime with ground granulated blast furnace slag (GGBS) on the strength properties of lime-stabilised sulphate-bearing clay soils 51, 37–53.

Zhang, M., Guo, H., El-Korchi, T., Zhang, G., Tao, M., 2013. Experimental feasibility study of geopolymer as the next-generation soil stabilizer. Constr. Build. Mater. 47, 1468–1478. https://doi.org/10.1016/j.conbuildmat.2013.06.017.

2. LITERATURE REVIEW

In this chapter a description of the state of art about the main topics of this experimental work is presented. It is divided into three sections: the first one is about the mechanical behaviour of cemented soils and lightweight cemented soils; the second one is dealing with the non-destructive testing method; finally, the third one is about durability aspects.

2.1. CEMENTED SOILS

2.1.1. NATURAL AND ARTIFICIAL CEMENTED SOILS

Leroueil and Vaughan (1990), in one of the most cited and influential paper of the last century, observed that many natural materials have strength and stiffness characteristics that cannot be treated by reference to the porosity and tensional history of the material. They are natural soils and weak rocks (i.e., soft and stiff clays, granular and residual soils, weak and eroded rocks). What these materials have in common is the “structure”. Soil structure includes soil fabric used to describe the particle arrangement in both cohesive soils (clays) and granular soils (silts, sands, and gravels) and bonding. The formation of structure in a material, in terms of bonding, may depend on artificial causes (as the addition of a bonding agent) and natural ones such as solution and deposition of silica in sands between particle contacts, cold welding under high pressures between inter-particle contacts, deposition of carbonates, solution of hydroxides and organic matter, recrystallisation of minerals during erosion, modification of the adsorption water layer and inter-particle attraction forces in clayey soils (Leroueil and Vaughan, 1990).

Their mechanical behaviour, both in situ and in the laboratory, cannot be analysed without considering their structure properties, as well as their initial porosity and stress history. Several publications have appeared in the past years documenting the effects of cement and lime addition on the mechanical behaviour of soils in terms of strength increase (Clough et al., 1981; Locat et al., 1990; Mitchell, 1981; Sariosseiri and Muhunthan, 2008). For instance, Consoli et al. (2007) argued that a small addition of cement to a compacted cemented silty sand is already enough to obtain an increment in strength as it can be seen from the linear increase of the Unconfined Compressive Strength (UCS) with the cement content. Horpibulsuk et al. (2003) studied the effect of cement addition on unconfined compressive strength of cemented high water content clays, considering the variation of cement content between 5% and 200%. What they saw was a significant increase in the strength of the cemented clays by passing from a cement content of 5% to up of 70%. In fact, at cement content of 5% the augment of strength was marginal, owing to the small amount of cement per intercluster site, compared to a cement content of 40%. In that last case, the authors thought of a continuity in clay fabric and a discontinuity in the hardened structure of the cement paste. Going beyond a cement content of 70%, the clay particles were completely embedded in a continuous cement paste.

2.1.2. MECHANICAL BEHAVIOUR OBSERVED UPON ISOTROPIC AND K_0 COMPRESSION

In Figure 2-1 is illustrated a schematic diagram of the compressibility behaviour of a cemented soil (Cuccovillo and Coop, 1999; Lade and Trads, 2014; Leroueil and Vaughan, 1990).

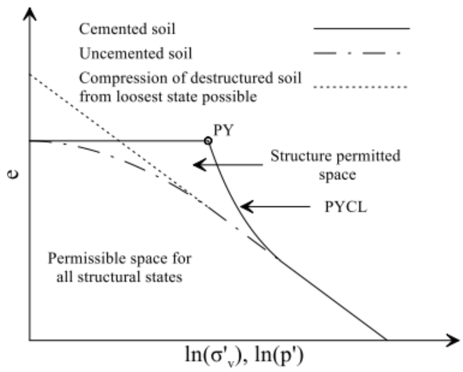

Figure 2-1. Schematic representation of compressibility behaviour of strongly cemented soil, after Leroueil and Vaughan (1990), Cuccovillo and Coop (1999); PY: Primary Yield, PYCL: Post-Yield Compression Line (Rotta et al., 2003).

Although the causes are different, the effects produced by the structure on the materials are ultimately similar. There is an increase in strength and a widening of the tensional domain within which these materials exhibit rigid behaviour, both together and separately from the tensional history they have undergone. The concept of yielding, thus developed to explain the effects of the tensional history, can also be safely adopted with regard to the effects produced by the structure. The shape of the yield curve and the yielding stress itself, due to the structure, reflect both density and bond strength. Furthermore, in a clay with structure or in sedimentary rocks, the shape of the yield curve reflects the anisotropy induced during initial sedimentation (Leroueil and Vaughan, 1990).

In agreement with the previous authors, Cuccovillo and Coop (1999) studied by experimental investigations the mechanical behaviour of artificially cemented carbonate sands. The addition of cement induced an enlargement of the elastic domain in the stress space (the space where the strains are reversible) and an increment of the initial stiffness at small strain level; higher strains were observed after the yielding condition. What is important to underline, is the behaviour in the tension-void ratio plane after the execution of isotropic compression tests on cemented sand: it is possible to obtain points that can reach states impossible for a reconstituted uncemented sample of the same sand. They showed that in a calcarenite, in which the structure is predominantly characterized by bonding, the shear behaviour is cohesive. The peak strength is only cohesive and the soil exhibits brittle behaviour. For these soils, frictional behaviour is only shown at high confining stresses leading to bond failure due to yielding. Frictional behaviour is then dominated by compression and particle crushing. On the other hand, for a sandstone in which the predominant aspect of the structure is the fabric, several characteristics of its behaviour can be identified. The shear mechanism is dominated by the dilatancy that causes the peak resistance; the shear stress-strain behaviour is non-linear for most of the confinement stress range and linearity is only present in the first part of the shear phase. Compression and fracture of the particles are only limited to the case of high confining pressures and, if the sand in question has a low degree of bonding, the cohesion peak can only be seen at low confining stresses.

As reported by Rotta et al. (2003), curing stress had an effect on the isotropic yielding stress for a compacted cemented silty sands. In fact, it was observed that raising the curing stress before the cementation process starts, in that case by simulating the curing of samples at different depths in a sedimentary deposit, there was an increment in the isotropic yielding stress. What is more after the achievement of the primary yield (PY) in Figure 2-1, considering samples at different initial void ratios, their compression paths followed a post-yield compression line (PYCL). There was a single PYCL for each cement content and, when the confining stresses were up to 30 MPa, it joined the intrinsic compression line (ICL) of the soil without cementation. The PYCL widened and became sharp at the increase of cement content. As shown in Figure 2-1, there is also an area called “Structure permitted space” by Leroueil and Vaughan (1990), between the intrinsic compression line (ICL) and the post-yield compression line (PYCL). In this space, there are structured materials with a higher initial void ratio than a material without structure, that reach stress states not possible for the latter one.

The results obtained by Verástegui Flores and Van Impe (2009) on an artificially cemented clay were in good agreement with the previous authors. In particular, they observed the behaviour of an artificially cemented kaolin beginning from a slurry state prepared at a water content equal to two time the liquid limit w_L: by executing a k_0 compression test and increasing the cement content, the yield stress reached values above the reconstituted soil’s ICL, showing a higher post-yield compressibility behaviour.

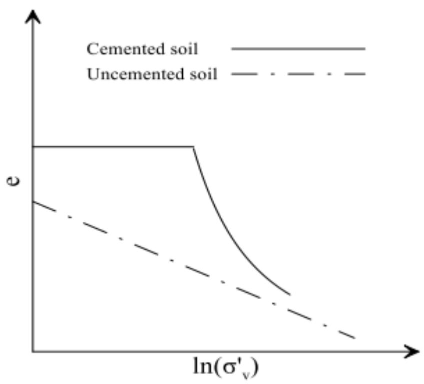

Figure 2-2. Schematic diagram of compressibility behaviour of cemented clay (Sasanian and Newson, 2014).

As it can be seen in Figure 2-2, the value of void ratio for a cemented soil is higher than the value of an uncemented soil, at very low confining stress. Sasanian and Newson (2014) studied the behaviour of the Ottawa clay, artificially cemented with a bonded structure in also its natural state. In both the cases (i.e., undisturbed and artificially cemented with a water content up to the liquid limit w_L and after 28 days of curing time), the initial void ratio values and the stiffness before the yield were higher than the reconstituted soil.

2.1.3. STRESS-STRAIN AND VOLUME CHANGE BEHAVIOUR IN TRIAXIAL COMPRESSION

Much research on the triaxial compression behaviour of cemented soils and their shear strength has been done in literature. Bressan and Vaughan (1989) showed that a yielding surface can be defined by the results of drained triaxial compression tests. Yield strength for low stress levels could occur only slightly before peak deviatoric stress. At higher stresses it occurred well before failure. Failure coincided with the critical state and complete destruction of the bonds at large strain levels. According to Lade and Overton (1989) after yielding, debonding occurred and the stress-strain behaviour was highly non-linear. The triaxial compression behaviour became more contractive due to the increase in the confining pressure.

Similar results were achieved by Airey (1993). He studied the behaviour of a calcarenite, carbonate cemented soil, after the execution of conventional and stress-path triaxial tests. The stress-path tests were carried out to investigate the shape of the yield loci. The soil response was similar to that of other cemented and structured soils. Cementation contributed to the enlargement of the yielding loci but had a small effect on the volumetric soil response. Airey agreed with the previous authors saying that when the bonds broke due to the application of deviatoric stress, the samples reached the critical state. During the drained triaxial tests the deviatoric stress increased linearly up to the yield point, followed by a further gradual increase towards the ultimate state, accompanied by significant volumetric strains. The linear response of deviatoric stress and axial strain suggested an elastic response up to yielding, however, a more detailed analysis of the response in terms of volumetric deformation reveals a departure from linearity well before the yield point. As in the case with rocks, there was a detachment from linearity in soils associated with the breaking of the weakest and most highly stressed bonds up to the yield point where there was a more rapid and progressive disintegration of the bonds. The point of detachment from linear behaviour was defined as an elastic limit. It was thus distinguished from yielding, defining the boundary of a rigid, low-strain response.

Together with Airey (1993), also Coop and Atkinson (1993) investigated the behaviour of a natural calcarenite that was shown to agree with the general framework developed for tests on artificially cemented carbonate sand and this framework can also be applied to other naturally cemented soils. Yielding was associated with the breakage of cementation bonds, and in the case of carbonate soils, with the initial breakage of soil particles. The most important effect of cementation was on stiffness and stress-strain behaviour at high confining stresses, while at low confining stresses there was a little influence in relation to bond strength. Moreover, at lower confining stresses the shear phase resulted in yielding at higher strengths than the frictional failure envelope of uncemented soil and continued loading of the specimen led to softening. At high confining stresses yielding occurred during the compression phase, in which case the soil had a behaviour characterized by hardening and its strength was frictional. The results show that the transition from cohesive to frictional behaviour was not well defined. Finally at intermediate confining stresses, there was the yielding of the specimens during the initial shear phase. Their peak strengths were slightly above the frictional failure envelope, indicating some post-yielding influences of cementation.

Another example of the mechanical behaviour of artificially cemented sand was reported by Schnaid et al. (2001). They put in evidence the effect of the increase of cement content on the peak strength and stiffness of the soil. The deviatoric stress, after the maximum value, tended to reach a constant value regardless of the level of cementation. From the point of volumetric behaviour, there was an initial phase where the behaviour was mostly contractive, then followed by a dilatative behaviour and the maximum dilation was right after the peak strength.

Studies on the undrained behaviour of a cemented clay were made by Horpibulsuk et al. (2004). They showed the typical stress-strain curve for a cemented soil, identified by a peak value of the deviatoric stress, followed by softening. They attributed peak strength to cementation instead of particles interlocking.

Sariosseiri and Muhunthan (2008, 2009) studied the effect of cement content and confining pressure on the behaviour of two soils, called Aberdeen and Everett soils, from Washington state in America. They observed an increment in the deviatoric stress at peak stage by increasing the confining pressure; in addition, the effect of the increase of cement content was reflected in the increase of peak deviatoric stress at low strain levels. They also noted that the increase in cement content was responsible for the high brittleness and the stress-strain curve was characterised by a relevant softening in the final part.

Another study on the mechanical behaviour of an artificially cemented clay was conducted by Jiang at al. (2017). They said that during the isotropic compression tests, the interparticle bonds increased the yielding stress for the structured soil. The compressibility of the cemented clay before yielding was very low, and then increased rapidly when the yielding stress was exceeded. The microstructure, linked to the interparticle bonds, was damaged and the compressibility increased in the loading-unloading cycles. For the anisotropic compression tests and at high stress level the damage of the soil structure was controlled by the mean effective stress and volumetric strains. In case of low stress level, it was controlled by the deviatoric stress and shear strains. During the drained and undrained consolidated triaxial tests, the elastic strains were predominant before the yielding where the confining stress was lower than the yielding stress.

Ali Rahman et al. (2018) presented the results about a series of drained triaxial tests on soil samples without structure and with bonds to study the stress-strain behaviour and the critical state for soils with weak bonds. The bounding surface for samples without structure could be defined as a straight line characterized by q/p′ and friction angle. On the other hand, structured soils had a bounding surface with curvature but it went back to that of structureless soils at high stress levels. That phenomenon indicated the presence of bonds resulted in higher strength until when there was the breakage of the bonds. At low stress levels, the influence of bonds on the shear strength was relevant until the applied stress was lower than the yielding stress. As that threshold was exceeded, the degradation of the cementing began. At higher stress levels, the strength attributed to the bonds was completely destroyed and the behaviour of those soils tended to follow that of unstructured soils. The critical state was defined as a sudden change that could be associated with the formation of a shear surface. In the v-lnp' plane, the critical state showed a curvature of the critical state line for cemented soils towards structureless soils. That meant that the effect of cementation decreased as soon as the stress level went beyond the yield stress of cemented soils. Samples on the dense side of the critical state were bounded by the Hvorslev surface, while those on the loose side were bounded by the Roscoe surface.

2.1.4. FAILURE ENVELOPE

Mohr-Coulomb criterion has been widely used to describe the failure of soil.

The theory of Mohr-Coulomb failure criterion is based on two variables: the shear strength (τ) and the effective normal stress (σ’). It is represented in (τ- σ’) space by drawing Mohr semi-circles, that symbolize stress states at failure, and a tangent line to the semi-circles which is a depiction of Mohr-Coulomb failure envelope. An assumption of this criterion is a linear variation of the shear strength (τ) with the effective normal stress (σ’). Two parameters characterize the equation of this criterion: effective cohesion intercept (c’) and effective angle of shearing resistance (φ’), as follows in Eq. (2-1) and Figure 2-3.

$$\tau = c' + \sigma' \tan \varphi' \tag{2-1}$$

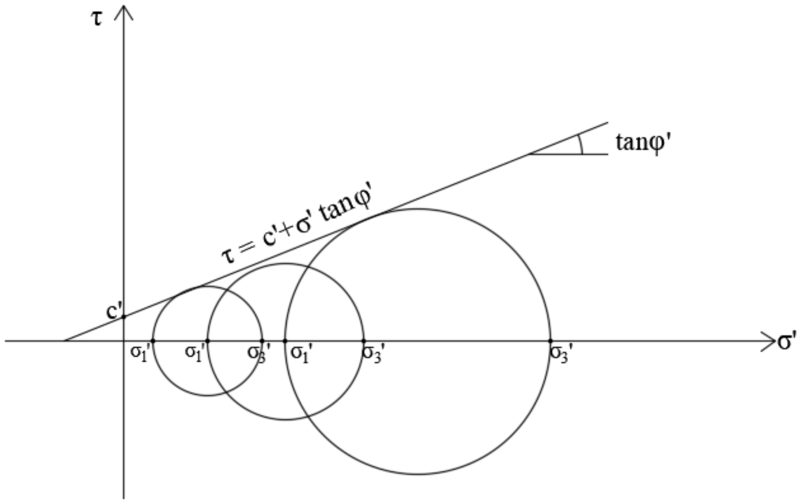

Figure 2-3. Mohr-Coulomb failure criterion.

Several authors have seen that the determination of the Mohr-Coulomb failure criterion requires the performance of many triaxial tests (Consoli et al., 2000, 2007; Dalla Rosa et al., 2008) or of simple shear tests (Festugato et al., 2013), instead of other complicated tests that take much longer. As reported by Consoli et al., (2012) the Mohr-Coulomb criterion requires a large number of experimental tests at different confining stresses on artificially cemented soils to define the failure envelope considering two different factors: cement content and porosity.

However, Sariosseiri and Muhunthan (2008) evidenced some irregularities when Mohr-Coulomb was applied to cement treated soil. It is owing to the fact that in a range of confining pressures the failure envelope shows a curvature that makes it not possible to establish only one friction angle parameter. The authors suggested to adopt other failure criteria in order to illustrate the failure behaviour of geomaterials, for example Hoek and Brown (1988) and Johnston (1985).

Consoli et al., (2012) proposed the application of Griffith criterion (Griffith, 1924) to describe the behaviour of cemented soils. Griffith's failure criterion is characterized by a parabolic envelope and in same features could be more reasonable than the Mohr-Coulomb criterion with a linear failure envelope. The representative Griffith failure envelope is the following one:

$$\tau^2 = 4\sigma_t(\sigma_t - \sigma_n) \qquad \textit{(2-2)}$$

where σ_t is the tensile stress, σ_n is the normal stress acting on the failure surface and τ is the shear stress acting along the failure surface. Nevertheless, Hoek and Bieniawski (1965) put in evidence a phenomenon of the closure of the cracks in compressive stress conditions: when it happened, it meant that the tensile stress at crack extremity was not so high to cause the fracture and the shear resistance among the two faces of the crack had to be surmounted before the propagation of crack started. A modification of the Griffith failure criterion was made by McClintock and Walsh (1962) to take account of that issue. In fact, with the Modified Griffith theory formulation, the failure criterion could be utilized also when the normal stress was in compression case.

The modified equation is as follows:

$$\tau = \mu\sigma_n - 2\sigma_t \qquad (2\text{-}2)$$

where μ is the internal friction coefficient. The modified equation was a straight-line similar to Mohr-Coulomb envelope.

In addition, Schnaid et al., (2001) found a linear equation at failure conditions, obtained from conventional drained triaxial tests:

$$q_f = k_1 \cdot p_i' + k_2 \cdot C \qquad (2\text{-}3)$$

where $k_1 \cdot p_i'$ is the deviatoric stress at failure for the uncemented soil, obtained in drained triaxial tests; k_2 corresponds to the rate of change in the deviatoric stress with cementation, which is not dependent on the effective stress level; and C is the quantity representing the degree of cementation, which is suggested to be expressed by the unconfined compressive strength.

2.1.5. CONSTITUTIVE MODELLING

The literature on structured soils shows a variety of constitutive models. Gens and Nova (1993) described the basic concepts to develop a constitutive model for structured soils and weak rocks, in reference to the framework of hardening plasticity. The starting point was the yielding phenomenon, as separation threshold between linear soil behaviour, in which there were reversible strains, and the one in which the behaviour became nonlinear with irreversible strains. In their model they formulated the expression of a yielding surface. What is important to put in evidence is the consideration of the bonding effect on the yielding loci. In Figure 2-4, the presence of bonding is visible in the different yielding surface size between a structured and structureless soil. For the first one, the surface is bigger than the second one.

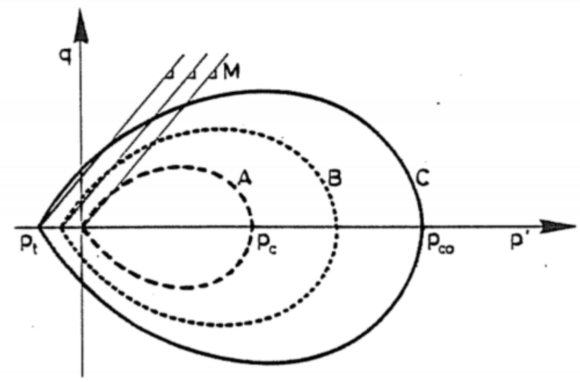

Figure 2-4. Successive yield surfaces for increasing degrees of bonding. Surface A corresponds to unbonded material (Gens and Nova, 1993).

Moreover, the bonding gave a real cohesion and a tensile strength (p_t) to the soil, that was reflected in the expansion of the yield surface to the left. The p_{co} stress controlled the yield of bonded soil during isotropic compression; the p_t stress instead was relative to the cohesion and the tensile strength of the material. The evolution of yield surface was regulated by two different phenomena: from one side to the plastics conventional hardening or softening without bonding and to the other side by the bonding degradation. The bonding amount diminished with the developments of irreversible plastic strains. When there was bonding degradation, the hardening modulus could become negative and there was a reduction of yield domain and strength.

An extension to the models of Nova (1988, 1992) was proposed by Lagioia and Nova (1995). They presented an elasto-plastic strain hardening model that considered the material degradation owing to debonding, by studying the mechanical behaviour of a natural calcarenite. The expression of yield surface derived from the previous formulation of Nova (1988), but two new parameters were introduced: p_t and p_m; the first one was linked to the tensile strength and the second one to the widening of the elastic domain in the compression range.

Rouainaia and Miur Wood (2000), Kavvadas and Amorosi (2000) developed two constitutive models characterized by more than one yielding surface. The latter authors introduced the Plastic Yield Envelope (PYE) and the Bond Strength Envelope (BSE). By means of the second surface, the pre-consolidation stress was described as a process that induced structure in the soil. Another important distinction was among the yield concept viewed as the beginning of irreversible strains and the achievement of PYE while, on the other hand, the beginning of loss of structure when the frontier of the second BSE surface was reached. As a consequence, that new model bypassed the concept of elastic domain typical of Critical State Model and allowed the development of important irreversible plastic strains also for little variations of the tensional state.

Liu and Carter (2002) proposed a constitutive model called Structured Cam Clay (SCC) which had at the base the Modified Cam Clay (MCC) but generalized it considering the isotropic variation of mechanical properties resulting from the presence of structure in the soil. Successively, some authors (Carter and Liu, 2005; Horpibulsuk et al., 2010; Suebsuk et al., 2011) presented a modification of the SCC model and developed the Structured Modified Cam Clay model (SMCC) in order to take in account the effect of cementation. In fact, the SCC model was suitable for naturally structured clay with low or negligible cementation. They borrowed from the SCC model the elliptical shape of the yielding surface but considered the cementation effect by the introduction of a Δe, the difference in void ratio between cemented and uncemented clays. When the yielding was achieved the breakage of cementation intervened and the additional voids diminished. Horpibulsuk et al., (2010) proposed a modification of the mean effective stress to consider the cementation in the following way:

$$\overline{p'} = p' + C/M \tag{2-4}$$

where C was the shear strength contribute of cementation, and M is the slope of failure envelope of cemented clay. There were three different conditions: in the first one C was constant until the strength peak with $\overline{p'} > p'$; the second one from the post-peak zone, where $\overline{p'}$ decreased due to the degradation of cemented soil structure; finally the third one, $\overline{p'} = p'$ when the critical state was achieved and C was equal to 0.

According to Nova et al. (2003), Nova (2005) and Suebsuk et al. (2011) the destructuration phenomenon depended also on the deviatoric plastic strains (ε_d^P). Suebsuk et al. (2011) described the effect of degradation and breakage of the cemented soil structure, through the reduction of the mean effective stress due to the structure (p'_b). There were three diverse cases for the p'_b value: one where it was constant until the yielding on the virgin line; two where p'_b during the yielding gradually diminished and then three when p'_b was equal to zero and there was structure breakage.

Before and after structure breakage the following equations were applied, respectively for the two cases:

$$p'_b = p'_{b0}\, e^{-\varepsilon_d^p} \tag{2-5}$$

$$p'_b = p'_{bf}\, e^{-\xi\left(\varepsilon_d^p - \varepsilon_{df}^p\right)} \tag{2-6}$$

Another constitutive model proposal was proposed by Nguyen et al. (2014). They introduced a model, based on the original Cemented Cam Clay model (CCC), to describe the behaviour of cemented clay. The formulation of the failure envelope in that model was thought to agree with the Critical State Line of reconstituted clay-cement mixture: they illustrated that the effect of cementation decreased owing to the fact that there was the bonding degradation when the confining stress increased. One of the most important features of the new model was the modified formulation of the mean effective stress to take into account the cementation decline. Moreover, it is important to underline that when effect of cementation is null, the CCC model goes back to MCC model. In fact, CCC model was formulated in the background of the Modified Cam Clay and of the Critical State concept.

The shape of CCC yield surface is represented in Figure 2-5, compared to that of the Modified Cam Clay. The CCC model yield function was different than the one of MCC model by the means of a new function that considered the effect of cementation (p'_{Ω}), influenced by the parameter C.

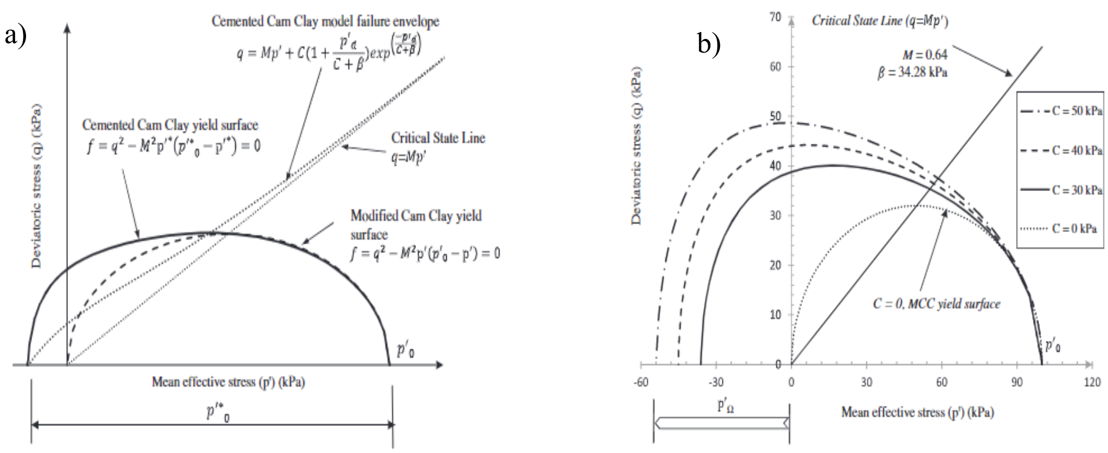

Figure 2-5. a) Yield surface and failure envelope of Cemented Cam Clay model compared to the Modified Cam Clay yield surface and Critical State Line. b) Proposed yield surface with increasing effect of cementation (Nguyen et al., 2014).

2.1.6. PARAMETERS CONTROLLING THE BEHAVIOUR OF CEMENTED SOILS

Several papers have appeared in the last twenty years with the aim to find the parameters that affected the behaviour of cemented soils. One of the first examples is presented in Schnaid et al. (2001), where they linked the deviatoric stress at failure q_f with the degree of cementation (equation 2-3), expressed by the Unconfined Compressive Strength (q_u). According to Schnaid et al. (2001), UCS parameter took into account density, gradation, amount and nature of cement, and mineralogy of soil:

$$q_f = \frac{2 \cdot sin\,\varphi}{1 - sin\,\varphi} \cdot p'_i + q_u \tag{2-7}$$

where φ is the friction angle and p'_i is the initial mean effective stress.

Consoli et al. (2007) evaluated the effect of water/cement and voids/cement ratios on the unconfined compressive strength (UCS) for an artificially cemented sand. The results of their experimental tests showed that it was not possible to demonstrate the existence of a relationship between the water/cement ratio (w_c/c), defined as the water mass divided by the cement mass, and the UCS. The problem was the non-complete filling of pores by water, so as a result the water content did not reflect the amount of voids. Due to that fact, for a soil in unsaturated conditions, it was more appropriate to establish a relationship between porosity and cement content in order to control the mechanical strength of soil, instead of using water/cement ratio that affected the soil structure and not the strength features. For this reason they proposed a relationship between UCS and V_v (absolute volume of voids (water+air))/V_{ci} (absolute volume of cement). However, they found that a more elegant formulation to express that function was to use the porosity η and the volumetric cement content C_{iv} (as percentage of the total volume) in place of voids and cement volumes, respectively.

The final form of the equation was as follows:

$$UCS\ (kPa) = c_1 \left[\frac{\eta}{(C_{iv})^{c2}}\right]^{-c3} \tag{2-8}$$

where c_1, c_2, c_3 were constants.

Consoli et al. (2009) correlated the ratio between the volume of voids (V_v) and the volume of cement (V_{ci}) with initial shear modulus (G_0) and effective strength parameters (c', φ') of an artificially cemented sand. The results reported that q_u, G_0, c' and φ' diminished as the value of V_v / V_{ci} increased. They said that void/cement ratio in (V_v/V_{ci}) shape was more useful than in (η / C_{iv}) shape for the designers to decide the optimum amounts of cement and compaction stress to calculate the right mixture with the appropriate strength and stiffness features. Finally, Consoli et al. (2011) demonstrated that it was possible to write a direct relationship between η/ C_{iv} and q_u also for artificially cemented clays.

Abram (1918) stated that the strength (S) was only dependent on water/cement ratio (w/c), with A and B two empirical constants:

$$S = \frac{A}{B^{(w/c)}} \tag{2-9}$$

Horpibulsuk et al. (2011a, 2011b, 2012a) proposed a new formulation for blended cement admixed clay:

$$q_u = \frac{A}{\left(\frac{w_c}{C_i + C_e}\right)^B} = \frac{A}{\left(\frac{w_c}{C_i(1+ka)}\right)^B} \tag{2-10}$$

where q_u was the compressive strength of blended cement admixed clay at a specific curing time, A, B and k empirical constants, w_c was the clay water content in (%), C_i was the cement content in (%), a was the ash content in (%). Moreover they proposed an interrelationship among strength, clay-water/cement ratio, and curing time. Starting from the equation (2-10), they introduced the effect of the curing time as:

$$\frac{q_{(w_C/C)_D}}{q_{(w_C/C)_{28}}} = \left[\frac{(w_C/C)_{28}}{(w_C/C)_D}\right]^B (c_1 + c_2 \ln D) \qquad (2\text{-}11)$$

where $q_{(w_C/C)_D}$ was the strength of the blended cement admixed clay to be estimated at clay–water/cement ratio of $(w_C/C)_D$ after D days of curing and $q_{(w_C/C)_{28}}$ was the strength of the blended cement admixed clay at clay–water/cement ratio of w_C/C after 28 days of curing and $C = C_i(1 + 0.75a)$; c_1 and c_2 were two constants.

In a recent paper by Sassanian and Newson (2014), the authors proposed an expression to correlate the undrained shear strength c_u to the curing time. They noted that there was an increase in residual strength with the curing time, attributed to the progressive formation of hydration products of cement. They normalized the undrained shear strength c_u by the one at 28 days (the reference time) and proposed the following equation:

$$\frac{c_u}{c_{u,28\ days}} = 0.96\left(\frac{t}{t_{28\ days}}\right)^{0.31} \qquad (2\text{-}12)$$

To derive the equation (2-12) they analysed more than 440 data for 12 types of clay, with a wide range of liquidity index (LI = 0.4 - 3.0) and cement content (c = 1 – 100%). In addition, they studied the effects of clay activity (A) and cement/water ratio (c/w) on the undrained shear strength (normalized by the atmospheric pressure P_a=101.3 kPa), by introducing the parameter β:

$$\beta = A^{3.2}\frac{c}{w} \qquad (2\text{-}13)$$

$$\frac{c_{u,28\ days}}{P_a} = 125.24\beta^2 + 7.47\beta + 0.42 \qquad (2\text{-}14)$$

2.1.7. LIGHTWEIGHT CEMENTED SOILS (LWCS)

Very few publications are available in the literature to address the issue of the foam effect on the physical and mechanical behaviour of cemented soils. Tsuchida and Egashira (2004) proposed an in-depth investigation on the Lightweight Treated Soil Method.

The use of Lightweight Treated Soils responds well to two different demands: from one side the lack of waste disposal sites in seaports has become a serious problem and, moreover, there have been strong calls due to social and environmental aspects for the reuse of dredged soils in port and harbour construction works. The authors described the Lightweight Treated Soils as a ground materials with a density between 0.6 and 1.5 g/cm^3, made by mixing sea water, lightener and stabilizing agent with dredged soil or other source soil. What they put in evidence was the Lightweight Treated Soils flowability immediately after the material was mixed; in addition, the reaction with the stabilizing agent ultimately produced hardened soil with strength properties equal to or superior to good quality material.

2.1.8. MAIN TECHNICAL APPLICATIONS OF LWCS

The first use of Lightweight Treated Soil as a ground material in the history of port construction projects in Japan was for quay wall damaged by Hanshin-Awaji Great Earthquake in 1995. After that first application, Lightweight Treated Soils were used in many other seaports and airports projects in Japan (Wako et al., 1998; Okumura et al., 2000; Hirasawa et al., 2000).

Satoh et al. (2001) presented the case study of Kumamoto Port (Kyushu Island, Japan) where to build a new quay wall to the depth of 10 m below the sea level the LWTS technology was employed. Full scale field placing tests were carried out and summing up the results it was found that LWTS technology could be applied to a water depth of 10 m. Thanks to lightweight of the whole quay wall structure due to the backfill of LWTS and the reduction of 10 m in the width of the concrete caisson owing to the decrease of the seismic earth pressure, the proportions of the ground improvement was drastically reduced and the economic costs of the works decreased by 20≈25% with respect to an ordinary technology. The UCS value after 1 year of curing was higher than the one at 28 days of curing. Moreover, the mean UCS value was around 1 MPa, higher than 200 kPa selected value. Otani et al. (2002) proposed a study about evaluation of physical and mechanical properties of an in-situ (Kumamoto Port) lightweight soil with air foams by the means of X-Ray CT scanner. The instrument was employed during the execution of unconfined compression tests to determine the density evolution of the sample. The result showed that the changes of density during the UCS tests was due to the effect of strains localization development. The progression of shear bands was not monotonic but intermittent. Watabe et al. (2009, 2011) summarized 10-year follow-up study of the lightweight soils that were placed as backfill at the seawall in Kobe Port Island and Tokyo International Airport. Those two sites were the early case examples of construction undertaken in 1996 after the Kobe earthquake disaster and the offshore expansion project of the Tokyo International Airport. For Kobe Port Island, its earthquake seismic resistance was improved after the utilization of airfoam-treated lightweight soil. The layer of LWTS was covered by sand and then a pavement. In agreement with the framework of cement-treated soils, the shear strength of the airfoam-treated lightweight soils was much higher than the target value and, in addition, it increased with curing time. The compressive yield stress p_y tended to increase with the depth and was lower in the upper part, due to the heterogenicity of the material, and not for the deterioration from the surface. The airfoam content was lower than 30%, with a target unit weight around 11 kN/m^3 and minimum UCS value of 196 kPa.

2.1.9. EXPERIMENTAL EVIDENCES OF LWCS MECHANICAL BEHAVIOUR

Tsuchida and Egashira (2004) confirmed the agreement of the Lightweight Cemented Soils behaviour in the general trend of cemented soils: in fact, the UCS of LWCS tended to increase as the cement content raised and to decrease as the slurry water content increased. Moreover, they indicated that E_{50} (i.e., secant Young modulus at 50% of deviator stress) was about

100≈200 times UCS and also it depended on the confining cell pressure (σ_c/q_{max}): when the relative cell pressure was less than 0.5 its effect on E_{50} could be neglected, otherwise when it was higher than 0.5 the effect needed to take in account. The minimum range value for the Poisson's ratio was 0.1≈0.2 for axial strains around 1% to 2% to reach an ultimate value of 0.4 for larger strains. Finally, they executed K_0-consolidation tests and they showed a reduction in the K_0 value up to 0.1 for axial strains about 0.5≈1%, and it meant an important diminution of the earth pressure. Some authors focused on studying the effect of the foam (i.e., air content) on the permeability of LWCS. They noted than an increase in the foam content caused an augment in the permeability, due to the fact than beyond an air content of 30% the pores could not be impermeable (Kikuchi et al., 2005, 2006, 2011).

The effects of water and air content on the compressibility behaviour of lightweight cemented clays was studied by Horpibulsuk et al., (2013). The void ratio increased with increasing water and air contents. As a consequence of the higher void ratio, samples were characterised by a lower yield stress and higher rate of destructuring in terms of fabric (pore space among the clay particles). The residual additional void ratio e_{sr} played a crucial role in compressibility behaviour of lightweight cemented clays, it was intrinsic and irrespective of the initial void ratio parameter. At higher effective vertical stresses, all the compression curves tended to come closer together but they were not identified by a unique final path (destructuration line). Those results were in agreement with others about the Bangkok clay on features of residual additional void ratio $e_{sr,}$ presented by Horpibulsuk et al., (2007).

Several authors proposed the individualization of parameters that could define the behaviour of lightweight cemented soils. For instance, Jongpradist et al., (2011) identified a parameter, namely effective void ratio e_{st}, in order to estimate the relation between the mechanical properties of cemented-clay admixtures on the influencing parameters, starting from mechanical tests (i.e., triaxial, oedometer and unconfined compression tests):

$$e_{st} = C_w \cdot ln(e_{ot}/A_w) \tag{2-15}$$

where C_w was the clay-water content, e_{ot} was the void ratio after curing time and A_w the desired cement content (%), defined as the percentage ratio of the weight of cement to the dry weight of soil.

For a mix design aims, Horpibulsuk et al., (2012b) identified a relationship between strength and V/C at a certain water content, taking in account the Abram's law and their findings for cemented clays (Horpibulsuk et al., 2011a, 2011b, 2012a):

$$q_u = \frac{A}{(V/C)^B} \tag{2-16}$$

where q_u was the unconfined compressive strength, A and B were two constants and V/C was the absolute volume of void/absolute volume of cement ratio. Moreover, to consider the effects of water content and curing time the authors proposed another relationship about the lightweight cemented Bangkok clay:

$$\frac{q_{(wV/C)_D}}{q_{(wV/C)_{28}}} = \left[\frac{(wV/C)_{28}}{(wV/C)_{28}}\right]^B (c_1 + c_2 \, ln \, D) \tag{2-17}$$

where $q_{(wV/C)_D}$ was the strength of the lightweight cemented Bangkok clay to be estimated at water-void/cement ratio of $(wV/C)_D$ after D days of curing, $q_{(wV/C)_{28}}$ was the strength of the lightweight cemented Bangkok clay at water-void/cement ratio of wV/C after 28 days of curing and c_1, c_2 were two constants.

Teerawattanasuk et al., (2015) carried out a study about the possibility to use the Bangkok clay to build a lightweight pavement material. The results of the UCS tests showed that the unconfined compressive strength tended to increase with the cement content and to decrease as the foam content became higher. They developed three different mix design charts characterized by a specific cement content that could be used to fix the input values of foam and cement contents for a unit weight target to reach, time after time for each lightweight pavement material.

De Sarno (2019) and De Sarno et al., (2019) deeply investigated the chemo-physical evolution and mechanical behaviour of lightweight cemented soils (LWCS). They carried out microstructural (i.e., XRD, TGA analyses, MIP and SEM observations) and mechanical tests (i.e., oedometer and direct shear tests) on two different types of soils: Speswhite Kaolin and Caposele Clay. The first one was a clayey silt commercially produced and the second one a natural clay with silt.

From the point of view of the chemo-physical evolution of the soil-cement-foam system, the hydration of cement played a crucial role together to the development of pozzolanic reactions. In particular, the addition of foam did not affect the chemo-physical evolution of the LWCS. In fact, the XRD and TGA analyses highlighted the presence of Portlandite ($Ca(OH)_2$) precipitation and successive cement hydration products since the early stages of curing (i.e., 24 hours). The progressive dissolution of clay minerals and $Ca(OH)_2$ precipitation determined the development of pozzolanic reactions.

The creation of a well joined interconnection due to the formation of hydration products had an effect on the microstructural features of LWCS studied. In particular, the MIP results showed at increasing curing time a slight shift in modal pore size towards a smaller pore size, as hydrated compounds increased the frequency of smaller pores between 0.6 – 4 μm. The SEM observations were in agreement with the MIP results. In fact, they showed how the interconnection of cement hydration products tended to fill the gap around groups of particles.

Vitale et al. (2020) noted in the SEM observations the existence of large voids as footprints left by air bubbles during mixing. Those led to an increase in the porosity and reduced the unit weight of the sample, thanks to an increment of the void ratio, but did not alter the microstructural matrix. As reported by De Sarno (2019), foam bubbles had the capacity to maintain the soil-water-cement system during the mixing phase. They were stable along the cement setting phase and the hardening of the matrix: those two phenomena were responsible for the augment of LWCS porosity. Moreover, MIP analyses put in evidence the inability of detecting the footprints of foam bubbles on the external sample surface with diameter > 300 μm; on the other hand, the bubbles in the inner part of the samples could be discovered only in the case they were linked to the pores of soil matrix, accessible from the outer surface. That feature was confirmed from the cumulative curves characterized by higher mercury intrusion volume that was related to the modal size of soil matrix, the volume of the internal bubbles and the high porosity of the lightweight cemented sample. In addition, the foam content had an effect on the pores frequency that was higher relative to the largest voids. At the increasing curing time, the pores frequency reduced due to the progressive filling of cement hydration products of the voids and it was more evident as the foam content increased (pores entrance diameter 10 mm – 250 μm).

De Sarno (2019) also investigated the effects of foam on the bulk density for Lightweight Cemented Soil samples and for the ones only cemented. For the latter, the theoretical value of bulk density was almost the same as the measured one; however, for the LWCS samples the theorical value was lower than the measured one, due to the breakage of air bubbles during the mixing phase. The mechanical tests (i.e., oedometer tests) showed a reduction in the yield stress owing to the addition of foam; on the other hand, yield stress increased with increasing the cement content from 20% to 40% and direct shear tests evinced an increase in the peak strength with a more brittle and dilatative behaviour, due to the increased cement content and curing time. When foam was added to the soil-cement-water system, there was a decrease in the peak strength with a more ductile and contractive behaviour. It was owing to the higher porosity present in the Lightweight Cemented Soil samples.

The void ratio of bonds e_b, defined by the ratio between the volume of hydrate cement (i.e. volume of bonds) and volume of solid soil, was a unique identified parameter in order to describe the degree of cementation, but considering the cement content and curing time. Finally, a failure surface was determined that was dependent on different parameters such as vertical stress, degree of cementation, foam content and three other constants φ (friction angle), c_{b0} (parameter that took into account the effect of bonds on cohesion) and c_f (fitting parameter).

2.2. NON-DESTRUCTIVE TESTING

Non-Destructive Testing (NDT) is defined as the course of inspecting, testing, or evaluating materials, components, or assemblies without destroying the serviceability of the part or system (Workman and O. Moore, 2012). The goal of using Non-Destructive Testing methods is to be able to carry out quality checks on the material without compromising its integrity. This contrasts with destructive testing techniques that investigate failure mechanisms to determine certain mechanical properties of materials: for instance, yield stress, compressive strength, and tensile strength.

Non-Destructive Testing are techniques used to apply physical principles in order to determine properties of materials, components and systems and moreover, with the aim of identify inhomogeneities and defects without compromising the integrity and subsequent use of the analysed object. In Table 2-1 are reported pros and cons of Non-Destructive Testing versus Destructive Testing (Beldev et al., 2002).

	Destructive tests	*Non-destructive tests*
	Advantages	**Limitations**
1.	Measurements are direct and reliable.	Measurements are indirect reliability is to be verified.
2.	Usually quantitative measurements.	Usually qualitative measurements. Measurements can also be done quantitatively.
3.	Correlation between test measurements and material properties are direct.	Skilled judgment and experience are required to interpret indications.
	Limitations	**Advantages**
1.	Tests are not made on the objects directly. Hence correlation between the sample specimen used and object needs to be proved.	Tests are made directly on the object. 100% testing on actual components is possible.
2.	A single test may measure only one or a few of the properties.	Many NDT methods can be applied on the same part and hence many or all properties of interest can be measured.
3.	Inservice testing is not possible.	Inservice testing is possible.
4.	Measurement of properties over a cumulative period of time cannot readily be possible.	Repeated checks over a period of time are possible.
5.	Preparation of the test specimen is costly.	Very little preparation is sufficient.
6.	Time requirements are generally high.	Most test methods are rapid.

Table 2-1. Destructive and Non-Destructive tests comparisons (Beldev et al., 2002).

In the following sections it is reported a brief description of two different non-destructive testing methods that are applied in this experimental study: ultrasonic testing and electrical resistivity measurements.

The decision to use these two non-destructive techniques lies in their ability to provide indications of the physical and mechanical properties of the studied material, which are highly dependent on its microstructure. These techniques can be used during various stages of curing time of cemented soils and lightweight cemented soils, to study the chemo-physical evolution of the soil-water-cement and soil-water-cement-foam systems, respectively.

They are a good tool to realize in situ quality checks about the right execution of the treatment on the material, due to the possibility of detecting the presence of hydration products by means of P-waves velocity or electrical resistivity trends. An increase in the measured geophysical quantities (i.e., P-waves velocity and electrical resistivity) is due to the increase in the gel/space ratio during paste hydration. The lower volume of pores leads to an increase in P-waves velocity and electrical resistivity through the samples. In addition, also the effects of artificial porosity can be checked by means of these techniques. In fact, the presence of additional voids determines on the one hand the reduction in P-wave velocity and, on the other hand, the increase in electrical resistivity.

Finally, there is the possibility to find relationships between the measured quantities and geotechnical parameters (for example UCS, E_{oed}). The relevance of these technologies is the capability of using the measured geophysical quantities (i.e., P-waves velocity and the electrical resistivity) to estimate certain geotechnical parameters, in all those cases where mechanical tests cannot be performed.

2.2.1. ULTRASONIC TESTING METHOD

The concept behind the ultrasonic testing method is the generation, transmission, and reception of a train of small amplitude waves with varying pulse lengths and frequencies. Wave propagation can be defined as a passage of strain energy in a medium (Eringen, 1980; Jaeger et al., 2007). The microstructure of a material, in terms of void index, size, shape, grain distribution and arrangement, can determine the rate of dissipation energy by defining the velocities of different modes of propagation, such as compression and shear. The wave velocity is related to the physical and mechanical properties of the material and strongly depends on its microstructure. Rummel and Van Heerden first and ISRM after (Rummel and Van Heerden, 1978; ISRM, 2007) proposed the original methods that consisted of three different approaches utilizing waves characterized by different frequency ranges and specimens of different shapes, testing and analysis procedures. In a recent paper by Ulusay (2014), it is presented an upgrade method that joins the high (100 kHz-2 MHz) and low (2-30 kHz) frequency ultrasonic pulse technologies in a generalized scheme applicable to any kind of specimens in terms of shapes, size, and frequency within ultrasonic range >20 kHz. In this procedure of ultrasonic testing, called pulse method, the wave trains propagation through solids can be detected by a single transducer (pulse-echo technique) or by a pair of transducers (pitch-catch technique). The first one is used to determine flaws that constitute seismic impedance contrasts inside the material. The second one is characterized by three different modes to set the transducers on the surface of the specimen: direct (through) transmission, indirect (surface) transmission, and semi-direct (edge) transmission, as represented in Figure 2-6.

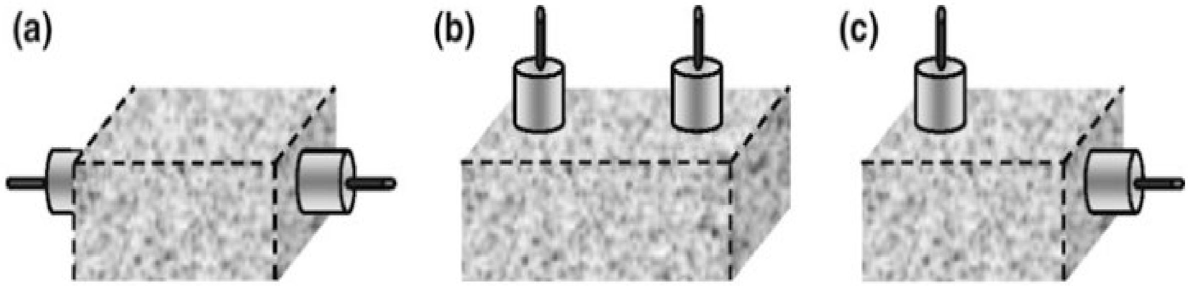

*Figure 2-6. Basic configurations of transducer pairs (transmitter-receiver) used in pitch-catch technique: **(a)** direct (through) transmission; **(b)** indirect (surface) transmission; **(c)** semi-direct (edge) transmission. (ISRM, 2007-2014)*

The direct transmission is better than the others because in this case the length and the direction of the wave trains are known and there are not effects of damage or deterioration of specimen surface and edges on the results (ISRM, 2007-2014).

Ultrasonic test apparatus is made up of these components: a signal generator to trigger timer to mark the beginning of each excitation pulse interval, an arrival timer in form of a threshold trigger and/or an oscilloscope for visual analysis of the wave form, amplifiers and filters for signals enhancement, and a data acquisition unit interfacing with the apparatus (Figure 2-7). Two different transducers are necessary to detect P- and S-wave velocities. The piezo-electric transducers are characterized by an interval of frequency that goes from 20 kHz to 2 MHz, but for the practical utilization the suggested range is 50-500 kHz.

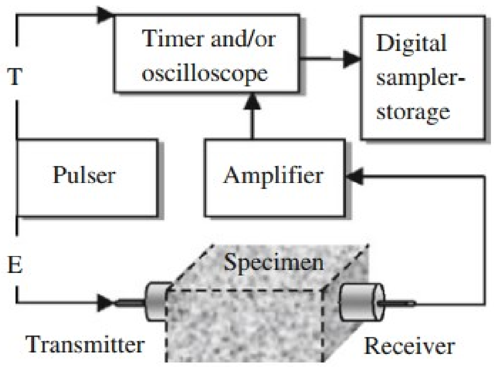

Figure 2-7. A simplified layout of basic components of an ultrasonic apparatus: E transmitter excitation signal, T timer trigger signal (ISRM, 2007-2014).

In the test procedure the length of wave travel path L and the length of travel time of each wave type t_P and t_S are necessary to determine V_P and V_S.

It is important to highlight that: a) a thin layer of coupling medium must be used to guarantee the most uniform and efficient energy transmission from one transducer to the other one; b) the pair of transducers must be positioned in the right centre of the two opposite surfaces of the specimen; c) to have a coaxial positioning of the transducers a benchtop load frame with a low capacity load transducer can be used in direct-transmission configuration.

The velocities of P- and S-waves can be estimated considering that $V_P= L/t_P$ and $V_S= L/t_S$, where L is for the travel path length and t_P and t_S are for travel times of P- and S-waves (ISRM, 2007-2014).

Galaa et al. (2011) studied the applicability of the ultrasonic testing technique to cemented paste backfill and they showed the evolution of stiffness of that material during one week of curing time in two different conditions: air-dried and submerged under water. The degree of saturation was responsible for the variations in the measured values of V_P. In particular, the air-dried samples showed a reduction in V_P due to the air entry into the samples, that caused the loss of pore fluid influence on the bulk modulus of the overall material. Hence changes in the stiffness of soil skeleton can be seen in the measured V_P values. On the other hand, for samples submerged under water V_P does not change.

Yesiller et al. (2000) demonstrated the applicability of the ultrasonic testing method to detect the characteristics of stabilized clay with lime, cement, and lime-fly ash mix. Curing time is one of the main factors that influenced the velocities of the treated soil. In addition, they observed that soil stabilized by cement had higher velocities values than the mixtures with lime and lime-fly ash. An increase in the soil strength, together to an augment of samples density, matched to higher velocity values.

As reported by (Hasanzadeh A. & Shooshpasha I., 2019), the ultrasonic pulse velocity depends on different parameters, for example type of materials, age and length of the sample and the pore distribution inside it. As a result, the lower the number of discontinuities (pores, cracks, poor quality) within the sample, the higher the velocity value; on the contrary the higher the number of discontinuities, the lower the velocity value. Moreover, they studied the effects of silica fume on the characteristics of resistance of those cemented soils. There was an increment in ultrasonic pulse velocity and in unconfined compressive strength because silica fume was responsible for filling and pozzolanic reactions. Therefore, materials became less porous and so there were an augment of ultrasonic pulse velocity and unconfined compressive strength.

In a recent paper, Pu et al. (2019) examined the applicability of the ultrasonic wave transmission method to find a correlation between the ultrasonic parameters and the properties of Foamed Mixture Lightweight Soil (FMLS). They found that the ultrasonic wave transmission method was useful to determine the crack evolution inside the FMLS earthwork. Moreover, the ultrasonic parameters were linked to the curing age of the FMLS: at 30 days of curing time, the velocity was constant.

2.2.2. ELECTRICAL RESISTIVITY MEASUREMENTS

Geophysical methods are widely used in site investigations, and they may avoid the limitations of traditional site investigation methods. In particular, electrical resistivity imaging (RI) has been gaining importance in recent years from the whole field of engineering for site surveys. Resistivity imaging is a method identified to be non-destructive, fast, and cost-effective that can be useful in soil characterization. There are several advantages in comparison to conventional in situ investigation methos, for instance to have a continuous image of subsurface conditions, to cover a large area in a reduced time, to detect the heterogeneity and zones characterized by high moisture content and to have simple and quick data processing. Moreover, one of the most important features of this non-destructive method is the possibility to determine engineering parameters necessary in analysis and design (Hossain et al., 2019).

Early examples of the use of electrical resistivity method were in 1720 by Gray and Wheeler with the aim to define the conductivity of rocks (Jakosky, 1950; Van Nostrand and Cook, 1966). In 1912, Conrad Schlumberger made one of the most rewarding experiments to quantify the electrical resistivity by means of the application of the DC current. In 1915, Frank Wenner developed the idea of different electrode combinations to improve the quality of subsurface images. Since then, they were used together to inversion models (Aizebeokhai, 2010).

It is possible to perform electrical resistivity measurements of soil in situ or in laboratory on collected samples, using a resistivity meter. At laboratory scale, direct current (DC) and alternative current (AC) are used to determine the electrical properties of soil. Regard to AC, the range of adopted frequencies is between low Hertz and microwave. On the contrary, DC method is based on the principle of Ohm’s law, in which an application of electrical current makes possible the measurement of voltage drop across the electrodes. There are two different electrode combinations to employ in the measurements: two and four electrode configurations (Hossain et al., 2019).

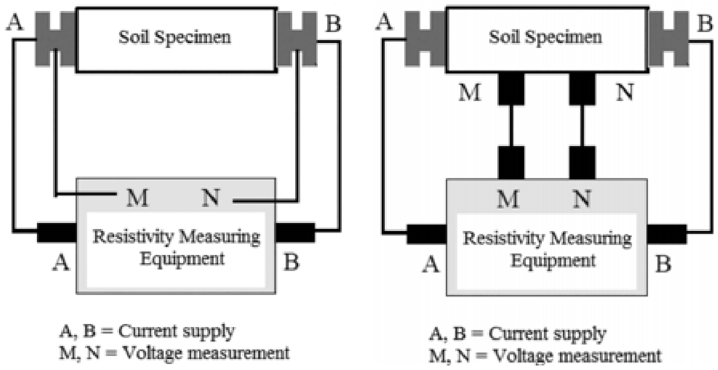

Figure 2-8. On the left, two-electrode electrical resistivity measurement system. On the right, four-electrode electrical resistivity measurement system (Hossain et al., 2019).

Representative schemes of two-electrode and four-electrode configurations are shown in Figure 2-8. On the left, the two-electrode electrical resistivity measurement system is made up of soil box, current source, resistance measuring equipment and electrical connections. In this set up, the two electrodes are used for both current application and voltage measurements. The soil box needs insulated and durable material in order to avoid problems of short circuiting during the development of the experimental measurements. Polished and anti-corrosion metal is necessary for the two end plates utilized for the current flow and voltage measurements. The most important phenomenon that affects the two-electrode configuration is the polarization.

Because of the electrical conduction in the electrode and cable, it is possible to have an electron flow together to the flow of the current. As a result, there will be a charge accumulation at the soil-metal interface. Moreover, air space at the interface, non-uniform electric field and chemical reactions could be the reason for other errors in this electrode's arrangement (Santamarina et al., 2001).

In Figure 2-8, the four-electrode configuration is depicted on the right. Two electrodes are positioned at the two opposite extremities of the soil box, and they are used to supply the current; on the other hand, the potential drop is measured between the previous points by means of other two electrodes. The advantage of this kind of configuration is the possibility of avoiding the polarization phenomenon, thanks to the fact that potential drop is measured within the samples. What is more, the impact of chemical reactions on the electrical resistivity measurements is not relevant since there are different electrodes for voltage and current.

Geotechnical parameters can influence the electrical resistivity of soils. In particular, one of the most important factors that has a relevant effect on the electrical resistivity is the moisture content. Moreover, also the degree of saturation, the pore water composition, the organic content, specific surface area and mineralogical and geologic formation can influence the electrical resistivity.

First of all, an increase in moisture content causes a decrease in the electrical resistivity. In fact, moisture content is strictly linked to the electrical conductivity, that occurs through the precipitated ions in the soil pore water. Pozdnyakov et al., (2006) showed that the electrical resistivity is linked to the natural logarithmic of moisture content and different zones can be identified. They are called adsorbed water, film water, film capillary water, capillary water and gravitational water, as reported in Figure 2-9. An important decrease in electrical resistivity can be observed in the adsorption water zone. Then, the rate of reduction tends to decrease in the film water zone, due to the increase in van der Waals. Moreover, in film capillary water and capillary water zones the electrical resistivity decreases less quickly, owing to the fact that the molecular attraction force is higher than the capillary force. Finally, in the gravitational water zone the electrical resistivity becomes independent of water content, because of the mobility of electrical charges is no longer linked to the movement of water molecule ions (Hossain et al., 2019).

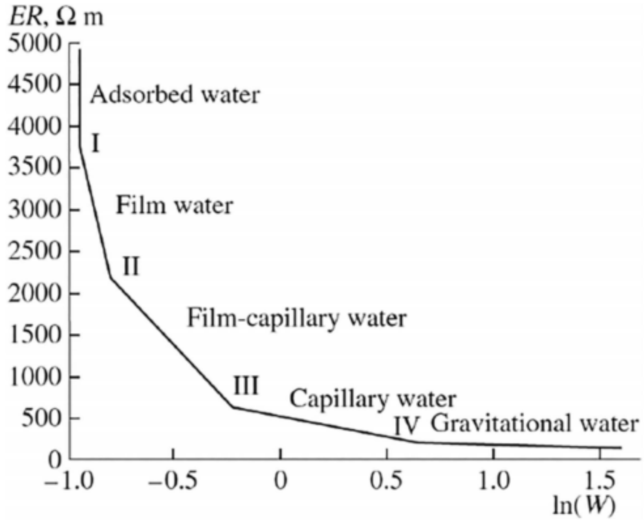

Figure 2-9. Soil moisture content and electrical resistivity relationship (Pozdnyakov et al., 2006).

Several publications have appeared in recent years documenting the effects of cemented soils properties on the characteristics of the electrical resistivity. As reported by Liu et al. (2008), cement-mixing ratio, water content, degree of saturation, water-cement ratio and curing time have been investigated to analyse their effect on the electrical resistivity measurements. In that work it was observed that the electrical resistivity of cemented soil increased with the increment of cement-mixing ratio and curing time, whereas the higher the degree of saturation and water-cement ratio the lower the electrical resistivity. In addition, the authors showed that there was a good relationship between the measurements of electrical resistivity and the results of the unconfined compression tests.

This kind of relationship between cemented soil and electrical resistivity has been confirmed by the experimental study of Chen et al. (2011) on cement-stabilized lead-contaminated soils. In particular, they investigated the effects of a change in porosity and degree of saturation on the electrical resistivity and its link with the unconfined compression strength of those materials. Moreover, the authors analysed the trend of the electrical conductivity of soil pore fluid during the curing time: in fact, the electrical conductivity of soil pore fluid decreased with increasing the curing period, and, on the other hand, it increased with the cement content.

A correlation between the standard compressive strength of cement and electrical resistivity was the aim of the experimental work of Wei et al. (2012), by measuring the ISO 679 cement compressive strength and the electrical resistivity of cement pastes, characterized by different strength grade cements. It is appropriate to emphasize the role of the hydration time on the electrical resistivity development for the pastes with different cements. In general, the development of hydration time determined an increase in the electrical resistivity values, even if there was a first drop to minimum point. What is more, the past with higher cement strength exhibited higher electrical resistivity values than the past with lower one.

Relationships between electrical resistivity and geotechnical data in clays were also proposed by Fallahsafari et al. (2013). They put much attention on these geotechnical parameters: water content, degree of saturation, wet unit weight, air void ratio and compressive strength. Those parameters showed an important effect on the electrical resistivity; for instance, clays characterized by high water content or degree of saturation had low electrical resistivity compared to clays with high air void ratio. In addition, increasing of wet unit weight led to increase in the electrical resistivity.

A study of the effect of soil parameters on the electrical resistivity has also been conducted by Zhou et al. (2015). For instance, the authors analysed the effects of the degree of saturation on the electrical resistivity: the lower the degree of saturation, the higher the electrical resistivity values. In addition, they underlined the importance of pore fluid on the measurements of the electrical resistivity. In fact, different kinds of electrolytes had dissimilar effects on soils electrical resistivity, because of the mobility of ions. In the end, they described the influence of temperature, and they said that abrupt variations of temperature lead to “jumps” in the electrical resistivity measurements; thus, it is important to take in account this parameter to avoid wrong analysis of the data.

In their research work, together to quantify the effects of cement content, porosity and curing time on the electrical resistivity and unconfined compression strength of cemented soils, Zhang et al. (2012) also proposed a modified Archie empirical law to put in evidence the role of cement content and curing time on the electrical resistivity values. The original Archie law is empirical and which relates the electrical resistivity of a saturated sand (ρ) to the electrical resistivity of its pore fluid (ρ_w) and the geometry of the porosity in the soil (n), as it can be seen in Equation 2-30:

$$\frac{\rho}{\rho_w} = n^{-m} \tag{2-30}$$

where m is the material-dependent empirical exponent, that measures the pore tortuosity and the interconnectivity of the pore network. During the years, in 1966 the Archie's law went as far as partially saturated soils thanks to Keller and Frischknecht, as it can be seen in equation 2-31:

$$\frac{\rho}{\rho_w} = a \cdot n^{-m} S_r^{-p} \tag{2-31}$$

where S_r is the degree of saturation, a is a constant and p is saturation exponent. However, those two models did not consider the effect of cement stabilization process on the electrical resistivity and the curing time. For those reasons, Zhang et al. (2012) introduced a new parameter called "after-curing porosity/cement content-curing time ratio", n_t/ (a_wT). They found a good correlation between that ratio and electrical resistivity of cement stabilized soils, expressed by the following equation.

$$\rho = A\left(\frac{n_t}{a_w T}\right)^{-B} \tag{2-32}$$

where A and B are dimensionless constants. If a comparison between the equation (2-32) and the original Archie's law is made, the Archie's model can be applied to cement stabilized soils by means of a term called "after-curing porosity/cement content-curing time ratio". They also argued that the cement content and the curing time influence the UCS of treated soils. Therefore, they added another parameter, the ratio $n_t/(a_w T^{1/2})$. Consequently, they determined a power function for the relationship between UCS (q_u) of cemented soils and the ratio $n_t/(a_w T^{1/2})$, as:

$$q_u = C\left(\frac{n_t}{a_w\sqrt{T}}\right)^{-D} \tag{2-33}$$

where C and D are dimensionless constants.

Kibria and Hossain (2014) agreed to the previous authors about the dependency of electrical resistivity on the geotechnical parameters (i.e., moisture content, unit weight, degree of saturation, void ratio, specific surface area, cation exchange capacity), but they also put the accent on the presence of different clay minerals that can influence the electrical resistivity of clayey soils. In particular, they focalized the attention on the bentonite minerals and their effects on the variations of electrical resistivity values. It was observed that there was a decrease in the electrical resistivity with increasing the Na-bentonite content from 20% to 100%, at a degree of saturation equal to 40%, and also for an increase in Ca-bentonite content from 20% to 100%, at the same degree of saturation. Summing up the results, it was clear that the presence of bentonite influenced a lot the soils electrical resistivity.

Another insight into the aspect of the electrical resistivity measurements related to clay minerals was made from Kibria and Hossain (2019). They carried out a study to determine the electrical resistivity response of diverse clay minerals (i.e., smectite, illite and kaolinite), considering three degrees of saturation (i.e., 40, 60, 80 %) and their rapport to activity, porosity, cation exchange capacity, pore water properties. It was shown that the physical-chemical properties had an impact on electrical resistivity of the clay materials investigated. In particular, an increment of pore water conductivity, pH, and sulphate concentration lead to a decrease in the electrical resistivity of the samples. Moreover, the rate of diminution decreased with the increase of the degrees of saturation. In addition, activity and cation exchange capacity had effects on the electrical resistivity since it decreased with the increments of those two properties.

The electrical resistivity monitoring and its correlation with volume, strength and stiffness during curing time of expandable foam grout (EFG) was experimentally studied by (Han et al., 2020). The results of the research work highlighted the effects of the hydration process on the electrical resistivity and on the strength of the cementitious material. In fact, strength, and stiffness of EFG developed because of the hydration of C_3S. Throughout the time of that process, electrical conductivity decreased, as a result of the precipitation of hydration products that filled the pores, reducing the passage for ions flow. Consequently, the electrical resistivity tended to increase along the hydration process of calcium silicates.

The objective of this study is to verify the applicability of a non-destructive investigation technique for the chemo-physical and mechanical characterisation of Lightweight Cemented Soils (LWCS). Electrical resistivity measurements of two different soils (i.e., SW Kaolin and Caposele Clay) prepared with different percentages of foam, will be performed in order to investigate the influence of the mineralogical characteristics of the untread soils and the treatment parameters on the electrical resistivity values and their evolution over the curing time. In fact, electrical resistivity could represent one of the relevant parameters in site applications in the quality control of LWCS, in order to check the development of cement products in a reliable and expeditious manner, and the consequent suitability of the treated material.

2.3. DURABILITY OF TREATED SOILS UNDER ENVIRONMENTAL LOADS

Durability is an important issue in geotechnical field and by this concept is meant the ability of the material to retain its stability and integrity while maintaining adequate long-term residual strength to cope with environmental stresses (Dempsey & Thompson, 1967). Under severe climatic stresses (i.e., wetting-drying, freezing-thawing, etc.), durability is a vital parameter in case of treated soil used as a building material: such as embankments, filling of underground cavities or excavations, infrastructures, and road pavements. Climatic stresses, especially in terms of wetting-drying cycles, can be considered one of the most destructive actions that may damage geotechnical engineering works, in particular infrastructures and road pavements (Allam & Sridharan, 1981; Sobhan & Das, 2007). During the alternance of wetting-drying cycles majority of engineering properties of soils, above all the strength, are severely compromised and, as a result, settlements and crack propagation occur (Al-Obaydi et al., 2010; Al-Zubaydi, 2011).

In nature, soils are subjected to periodic wetting-drying cycles owing to the alternation of the rainy and dry seasons. Their variation produces effects on the mechanical behaviour and performance of treated soils used in geotechnical and environmental applications (Chen and Ng, 2013; Tang et al., 2016; Pasculli et al., 2017).

Several studies have been proposed about the effects of wetting-drying cycles on the hydro-mechanical behaviour of unsaturated soils. In particular, this type of climatic stress involves irreversible volumetric variations due to swelling and shrinkage strains: an accumulation of the latter occurs in an expansive soil after it has been subjected to wetting-drying cycles (Alonso et al., 2005; Cuisinier and Masrouri, 2005). The occurrence of irreversible swelling or shrinkage is a function of compaction conditions and the resulting change in net stress and suction, rather than being determined solely by the soil type (Nowamooz and Masrouri, 2008). Moreover, the authors investigated the influence of suction cycles on the soil fabric of two reconstituted clayey soils, by the means of MIP technique. They observed that suction cycles determine a cumulative swelling strain for dense soil, while a cumulative shrinkage for a loose one. In addition, they show a presence of an equilibrium in which samples have an elastic behaviour. The analysis of fabric in that stage reveals how suction cycles provide macrostructural modification in terms of reorganization of meso-pores towards a smaller dimension (Nowamooz and Masrouri, 2010).

On the other hand, Kalkan (2011) suggested that the addition of silica fume can reduce the progressive swelling strain of a clayey soil, when it is submitted to wetting-drying cycles. In fact, when silica fume is added to clayey soil, the pH values increase. This phenomenon causes the dissolution of silica from clay minerals. As a result, the soil with low values of clay minerals and a low liquid limit shows a reduction in swelling behaviour.

Chen and Ng (2013) proposed a study on the volumetric response of unsaturated compacted clay linked to the effects of wetting and drying cycles. The volumetric behaviour was characterized by irreversible swelling after wetting and irreversible shrinkage after drying phase. From the mechanical point of view, the swelling post wetting led to a reduction in the preconsolidation stress. This behaviour was attributed to irreversible modification in degree of saturation. Those two combined effects (i.e., swelling and increment of degree of saturation), led to a soil that was more susceptible to yielding and a softening effect.

Another study on the topic of durability against wetting-drying was carried out by Neramitkornburi et al., (2014), focusing on Lightweight Cellular Cemented construction material. They studied the effect of soil's cemented structure, in terms of fabric and bonding, on the strength of Lightweight Cellular Cemented construction material. It was found that the strength reduction is attributable to cemented structure degradation. Wetting-drying cycles involve swelling or shrinkage of clay particles, leading to crack formations. Because of fissures, the amount of pore spaces increases a lot leading to a rise in water content.

In the field of cemented soils, the condition of partial saturation plays an important role. In fact, suction is a key feature in the understanding of the mechanical behaviour of unsaturated soil. In particular, it exerts its influence through two different mechanisms (Karube and Kato, 1994; Wheeler and Karube, 1995):

a) by varying the skeleton stress through alterations in the average fluid pressure acting in the soil pores

b) by supplying an additional bonding force at the particle contacts, often attributed to capillary phenomena occurring in the water menisci.

The value of suction is related to the degree of saturation of the soil. The relative area over which the water and air pressures act depends directly on the degree of saturation (the percentage of pore voids occupied by water), and at same time this parameter influences the number and intensity of capillary-induced inter-particle forces. The authors have pointed out that the phenomenon of soil particle slippage, under partially saturated conditions, is inhibited by the presence of interparticle forces due to the menisci with negative pressure water inside, behaving as additional bonding. Thus, from the point of view of the elasto-plastic behaviour, many features depend on the phenomenon of *bonding* and *de-bonding* among soil particles owing to the presence or absence of water menisci at the contacts (Gallipoli et al., 2003).

The literature on this topic shows that suction contributes to the strength of the cementing materials, in the sense that its action goes to sustain together groups of particles and the behaviour of the soil becomes as if has a coarser grading, and thus it shows a dilatant tendency. It is opposed to what can be seen for a soil in saturated conditions where samples consolidated at higher effective confining pressures tend to reveal less dilatant behaviour. If in a condition of bonded soil, cementing bonds among soil particles play a dominant role in shear strength, on the other hand in an unsaturated soil the most important role in shear strength is due to the suction that helps the cementing fabric not to break completely at large strains, since it sustains groups of soil particles kept together by cementing agent (Toll et al., 2017).

Another contribution to literature on this topic was made by Rinaldi et al., (2007). They underlined that the stress-strain behaviour of soils characterized by the presence of structure is a combination of different factors: water content, degree of cementation, strain level and confining pressure. In fact, as stated by some other authors (Airey and Fahey, 1991; Maâtouk et al., 1995; Rinaldi and Capdevila, 2006), before yielding the stress-strain behaviour is that of cemented material, with a linear relationship between volumetric and axial strain. In fact, no plastic deformations appear, and the stiffness of soil depends on the cemented bonds. When the sample is in unsaturated condition, the process of decementation starts and the yield stress is dominated by water meniscus. In this case, the difference between saturated and unsaturated condition is the position of the yielding locus that takes place at a higher strain level in the latter condition. Right after the yielding, the shear resistance could be of frictional or cohesive nature, and it depends on the confining pressure, capillary forces, and cement resistance. As asserted by Lambe (1960), when the degree of cementation is high, high suction level and low confining pressure generate a very fixed structure and the frictional behaviour is due to the size distribution and the shape of the aggregates. Stress localization and shear bands occur.

Many studies have focused on the shear strength of unsaturated soils and they have shown that a higher shear strength is linked to a lower degree of saturation or water content, owing to the increase in suction (Fredlund et al., 1987; Fredlund et al., 1996; Goh et al., 2014).

Drying is responsible for the increase in soil stiffness, brittleness and a reduction in strain at failure. These effects are due to an increase in suction value. In fact, it is responsible for the improvement of soil cohesion and effective stress between particles. The increase of suction sustains soils structure and has positive effects on the strength and deformation of soils. In particular, suction goes to improve bonds between soil particles and strength of soil skeleton. Its importance on the mechanical behaviour of soils becomes even more relevant at lower water content. Moreover, when bonds between soil particles are broken due to external load, the positive effects of suction are completely lost (C.-S. Tang et al., 2020).

However, the issue of the durability of Lightweight Cemented Soil (LWCS) has not been deeply investigated in literature. Nevertheless, an insight into the effects of the addition of cement and foam on the water retention properties of LWCS, has been recently provided by Vitale et al., (2020b). They defined the water retention curves for kaolin treated by cement and foam at two different percentages by osmotic technique, at increasing curing time. The influence of the latter parameter is very low on the water retention properties of treated soils, owing to the fact that in long term the hydration process of cement is very slow and as a result there is a slight influence on the chemo-physical evolution of the soil-cement-foam system. What is important to know is that foam does not affect the water retention properties of these materials. Moreover, from the microstructural point of view, the increase of porosity due to the addition of foam, does not alter the soil matrix, which on the contrary is responsible for the water retention facility.

This is the starting point for the durability study of Lightweight Cemented Soil under the effect of environmental loads. In particular, the aim of this part of the research is to analyse the impact of wetting-drying cycles on the mechanical behaviour of Lightweight Cemented Soils.

References

Abrams, D.A., 1918. Design of Concrete Mixtures, Structural Materials, Research Laboratory. Lewis Institute, Chicago. Bulletin 1.

Airey, D.W., 1993.Triaxial testing of naturally cemented carbonate soil. Journal of Geotechnical Engineering. Vol. 119, Issue 9. https://doi.org/10.1061/(ASCE)0733-9410(1993)119:9(1379).

Airey, D.W., Fahey, M., (1991). Cyclic Response of Calcareous Soil from the North-West Shelf of Australia. Géotechnique, Vol. 41, No 1, pp. 101 – 121.

Aizebeokhai, A.P., 2010. 2D and 3D geoelectrical resistivity imaging: Theory and field design. Scientific Research and Essays, 5(23), 3592–3605.

Ali Rahman, Z., Toll, D.G., Gallipoli, D., 2018. Critical state behaviour of weakly bonded soil in drained state. Geomechanics and Geoengineering 13(6):1-13. https://doi.org/10.1080/17486025.2018.1454608.

Allam, M.B., Sridharan, A., 1981. Effect of Wetting and Drying on Shear Strength. Journal of the Geotechnical Engineering Division. https://doi.org/10.1061/AJGEB6.0001117.

Al-Obaydi, M.A., Al-Kiki, I.M., Al-Zubaydi, A.H., 2010. Strength and durability of gypseous soil treated with waste lime and cement. Al-Rafidain Engineering Vol.18 No.1 January 2010. https://doi.org/10.33899/rengj.2010.27985.

Alonso, E.E., Romero, E., Hoffmann, C., García-Escudero, E., 2005. Expansive bentonite-sand mixtures in cyclic controlled-suction drying and wetting. Engineering Geology 81 (2005) 213–226. https://doi.org/10.1016/j.enggeo.2005.06.009.

Baldev, R., Joyakumar, T., Thavasimuthu, M., 2002. Practical non-destructive testing. ISBN: 1-85573-600-4.

Bressani; L.A., Vaughan, P.R., (1989). Damage to soil structure during triaxial testing. Congrès international de mécanique des sols et des travaux de fondations. 12. 1989, pp 17-20.

Carter, J.P., Liu, M.D., 2005. Review of the Structured Cam Clay Model. Soil Const. Model. Eval. Sel. Calibration. GSP 128 40771, 99–132. https://doi.org/10.1061/40771(169)5.

Chen, L., Du, Y-J., Liu, S-Y., M. ASCE, Jin, F., 2011. Evaluation of Cement Hydration Properties of Cement-Stabilized Lead-Contaminated Soils Using Electrical Resistivity Measurement. Journal of Hazardous, Toxic, and Radioactive Waste, Vol. 15, No. 4, October 1, 2011. ASCE, ISSN 2153-5493/2011/4-312–320/$25.00.

Chen, R., Ng, CW.W., 2013. Impact of wetting-drying cycles on hydro-mechanical behavior on an unsaturated compacted clay. Applied Clay Science 86 (2013) 38–46. http://dx.doi.org/10.1016/j.clay.2013.09.018.

Clough, G.W., Sitar, N., Bachus, R.C., 1981. Cemented Sands under Static Loading. J. Geotech. Eng. Div.

Consoli, N.C., Rotta, G.V., Prietto, P.D.M., 2000. Influence of curing under stress on triaxial response of cemented soils. Géotechnique 50, No. 1, pp. 99-105. https://doi.org/10.1680/geot.2000.50.1.99.

Consoli, N.C., Cruz, R.C., B.S., C., Maghous, S., 2012. Failure envelope of artificially cemented sand. Géotechnique 62, 543–547. https://doi.org/10.1680/geot.11.P.037.

Consoli, N.C., da Silva Lopes, L., Foppa, D., Heineck, K.S., 2009. Key parameters dictating strength of lime/cement-treated soils. Proc. Inst. Civ. Eng. - Geotech. Eng. 162, 111–118. https://doi.org/10.1680/geng.2009.162.2.111.

Consoli, N.C., Dalla Rosa, A., Corte, M.B., Da Silva Lopes Jr, L., Consoli, B.S., 2011. Porosity-Cement Ratio Controlling Strength of Artificially Cemented Clays. J. Mater. Civ. Eng. https://doi.org/10.1061/(ASCE)MT.1943-5533.0000283.

Consoli, N.C., Foppa, D., Festugato, L., Heineck, K.S., 2007. Key Parameters for Strength Control of Artificially Cemented Soils. J. Geotech. Geoenvironmental Eng. https://doi.org/10.1061/(ASCE)1090-0241(2007)133:2(197).

Coop, M.R., Atkinson, J.H., 1993. The mechanics of cemented carbonate sands. Géotechnique. Volume 43 Issue 1, March 1993, pp. 53-67. https://doi.org/10.1680/geot.1993.43.1.53.

Cuccovillo, T., Coop, M.R., 1999. On the mechanics of structured sands. Géotechnique 49, 741–760. https://doi.org/10.1680/geot.1999.49.6.741.

Cuisinier, O., Masrouri, F., 2005. Hydromechanical behaviour of a compacted swelling soil over a wide suction range. Engineering Geology 81 (2005) 204– 212. https://doi.org/10.1016/j.enggeo.2005.06.008.

Dalla Rosa, F., Consoli, N.C., Baudet, B.A., 2008. An experimental investigation of the behaviour of artificially cemented soil cured under stress. Géotechnique. Volume 58 Issue 8, October 2008, pp. 675-679. https://doi.org/10.1680/geot.2008.58.8.675.

Dempsey, B.J., Thompson, M.R., 1967. Durability properties of lime-soil mixtures. Highway Research Record No. 235, Highway Research Board, Washington D.C. (1968), pp. 61-75.

De Sarno, D., 2019. Microstructure and mechanical behaviour of cemented soils lightened by foam. Ph. D. Thesis. University of Naples, “Federico II”.

De Sarno, D., Vitale, E., Deneele, D., Nicotera, M.V., Papa, R., Russo, G., Urciuoli, G., 2019. Effects of cement and foam addition on chemo-mechanical behaviour of lightweight cemented soil (LWCS). E3S Web Conf., 92. https://doi.org/10.1051/e3sconf/20199211006.

Eringen, A.C., 1980. Mechanics of Continua, 2nd edn. R.E. Krieger, New York.

Fallahsafari, M., Hafizi, M.K., Ghalandarzadeh, A., 2013. The relationship between clay geotechnical data and clay electrical resistivity. Bollettino di Geofisica Teorica ed Applicata Vol. 54, n. 1, pp. 23-38; March 2013. https://doi.org/10.4430/bgta0070.

Festugato, L., Fourie, A., Consoli, N.C., 2013. Cyclic shear response of fibre-reinforced cemented paste backfill. Géotechnique Letters 3, pp. 5-12. http://dx.doi.org/10.1680/geolett.12.000425

Fredlund, D.G., Morgenstern, N.R., Widger, R.A., 1987. The shear strength of unsaturated soils. Can. Geotech. J. 15(3), pp. 313-321.

Fredlund, D.G., Xin, A., Fredlund, M.D., Barbour, S.L., 1996. The relationship of the unsaturated soil shear strength functions to the soil-water characteristic curve. Can. Geotech. J. 33(3), pp. 440-448.

Galaa, M.A., Thompson, B.D., Grabinsky, M.W., Bawden, W.F., 2011. Characterizing stiffness development in hydrating mine backfill using ultrasonic wave measurements. Canadian Geotechnical Journal 3 August 2011 https://doi.org/10.1139/t11-02.

Gallipoli D., Gens, A., Sharma R., Vaunat J., (2003). An elasto-plastic model for unsaturated soil incorporating the effects of suction and degree of saturation on mechanical behaviour. Géotechnique. Volume 53 Issue 1, February 2003, pp. 123-135. https://doi.org/10.1680/geot.2003.53.1.123.

Gens, A., Nova, R., 1993. Conceptual bases for a constitutive model for bonded soils and weak rocks. International Society for Soil Mechanics and Foundation Engineering; French Committee / International Society for Soil Mechanics and Foundation Engineering; Hellenic Society. Vol. 1-3, 485-494, 1993. ISBN:9054103450, 9054103442.

Goh, S.G., Rahardjo, H., Leong, E.C., 2014. Shear strength of unsaturated soils under multiple drying-wetting cycles. J. Geotech. Geoenviron. 140(2), 06013001.

Griffith, A., 1924. The theory of rupture, in: First Int. Cong. Appl. Mech. pp. 55–63.

Han, W., Lee, J-S., Byun, Y-H., 2020. Volume, strength, and stiffness characteristics of expandable foam grout. Construction and Building Materials 274 (2021) 122013. https://doi.org/10.1016/j.conbuildmat.2020.122013.

Hasanzadeh, A., Shooshpasha, I., 2019. Effects of silica fume on cemented sand using ultrasonic pulse velocity. Journal of Adhesion Science and Technology. https://doi.org/10.1080/01694243.2019.1582890.

Hirasawa, M., Saeki, S., Kodama, S., Yakuwa, T. and Tsuchida, T., 2000. Development of light-weight soil using excavated sand and its application for harbor structures in cold regions, Coastal Geotech. Engrg. in Practice, Proc. of Int. Symp. on Coastal Geotech. Engrg. in Practice, Balkema, 1, 599-604.

Hoek, E., 1988. The Hoek-Brown failure criterion-a 1988 update, in: Proc. 15th Canadian Rock Mech. Symp. Toronto, Dept. Civil Engineering, University of Toronto, pp. 31–38.

Horpibulsuk, S., Shibuya, S., Fuenkajorn, K., Katkan, W., 2007. Assessment of engineering properties of Bangkok clay. Canadian Geotechnical Journal February 2007. https://doi.org/10.1139/t06-101.

Horpibulsuk, S., Liu, M.D., Liyanapathirana, D.S., Suebsuk, J., 2010. Behaviour of cemented clay simulated via the theoretical framework of the Structured Cam Clay model. Comput. Geotech. 37, 1–9. https://doi.org/10.1016/j.compgeo.2009.06.007.

Horpibulsuk, S., Miura, N., Bergado, D.T., 2004. Undrained Shear Behavior of Cement Admixed Clay at High Water Content. J. Geotech. Geoenvironmental Eng. 130, 1236–1249. https://doi.org/10.1061/(ASCE)1090-0241(2004)130.

Horpibulsuk, S., Nagaraj, T.S., Miura, N., 2003. Assessment of strength development in cement-admixed high water content clays with Abrams' law as a basis. Géotechnique 53, 439–444. https://doi.org/10.1680/geot.2003.53.4.439.

Horpibulsuk, S., Phojan, W., Suddeepong, A., Chinkulkijniwat, A., Liu, M.D., 2012a. Strength development in blended cement admixed saline clay. Appl. Clay Sci. 55, 44–52. https://doi.org/10.1016/j.clay.2011.10.003

Horpibulsuk, S., Rachan, R., Suddeepong, A., 2011a. Assessment of strength development in blended cement admixed Bangkok clay. Constr. Build. Mater. 25, 1521–1531. https://doi.org/10.1016/j.conbuildmat.2010.08.006

Horpibulsuk, S., Rachan, R., Suddeepong, A., Chinkulkijniwat, A., 2011b. Strength Development in Cement Admixed Bangkok Clay: Laboratory and Field Investigations. Soils Found. 51, 239–251. https://doi.org/10.3208/sandf.51.239.

Horpibulsuk, S., Rachan, R., Suddeepong, A., Liu, M.D., Du, Y.J., 2013. Compressibility of lightweight cemented clays. Eng. Geol. 159, 59–66. https://doi.org/10.1016/j.enggeo.2013.03.020

Horpibulsuk, S., Suddeepong, A., Chinkulkijniwat, A., Liu, M.D., 2012b. Strength and compressibility of lightweight cemented clays. Appl. Clay Sci. 69, 11–21. https://doi.org/10.1016/j.clay.2012.08.006.

Hossain, S., Kibria, G., Khan, S., 2019. Site Investigation using Resistivity Imaging. Taylor & Francis Group, London, UK.

Jaeger, J.C., Cook, N.G.W., Zimmerman, R.W., 2007. Fundamentals of rock mechanics, 4th edn. Blackwell, Singapore, 475 p.

Jakosky, J.J. 1950. Exploration Geophysics. Trija Pub. Co., Los Angeles, 119.

Jiang, M., Li, T., Cui, Y., Zhu, H., 2017. Mechanical behaviour of artificially cemented clay with open structure: cell and physical model analyses. Engineering Geology 221. https://doi.org/10.1016/j.enggeo.2017.03.002.

Johnston, I.W., 1985. Strength of Intact Geomechanical Materials. J. Geotech. Eng. https://doi.org/10.1061/(ASCE)0733-9410(1985)111:6(730)

Jongpradist, P., Youwai, S., Jaturapitakkul, C., 2011. Effective Void Ratio for Assessing the Mechanical Properties of Cement-Clay Admixtures at High Water Content. J. Geotech. Geoenvironmental Eng. 137, 621–627. https://doi.org/10.1061/(ASCE)GT.1943-5606.0000462.

Kalkan, E., 2011. Impact of wetting-drying cycles on swelling behavior of clayey soils modified by silica fume. Applied Clay Science 52 (2011) 345–352. https://doi.org/10.1016/j.clay.2011.03.014.

Karube, D., Kato, S., 1994. An ideal unsaturated soil and the Bishop's soil. International conference on soil mechanics and foundation engineering. 1994, pp 43-46.

Kavvadas, M., Amorosi, A., 2000. A constitutive model for structured soils. Géotechnique 50(3) : 263-273. https://doi.org/10.1680/geot.2000.50.3.263.

Kibria, G., Hossain, S., 2019. Electrical resistivity of compacted clay minerals. Environmental Geotechnics. Volume 6 Issue 1, February 2019, pp. 18-25. https://doi.org/10.1680/jenge.16.00005.

Kibria, G., Hossain, MS., 2014. Effects of Bentonite Content on Electrical Resistivity of Soils. Geo-Congress 2014 Technical Papers, GSP 234 ASCE 2014.

Kikuchi, Y., Nagatome, T., Mizutani, T.-A., Yoshino, H., 2011. The effect of air foam inclusion on the permeability and absorption properties of light weight soil. Soils Found. 51, 151–165. https://doi.org/10.3208/sandf.51.151

Kikuchi, Y., Nagatome, T., Otani, J., 2006. Visualization of permeability phenomena in lightweight treated soil mixed with air foam using microfocus x-ray CT scanner. GeoCongress 2006 Geotech. Eng. Inf. Technol. Age. https://doi.org/10.1061/40803(187)48.

Kikuchi, Y., Otani, J., Mukunoki, T., Yoshino, H., Nagatome, T., 2005. Permeability of lightweight treated soil mixed with air foam. Issmge2005 1721–1725. https://doi.org/10.3233/978-1-61499-656-9-1721.

ISRM (2007) The Complete ISRM Suggested Methods for Rock Characterization, Testing and Monitoring: 1974–2006. In: R. Ulusay and J.A. Hudson (eds.), Suggested Methods Prepared by the Commission on Testing Methods, International Society for Rock Mechanics, Compilation Arranged by the ISRM Turkish National Group, Ankara.

Lagioia, R., Nova, R., 1995. An experimental and theoretical study of the behaviour of a calcarenite in triaxial compression. Géotechnique. https://doi.org/10.1680/geot.1995.45.4.633.

Lade, P. V., Overton, D.D., 1989. Cementation Effects in Frictional Materials. J. Geotech. Eng. https://doi.org/10.1061/(ASCE)0733-9410(1989)115:10(1373).

Lade, P. V., Trads, N., 2014. The role of cementation in the behaviour of cemented soils. Geotech. Res. https://doi.org/10.1680/gr.14.00011.

Lambe, T.W., 1960. A Mechanistic Picture of Shear Strength in Clay. Res. Conf. on Shear Strength of Cohesive Soils. ASCE. Pp. 555 – 580.

Leroueil, S., Vaughan, P.R., 1990. The general and congruent effects of structure in natural soils and weak rocks. Géotechnique 40, 467–488. https://doi.org/10.1680/geot.1990.40.3.467.

Liu, M.D., Carter, J.P., 2002. A structured Cam Clay model. Can. Geotech. J. 39, 1313–1332. https://doi.org/10.1139/t02-069.

Liu, S.Y., Du, Y.J., Han, L.H., Gu, M.F., 2007. Experimental study on the electrical resistivity of soil-cement admixtures. Environ Geol (2008) 54 :1227–1233. https://doi.org/10.1007/s00254-007-0905-5.

Locat, J., Berube, M., Choquette, M., 1990. Laboratory investigations on the lime stabilization sensitive clays: shear strength development. Can. Geotech. J.

Maâtouk, A., Leroueil, S., La Rochelle, P., 1995. Yielding and Critrical State of a Collapsible Unsaturated Silty Soil, Géotechnique, 45, N0. 3, pp. 465-477.

McClintock, F.A., Walsh, J.B., 1962. Friction on Griffith cracks in rocks under pressure, in: Proc. 4th US Nat. Congr. Appl. Mech. pp. 1015–1022.

Mitchell, J.K., 1981. Soil improvement-state of the art report, in: Proc., 11th Int. Conf. on SMFE. pp. 509–565.

Neramitkornburi, A., Horpibulsuk, S., Shen, S.L., Chinkulkijniwat, A., Arulrajah, A., Disfani, M.M., 2014. Durability against wetting-drying cycles of sustainable Lightweight

Cellular Cemented construction material comprising clay and fly ash wastes. Construct Build Mater, 77 (2015), pp. 41-49. https://doi.org/10.1016/j.conbuildmat.2014.12.025.

Nguyen, L.D., Fatahi, B., Khabbaz, H., 2014. A constitutive model for cemented clays capturing cementation degradation. Int. J. Plast. 56, 1–18 https://doi.org/10.1016/j.ijplas.2014.01.007.

Nova, R., Castellanza, R., Tamagnini C., 2003. A constitutive model for bonded geomaterials subjected to mechanical and/or chemical degradation. https://doi.org/10.1002/nag.294.

Nova, R., 2005. A simple elastoplastic model for soils and soft rocks. Soil Const. Model. https://doi.org/doi:10.1061/40771(169)16.

Nova, R., 1992. Mathematical modelling of natural and engineered geomaterials. General lecture 1st ECSM Munchen. Eur. J. Mech. A/Solids 11, 135–154.

Nova, R., 1988. Sinfonietta classica: an exercise on classical soil modelling. Const. Equations Granul. non-cohesive soils 501–519.

Nowamooz, H., Masrouri, F., 2008. Hydromechanical behaviour of an expansive bentonite/silt mixture in cyclic suction-controlled drying and wetting tests. Engineering Geology 101 (2008) 154–164. https://doi.org/10.1016/j.enggeo.2008.04.011.

Nowamooz, H., Masrouri, F., 2010. Relationships between soil fabric and suction cycles in compacted swelling soils. Engineering Geology 114 (2010) 444–455. https://doi.org/10.1016/j.enggeo.2010.06.005.

Okumura, T., Noda, S., Kitazawa, S., Wada, K., (2000). New ground material made of dredged soil for port and airport reclamation, Coastal Cieotech. Engrg. In Practice, Proc. Of Int. Symp. On Coastal Geotech. Engrg. In Practice, Balkema, 1, 697-702.

Otani, J., Mukonoki, T., Kikuchi, Y., 2002. Visualization for engineering property of in-situ light weight soils with air foams. Soils Found. 42, 93–105. https://doi.org/10.1248/cpb.37.3229.

Pasculli, A., Sciarra, N., Esposito, L., Esposito, A.W., 2017. Effects of wetting and drying cycles on mechanical properties of pyroclastic soils. Catena 156 (2017) 113–123. http://dx.doi.org/10.1016/j.catena.2017.04.004.

Pozdnyakov, A.I., Pozdnyakova, L.A., Karpachevskii, L.O., 2006. Relationship between water tension and electrical resistivity in soils. Eurasian Soil Science, 39(1), 78–83.

Pu, S., Hong, B., Liu, X., Xu, F., Shan, H., 2019. Detection Technology of Foamed Mixture Lightweight Soil Embankment Based on Ultrasonic Wave Transmission Method. Advances in Materials Science and Engineering, vol. 2019, Article ID 9654819, 15 pages. https://doi.org/10.1155/2019/9654819.

Rinaldi, V., Capdevila, J., 2006. Effect of Cement and Saturation on the Stress Strain Behavior of a Silty Clay. Unsaturated Soil Conferences, Arizona, USA (In press) CAREFREE ASCE Vol. 1 pp.1157 -1168.

Rinaldi, V.A., Rocca, R.J., Zeballos, M.E., 2007. Geotechnical characterization and behaviour of Argentinean collapsible loess. T.S. Tan, K.K. Phoon, D.W. Hight, S. Leroueil (Eds.), Characterization and Engineering Properties of Natural Solis, CRC Press, Boca Raton (2007), pp. 2259-2293.

Rotta, G. V., Consoli, N.C., Prietto, P.D.M., Coop, M.R., Graham, J., 2003. Isotropic yielding in an artificially cemented soil cured under stress. Géotechnique 53, 493–501. https://doi.org/10.1680/geot.53.5.493.37508.

Rouainia, M., Muir Wood, D., 2000. A kinematic hardening constitutive model for natural clays with loss of structure. Géotechnique 50, 153–164. https://doi.org/10.1680/geot.2000.50.2.153.

Rummel, F., Van Heerden, W.L., 1978. Suggested methods for determining sound velocity. Int J Rock Mech Min Sci Geomech Abstr 15(2):53–58.

Santamarina, J.C., Klein, K.A., Fam, M.A., 2001. Soil and Waves: Particulate material behaviour, characterization and monitoring. John Wiley and Sons, New York.

Sariosseiri, F., Muhunthan, B., 2009. Effect of cement treatment on geotechnical properties of some Washington State soils. Eng. Geol. https://doi.org/10.1016/j.enggeo.2008.09.003.

Sariosseiri, F., Muhunthan, B., 2008. Interpretation of Geotechnical Properties of Cement Treated Soils, Washington State Department of Transportation.

Sasanian, S., Newson, T.A., 2014. Basic parameters governing the behaviour of cement-treated clays. Soils Found. 54, 209–224. https://doi.org/10.1016/j.sandf.2014.02.011.

Satoh, T., Tsuchida, T., Mitsukori, K., Hong, Z., 2001. Field placing test of lightweight treated soil under seawater in Kumamoto port. Soils Found. 41, 145–154. https://doi.org/10.3208/sandf.41.5_145.

Schnaid, F., Prietto, P.D.M., Consoli, N.C., 2001. Characterization of Cemented Sand in Triaxial Compression. J. Geotech. Geoenvironmental Eng. 0241, 857–868. https://doi.org/10.1061/(ASCE)1090-0241(2001)127:10(857).

Sobhan, K., Das, M., 2007. Durability of Soil-Cements against Fatigue Fracture. Journal of Materials in Civil Engineering, Vol. 19, No. 1, January 1, 2007. ASCE, ISSN 0899-1561/ 2007/1-26–32/$25.00. https://doi.org/10.1061/(ASCE)0899-1561(2007)19:1(26).

Suebsuk, J., Horpibulsuk, S., Liu, M.D., 2011. A critical state model for overconsolidated structured clays. Comput. Geotech. https://doi.org/10.1016/j.compgeo.2011.03.010.

Tang, C-S., Cheng, Q., Leng, T., Shi, B., Zeng, H., Inyang, H.I., 2020. Effects of wetting-drying cycles and desiccation cracks on mechanical behavior of an unsaturated soil. Catena 194 (2020) 104721. https://doi.org/10.1016/j.catena.2020.104721.

Tang, C-S., Wang, D-Y., Shi, B., Li, J., 2016. Effect of wetting-drying cycles on profile mechanical behavior of soils with different initial conditions. Catena 139 (2016) 105–116. http://dx.doi.org/10.1016/j.catena.2015.12.015.

Teerawattanasuk, C., Voottipruex, P., Horpibulsuk, S., 2015. Mix design charts for lightweight cellular cemented Bangkok clay. Appl. Clay Sci. 104, 318–323. https://doi.org/10.1016/j.clay.2014.12.012.

Toll, D.G., Ali Rahman, Z., 2017. Critical state shear strength of an unsaturated artificially cemented sand. Géotechnique, Volume 67 Issue 3, March 2017, pp. 208-215. https://doi.org/10.1680/jgeot.15.P.042.

Tsuchida, T., Egashira, K., 2004. The Lightweight Treated Soil Method: New Geomaterials for Soft Ground Engineering in Coastal Areas. CRC Press-Taylor & Francis Group, London.

Van Nostrand, R.G., Cook, K.L., 1966 Interpretation of resistivity data. Geological Survey, Professional paper; 499. U.S. Govt. Print. Off., Washington, 310.

Verástegui Flores, R.D., Van Impe, W.F., 2009. Stress-strain behavior of artificially cemented Kaolin clay. Proc. 17th Int. Conf. Soil Mech. Geotech. Eng. Acad. Pract. Geotech. Eng. 1, 283–286. https://doi.org/10.3233/978-1-60750-031-5-283.

Vitale, E., Deneele, D., Russo, G., De Sarno, D., Nicotera, M. V., Papa, R., Urciuoli, G. 2020. Chemo-mechanical behaviour of lightweight cemented soils. Acta Geotech. 15, 933–945. https://doi.org/10.1007/s11440-019-00797-8.

Vitale, E., Cuisinier, O., Russo, G., Deneele, D., De Sarno, D., Nicotera M.V., Papa, R., Urciuoli, G., 2020b. Water retention curves of lightweight cemented soils. E3S Web Conf. Volume 195. https://doi.org/10.1051/e3sconf/202019506004.

Wako, T., Tsuchida, T., Matsunaga Y., Hamamoto K., Kishida T., Fukasawa K., 1988. Application of lightweight mixed treated soil construction method to harbour facilities. Journal of Japan Society of Civil Engineers/Volume 1998 (1998) Issue 602. https://doi.org/10.2208/jscej.1998.602_35.

Watabe, Y., Saegusa, H., Shinsha, H., Tsuchida, T., 2011. Ten years follow-up study of airfoam-treated lightweight soil. Proc. Inst. Civ. Eng. Gr. Improv. 164, 189–200. https://doi.org/10.1680/grim.2011.164.3.189.

Watabe, Y., Tanaka, M., Saegusa, H., Shinsha, H., Tsuchida, T., 2009. LongTerm Properties of Airfoam-Treated Lightweight Soil Made from Dredged Clay. J. ASTM Int. 6, 1–10. https://doi.org/10.1520/JAI102134.

Wei, X., Xiao, L., Li, Z., 2012. Prediction of standard compressive strength of cement by the electrical resistivity measurement. Construct. Build. Mater., 31 (2012), pp. 341-346. https://doi.org/10.1016/j.conbuildmat.2011.12.111.

Wheeler, S.J., Karube, D., (1995). Constitutive modeling. State of the Art Report. Proc. 1st Int. Conf. on Unsaturated Soils, Paris, 3, 1323–1356. ISBN: 90-5410-583-6.

Workman, G.L., O Moore, P., 2012. Nondestructive Testing Overview. 594 Pages, Published 2012 by American Society For Nondestructive Testing. ISBN-13: 978-1-57117-187-0, ISBN: 1-57117-187-8.

Ulusay, R., 2014. The ISRM Suggested Methods for Rock Characterization, Testing and Monitoring: 2007-2014.

Yesiller, N., Hanson, J.L., Usmen, M.A., 2000. Ultrasonic Assessment of Stabilized Soils. Soft Ground Technology Conference May 28 - June 2 | Noordwijkerhout, the Netherlands https://doi.org/10.1061/40552(301)14.

Zhang, D-W., Chen, L., Liu, S-Y., 2012. Key parameters controlling electrical resistivity and strength of cement treated soils. J. Cent. South Univ. (2012) 19: 2991−2998. https://doi.org/10.1007/s11771-012-1368-8.

Zhou, M., Wang, J., Cai, L.,Fan, Y., Zheng, Z., 2015. Laboratory Investigations on Factors Affecting Soil Electrical Resistivity and the Measurement. IEEE Transactions on Industry Applications, vol. 51, no. 6, pp. 5358-5365, Nov.-Dec. 2015. https://doi.org/10.1109/TIA.2015.2465931.

3. SOIL, CEMENT AND FOAM

In this chapter a brief description of three components of the lightweight cemented soils is presented. They are soil, cement and foam. In this experimental work the attention was put on clayey soils, but the lightweight cemented soil technology can be adopted for different types of soils, except for the coarse ones that may provoke the segregation phenomenon of the particles to the bulk

3.1. CLAY AND CLAYEY MINERALS

As reported by Grim (1968) clay can be defined as “natural, earthy, fine-grained material which develops plasticity when mixed with a limited amount of water”. In geotechnical field, A.G.I (1963) referred to the term clay as particles with a diameter < 2 μm. Moreover, Andrade et al. (2011) described the plasticity property for a substance as its capacity to preserve the shape under the continuous deformation of a finite force, when it is removed or unless reduced. Clayey minerals are characterized by the presence of silica, alumina, water with percentage of iron, alkalis and alkaline soils.

The clayey minerals with a diameter <2 μm belong to the group of hydrated aluminosilicates (Barton ad Karathanasis, 2002). Martin et al. (1991) reported a nomenclature and classification of clay minerals, suggested by *The Clay Mineral Society* (Table 3-1).

Table 1. Classification of planar hydrous phyllosilicates.

Layer type	Interlayer material[1]	Group	Octahedral character	Species
1:1	None or H_2O only ($x \sim 0$)	Serpentine-kaolin	Trioctahedral	Lizardite, berthierine, amesite, cronstedtite, nepouite, kellyite, fraipontite, brindleyite
			Dioctahedral	Kaolinite, dickite, nacrite, halloysite (planar)
			Di-trioctahedral	Odinite
2:1	None ($x \sim 0$)	Talc-pyrophyllite	Trioctahedral	Talc, willemseite, kerolite, pimelite
			Dioctahedral	Pyrophyllite, ferripyrophyllite
	Hydrated exchangeable cations ($x \sim 0.2$–0.6)	Smectite	Trioctahedral	Saponite, hectorite, sauconite, stevensite, swinefordite
			Dioctahedral	Montmorillonite, beidellite, nontronite, volkonskoite
	Hydrated exchangeable cations ($x \sim 0.6$–0.9)	Vermiculite	Trioctahedral	Trioctahedral vermiculite
			Dioctahedral	Dioctahedral vermiculite
	Non-hydrated monovalent cations ($x \sim 0.6$–1.0)	True (flexible) mica	Trioctahedral	Biotite, phlogopite, lepidolite, etc.
			Dioctahedral	Muscovite, illite, glauconite, celadonite, paragonite, etc.
	Non-hydrated divalent cations ($x \sim 1.8$–2.0)	Brittle mica	Trioctahedral	Clintonite, kinoshitalite, bityite, anandite
			Dioctahedral	Margarite
	Hydroxide sheet (x = variable)	Chlorite	Trioctahedral	Clinochlore, chamosite, pennantite, nimite, baileychlore
			Dioctahedral	Donbassite
			Di-trioctahedral	Cookeite, sudoite
2:1	Regularly interstratified (x = variable)	Variable	Trioctahedral	Corrensite, aliettite, hydrobiotite, kulkeite
			Dioctahedral	Rectorite, tosudite

[1] x is net layer charge per formula unit.

Table 2. Classification of non-planar hydrous phyllosilicates.

Layer type	Modulated component	Linkage configuration	Unit layer, c sin β value	Traditional affiliation	Species
A. Modulated structures					
1:1 layer	Tet. Sheet	Strips	7 Å	Serpentine	Antigorite, bemenitite
		Islands	7 Å	Serpentine	Greenalite, caryopilite, pyrosmalite, manganpyrosmalite, feropyrosmalite, friedelite, mcgillite, schallerite, nelenite
		Other		None	None
2:1 layer	Tet. Sheet	Strips	9.5 Å	Talc	Minnesotaite
			12.5 Å	Mica	Ganophyllite, eggletonite
		Islands	9.6–12.5 Å	Mica/complex	Zussmanite, parsettensite, stilpnomelane, ferrostilpnomelane, ferristilpnomelane, lennilenapeite
		Other	12.3 Å	None	Bannisterite
			14 Å	Chlorite	Gonyerite
	Oct. Sheet	Strips	12.7–13.4 Å	Pyribole	Sepiolite, loughlinite, falcondoite, palygorskite, yofortierite
B. Rolled and spheroidal structures					
1:1 layer	None	Trioctahedral	–	Serpentine	Chrysotile, pecoraite
		Dioctahedral	–	Kaolin	Halloysite (nonplanar)

Table 3-1. Nomenclature and classification of clay minerals, Copyright "The Clay Minerals Society" (Martin et al., 1991).

3.2. CLAY-WATER INTERACTION BEHAVIOUR

Water is strongly correlated to the structure of clay minerals and in some cases is a principal component of the structure for a number of clay minerals. The interaction between water and clay minerals works through the presence of ion-dipole, hydrogen covalent bonding, dipole-dipole interactions, due to the water polarity (Johnston, 2018). The clay minerals surface is characterized by hydroxyl groups and oxygen atoms and there are electrons that can be derived from the replacement of cations of the grid.

It is possible to define the *electrical double layer* where there are the negative electrical layer on the surface of clay particles and the positive electrical layer present in the adsorbed water. A representation of electrical double layer in the simplest model by Helmholtz is presented in Figure 3-1a, as reported by Paunovic and Schlesinger (2006). Together to the Helmholtz model there is Gouy-Chapman model also known as the *diffuse layer model* (Figure 3-1b). The main reasons for the formation of diffuse layer model are the concentration of counter-ions that is higher on the particle surface, lower in the bulk solution and, as a consequence, there is a diffusive force of counter-ions through the bulk solution; the presence of an electrostatic surface repelling force that provokes a leak of ions of the same charge around the layer.

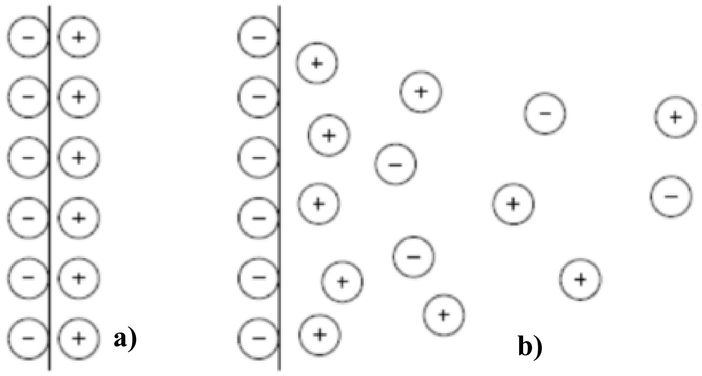

Figure 3-1. Nomenclature and classification of clay minerals, Copyright "The Clay Minerals Society" (Martin et al., 1991).

In the case of the double layer being characterized by adsorption of potential-determining ions the electrical potential Φ can be defined by Nernst equation (3-1):

$$\Phi_0 = \frac{k_B T}{ve} ln\left(\frac{c}{c_0}\right) \Rightarrow c = c_0 exp\left(\frac{ve\Phi_0}{k_B T}\right) \tag{3-1}$$

where k_B is the Boltzmann constant, T is the temperature, c is the concentration of the ions in bulk solution, ve is the valence of ions and c_0 is the concentration of ions at the zero point of charge when Φ = 0, (van Olphen, 1977).

When two particles come into contact with each other, there is a repulsive force between them and work needs to be done to move them together. Nevertheless, there are also attractive forces and the flocculation process proves their existence. These forces are defined as van der Waals forces and they are determined as the sum of all the attractive forces of all atoms constituent in one particle and all atoms of the other particle. The feature of this kind of force is that the sum of all the attractive forces contributes decreases with the increasing distance. If the attractive forces do not depend on solution, repulsive forces depend on ion concentration and valence. As represented in Figure 3-2, there are three different cases to show the behaviour of a suspension, with decreasing ion concentration.

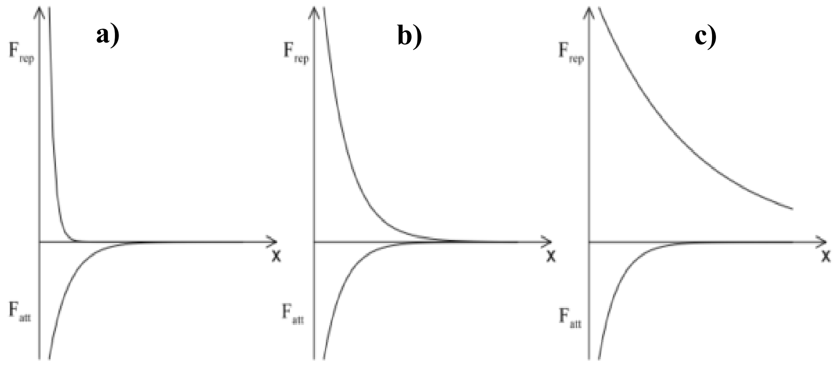

Figure 3-2. Double layer repulsive forces (F_{rep}) and Van der Waals forces (F_{att}) with the distance (De Sarno, 2019).

In case a, the high ion concentration at the contact between two particles determines flocculation, owing to the fact that attractive forces are dominant. The case b is a situation in the middle of the two other cases. In case c, the repulsive forces are dominant and there is no possibility of flocculation (van Olphen, 1977).

In the framework of diffuse double layer, there is also another model that is a combination of Helmholtz and Gouy-Chapman models and it is called Stern model. In fact as stated by Helmholtz, some ions are confined to a little plane near to the particle and others are present in solution, as said by Gouy-Chapman (Paunovic and Schlesinger, 2006).

3.2.1. CLAY PARTICLES ASSOCIATIONS

The flocculation of clay particles determines three different particles associations that depended on the plate-like morphology. It is possible to have Face to Face (FF), Edge to Face (EF) and Edge to Edge (EE) associations. The resulted agglomerates from EF and EE associations are called “flocs”, instead FF association is the “aggregate”; on the other hand, the dissociations of EF and EE is called “deflocculation” and FF separation is a “dispersion”. Explicative images of these clay particles associations is reported in Figure 3-3. The way in which clay particles tended to associate themselves has an effect on the rheological behaviour of clay suspensions.

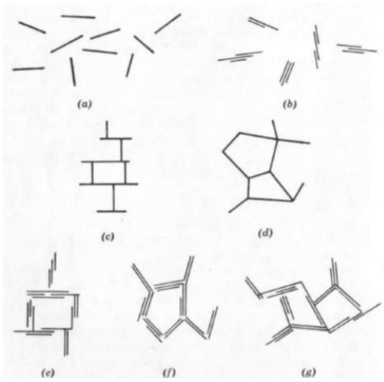

Figure 3-3. Clay particles associations: (a) Deflocculated and dispersed; (b) Deflocculated and aggregated; (c) EF flocculated and dispersed; (d) EE flocculated and dispersed; (e) EF flocculated and aggregated; (f) EE flocculated and aggregated; (g) EE and EF flocculated and aggregated (van Olphen, 1977).

3.2.2. RHEOLOGICAL PROPERTIES AND BEHAVIOUR OF CLAY SUSPENSIONS

The rheological behaviour can be described by the relationship between the shear stress τ and the rate of shear D, measured in sec^{-1}. When the relationship between the two terms is linear, passing through the origin, the fluid to deal with is Newtonian. Viscosity η is the constant of proportionality and it is expressed in Poiseuille (Pl), 1·Pa·sec.

$$\tau = \eta D \tag{3-2}$$

The dilute suspensions behave as Newtonian fluid, on the contrary concentrated suspensions behave as non-Newtonian fluid. It is possible to define a property that is valid only for suspensions dispersed enough and it is the relative viscosity, as the ratio between suspension viscosity η and liquid medium viscosity η_0, called relative viscosity of suspension η_r. As reported by van Olphen (1977), using a theorical relation derived by Einstein, it is possible to correlate the relative viscosity to the concentration of solids by volume C_s, considering a constant $k_{\eta r}$, equal to 2.5 for spheres and with higher value for anisometric particles.

$$\eta_r = 1 + k_{\eta_r} C_s \tag{3-3}$$

Typical examples of non-Newtonian fluids are presented in Figure 3-4. In these kinds of trends in each point it is possible to determine the apparent viscosity τ/D and the differential viscosity dτ/dD. The fluid is dilatant or shear thickening when apparent viscosity and differential viscosity increase with increasing shear stress; while the fluid is shear thinning when they both decrease with shear stress.

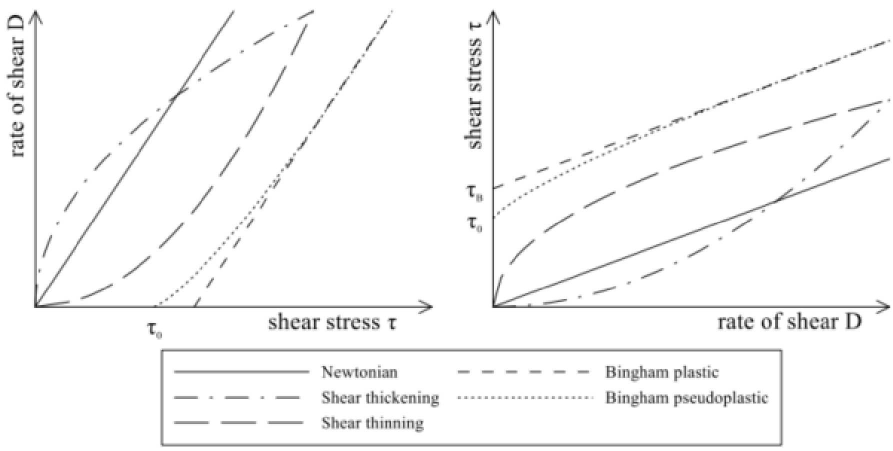

Figure 3-4. Rheological behaviour in laminar flow (De Sarno, 2019).

It is also possible to describe the two behaviours (shear thickening and thinning) by means of a power law model (3-4), characterized by two constants K and n (when $n > 1$ shear thickening, $n < 1$ shear thinning).

$$\tau = KD^n \tag{3-4}$$

Moreover, there is *Bingham pseudoplastic fluid* where it can be defined a threshold shear stress τ_0 (yield stress) and the differential viscosity decreases until a constant value, corresponding to linear τ-D trend. Considering the linear line, but at low shear rates, it can be defined the τ_B ordinate (Bingham yield stress) and the corresponding behaviour is the *Bingham plastic fluid* described by the equation (3-5) as follow:

$$\tau = \tau_B + \eta D \tag{3-5}$$

3.2.3. PROPERTIES OF SOIL SLURRY

In lightweight cemented soils technology the first phase is the soil slurry preparation. It is produced by mixing soil with water: to reach the slurry the sectioned water content is very high, above the soil liquid limit. The properties of soil slurry are independent of the initial condition of soil, due to the dispersion of soil particles in the water to obtain a suspension. In addition, the absence of air implies the absence of the gas phase.

It is possible to define some relationship about the bulk properties of soil slurry.

$$\rho_s = \frac{W_s^s}{V_s^s} \tag{3-6}$$

$$w_s = \frac{W_{ws}}{W_s^s} \tag{3-7}$$

where ρ_s is the density of the soil, W_s^s and V_s^s are the weight and volume of solid soil, while W_{ws} is weight of water in the slurry and w_s is the water content for the slurry.

$$W_{slurry} = (1 + w_s)W_s^s \tag{3-8}$$

Therefore, in absence of gas phase it is possible to define the volume and the unit weight of slurry:

$$V_{slurry} = V_s^s + V_{ws} = \frac{W_s^s}{\rho_s} + \frac{W_{ws}}{\rho_w} = W_s^s\left(\frac{1}{\rho_s} + \frac{w_s}{\rho_w}\right) \tag{3-9}$$

$$\gamma_{slurry} = \frac{W_{slurry}}{V_{slurry}} = \frac{1 + w_s}{\frac{1}{\rho_s} + \frac{w_s}{\rho_w}} \tag{3-10}$$

where ρ_w is the water density.

3.3. CEMENT

Cement is the binding agent used in lightweight cemented soil technology with the aim to gain strength, by the hardening of the fresh paste. As reported by Neville (2001), the patent of Portland Cement is due to Joseph Aspdin in 1824, but it was Isaac Johnson in 1845 that advanced the prototype of the cement that is known nowadays. Portland cement belongs to the category called CEM I and its percentage is more than 95%. CEM II is the category of cements that are a mixture of Portland cement and other materials, for instance fly ash, pozzolana, silica fume furnace slag, limestone. Then there are other cement categories namely CEM III, CEM IV and CEM V and they are characterised by blastfurnace, pozzolanic and composite cements respectively.

Moreover there is a classification based on the value of minimum compressive strength at a specific term of time, that is 28 days. In particular, there are three classes: 32.5, 42.5, 52.5 MPa. In addition, there are sub-classes that depend on the early stage of strengthening; cements characterised by ordinary early strength are *Normal hardening* with letter N, while cements characterised by higher early strength are *Rapid hardening* with letter R.

3.3.1. CHEMICAL COMPOSITION AND HYDRATION REACTIONS

Cements are made up of four different types of components, reported in the list as follows.

- Tricalcium silicate $3CaO{\cdot}SiO_2 \equiv C_3S$
- Dicalcium silicate $2CaO{\cdot}SiO_2 \equiv C_2S$
- Tricalcium aluminate $3CaO{\cdot}Al_2O_3 \equiv C_3A$
- Tetracalcium aluminoferrite $4CaO{\cdot}Al_2O_3{\cdot}Fe_2O_3 \equiv C_4AF$

There is a time during which the cement paste changes its state from fluid to rigid. This process in which cement gains stiffness is called setting. The setting time has a beginning and an end and they are arbitrary, but as suggested by ASTM (2008) they can be determined by

Vicat needle. It is important to make a difference between hardening and setting time: the first one is related to the gain of strength of a set cement paste. Both of them depend on the hydration process of cement compounds C_3S and C_2S and their hydration products. The hydration process is a question of time and its rate depends on the main compounds. For instance, calcium aluminates hydrate faster than calcium silicates, and moreover, tricalcium silicate (C_3S) than dicalcium silicate (C_2S).

Hydration reactions of calcium silicate can be written as follows:

$$2C_3S + 6H \rightarrow C_3S_2H_3 + 3Ca(OH)_2 \tag{3-11}$$

$$2C_2S + 4H \rightarrow C_3S_2H_3 + Ca(OH)_2 \tag{3-12}$$

where $Ca(OH)_2$ is called Portlandite and it is calcium hydroxide, $C_3S_2H_3$ is a lower basicity calcium silicate and it is usually reported as C-S-H gel. It is called gel due to its amorphous nature, even if the electron microscopy referred a crystalline nature. Taylor (1950) described its structure as disordered and made up of fibrous and plate particles like clay minerals.

The reactions of Portlandite with silica and alumina, due to a continuous supply of moisture, determine other hydration products and their name is pozzolanic reactions:

$$Ca(OH)_2 + SiO_2 \rightarrow CSH \tag{3-13}$$

$$Ca(OH)_2 + Al_2O_3 \rightarrow CAH \tag{3-14}$$

Bergado (1996) asserted that the first hydration reactions (3-11, 3-12) are stronger than the second ones (3-13, 3-14); however they always produce a contribution to the bond strength between particles by the presence of more cementing substance.

In the group of hydration reactions there is also the hydration of tricalcium aluminate that is faster than the (3-11, 3-12):

$$C_3A + 6H \rightarrow C_3AH_6 \tag{3-15}$$

This reaction is very impactful due to its exothermic nature thanks to the absence of gypsum; the produced effect is called flash set, that provokes an instantaneous stiffness of the fresh cement paste. On the contrary when gypsum is present in the system, there is a reaction between the tricalcium aluminate with SO_4^{-2} and water: the resulted product is called ettringite (3-16) and it goes to coat C_3A.

$$C_3A + 3CaSO_4 + 32H \rightarrow 3(C_3A \cdot C\bar{S} \cdot 32H) \tag{3-16}$$

It is important to underline that the presence of tricalcium aluminate is relevant only to lower the burning temperature of the clinker and to easily combine silica and lime. Its contribution to the resistance of hardened paste is not so relevant, in particular in the case of attack of sulphates where there is the expansion of ettringite and the breakage of the hardened cement paste.

Finally, there is also a temperature effect on the hydration products as reported by Alarcon-Ruiz et al. (2005).

- From 30 to 105 °C, there is the escape of all the evaporable and part of the bound water. Indeed, 120 °C is the temperature at which all the evaporable water is removed.
- From 110 to 300 °C, there is the loss of water present in the hydration products. In particular, between 110 – 170 °C there is the decomposition of gypsum and ettringite with part of carbo-aluminate hydrates. Between 180 - 300 °C there is the disintegration of the residual part of carbo-aluminate hydrates and of C – S – H.
- From 450 – 550 °C, disintegration of Portlandite occurs.
- From 700 – 900 °C, there the decarbonation of $CaCO_3$.

3.3.2. STRUCTURE OF CEMENT HARDENED PASTE

The cement hardened paste is characterized by a matrix with very small and joint crystals of calcium silicate hydrates (nanometre order of magnitude). They constituent a gel in which other hydration products are immersed (i.e., portlandite, aluminates, alumina-ferrites etc). The nature of the cement paste is highly porous due to the voids left by hydration water and water-filled spaces. Therefore, there are the presence of "capillary pores", in addition also the C – S – H gel matrix is porous (around 28%) and the voids are called in this case "gel pores", with a diameter of 3 nm, instead of capillary pores with a diameter of one or two order of magnitude higher than the previous ones.

It is possible to distinguish three types of water fraction that are present in the cement paste. The first one is called "chemically combined water"; the second one, namely "interlayer or zeolitic water", is retained between the surface of gel sheets; the third one is the "adsorbed water" and it is held by surface forces.

The condition of this water is not free and if the cement sample is sealed cured to avoid the evaporation of water, the components of cement will use the water present in the mix and the water content will decrease. In this case, a "self-desiccation" phenomenon occurs.

3.3.3. EFFECTS OF ALKALIA PRESENCE

Alkalis are minor components but they have an important effect on the cement paste. First of all, they have an effect on the alkalinity of cement paste in terms of pH that is equal to 12.5. Secondarily, they act on the early ages strength of cement paste (i.e., 3 days) even if it tends to diminish in long-term (i.e., 28 days).

Alkalis can also produce an alkali-silicate gel by means of their reaction with aggregates, in particular silica. This kind of gel could be a problem being a plane of weakness in the aggregates, or by coating them, or compromising the structure of cement paste with the alteration of bonds among aggregate surface and cement paste. In addition, alkali-silicate gel has swelling properties under the water imbibition, causing the formations of cracks and disintegration in the hardened paste due to its expansion and internal pressure produced. This type of phenomenon can be avoided by putting pozzolana in the mix, because in this way $Ca(OH)_2$ is eliminated and, as a result Ca^{+2} ions.

3.3.4. RHEOLOGY OF FRESH CEMENT PASTE

Two important concepts in the framework of rheology of cemented paste are the workability and the consistency. The definitions reported by ACI Committee (2008) for these two concepts are the following one: workability is the "property of freshly mixed concrete or mortar that determines the ease with which it can be mixed, placed, consolidated, and finished to a homogeneous condition", consistency is the "degree to which a freshly mixed concrete, mortar, grout, or cement paste resist to deformation". In addition other two properties are related to the rheological features of fresh cement paste: the viscosity and yield.

Taking into account the description of the rheological behaviour of clay suspension in paragraph (3.2.2.), the rheological behaviour of cement paste can be paragoned to that of Bingham fluid, by the Bigham plastic model. The majority of the tests made on the fresh cement paste are able to measure only one factor related to these two properties (i.e., viscosity and yield stress).

As reported by Banfill (1991), the cement paste in fresh state can be seen as a solid particles suspension in water at high concentration; in the early stage its behaviour can be assumed to be that of unreactive silica suspensions, in agreement with Chougnet et al. (2008). The increase of water/cement ratio by weight (w_c/c) determines a high workability, but low yield stress and viscosity.

From the experience of Struble and Sun (1995), it is possible to see that the behaviour of cement fresh paste tends to that of Newtonian fluid in case of dilute suspension and to that of Bingham pseudoplastic in case of concentrate suspension, and so decreasing viscosity with shear stress. The viscosity range of variation observed is between 5 and 0.01 Pl, and it depends on the typology of cement, the parameter w_c/c, strain rate and the presence of additives.

Chougnet et al. (2008) proposed two ranges of viscosity values in relation to w_c/c. The first one is 60 – 0.3 Pl with $w_c/c = 0.3$, the second one is 10 – 0.03 Pl with $w_c/c = 0.5$. As a result, the viscosity decreases as the shear strains increase. Considering the Bingham plastic behaviour, the yield stress value is comprised in the range from 200 – 40 Pa, by increasing the water/cement ratio by weight (w_c/c).

Finally, Banfill (1991) found another range of yield stress and viscosity values: 10 – 100 Pa and 0.01 – 1 Pl, respectively.

3.4. FOAM

It is possible to define foam as a system of dispersed bubbles that are separated by liquid layers. There are two different situations: one is called emulsion, with low gas content and the shape of bubbles is spherical; the other one is the case of gas content higher than 50% and polyhedral bubbles shape.

In addition there are different methods to produce foam, as reported by Ekserova and Krugli͡akov (1998). Condensation method comports the reduction of the external pressure to generate the gas bubbles, thanks to the increasing of temperature or by chemical reactions. Dispersion methods is characterized by the direct injection of gas into the foaming solution by means of capillaries, porous plates and gauzes or by blowing into wetted gauzes surfactant solutions. In other case, there is a flow of solution and gas to create foam, and gas can be pressurized by the use of compressor.

The “Foam Expansion Ratio” (FER), together with the foam dispersity and foam stability, are the fundamental parameters for polyhedral type of foam. The following equation can define the FER, as volume of foam and volume of the liquid content.

$$FER = \frac{V_f}{V_f^l} = \frac{V_f^g + V_f^l}{V_f^l} \tag{3-17}$$

where V_f^g is the volume of gas in foam. FER parameter is the ability of solution to foaming and, as a result, to create foam. By neglecting the weight of gas phase with respect to the weight of liquid phase, the weight of foam can be written as the weight of liquid phase:

$$FER = \frac{V_f}{V_f^l} = \frac{W_f\, \gamma_{sol}}{\gamma_f\, W_f^l} \cong \frac{\gamma_{sol}}{\gamma_f} \tag{3-18}$$

where γ_{sol} and γ_f are the unit weights of solution and foam. The lower the density of foam, the higher is the FER (i.e., it can reach value above 1000). The problem is that when the FER becomes higher the assumption of neglecting the weight of gas phase is no longer valid, and so to estimate the FER other methods should be used.

The other parameter is the foam dispersity and its kinetic of changes is the means to indicate at what rate the bubbles begin to break. The indicators are the bubbles size distribution, the average bubble size or, in addition, the specific foam surface ε can be used. ε is the ratio between total surface area of all liquid – gas interfaces in foam and volume of foam ε_f, the volume of liquid phase ε_l and the volume of gas phase ε_g.

Finally foam stability is defined as the capability of foam to keep the FER and foam dispersity constant during the time. The easier way to measure the stability of the foam is the foam lifetime. Owing to the fact that the foam is not thermodynamically stable because of the increasing interfacial area and interfacial energy, the foam will be destroyed. When the lifetime of foam is about days it is called “metastable”, otherwise when the lifetime is question of seconds the foam is “unstable”.

The key component for producing foam together with water is a surfactant, that is a surface-active agent.

3.4.1. SURFACTANTS CLASSIFICATIONS

The structure of a surfactant molecule is composed of two groups: one is the polar head, with hydrophilic character, the other one is the non – polar tail that is hydrophobic. Figure 3-5 shows the structure of soap, the simplest surfactant which is composed of only one head and one tail. But there are other more complex structures, such as two heads and one tail or one head and two tails etc.

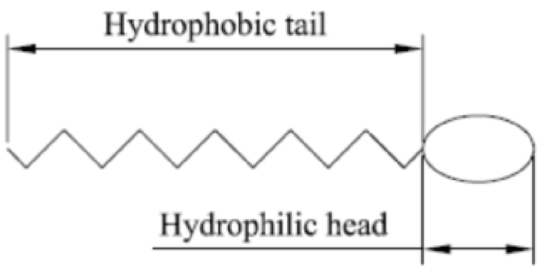

Figure 3-5. An example of surfactant molecule structure (De Sarno, 2019).

The hydrophilic group is at the base of the classification of surfactants, in fact it can be of different natures: anionic, cationic, non – ionic and amphoteric. The anionic and cationic dissociate in water in charged ions negative and positive and the hydrophilic head is negatively charged in the case of anion and positively charged in case of cation. The most common and less expensive are the anionic surfactants. Non – ionic surfactants have no dissociative characteristics in water and also the head is with neutral charge. The last ones, the amphoteric, have all the behaviour together, but it depends on the pH value.

The structure of the hydrophobic tail is characterized by a hydrocarbon chains, that derived from animal fats, vegetable oils or of petrochemical nature.

3.4.2. SURFACE TENSION

The surface tension (γ) is the amount of work (dW) needed to have a unit area expansion (dA). It is a thermodynamic property; for instance, the surface tension for water is equal to 72.8 mN/m at 20 °C.

$$dW = \gamma dA \tag{3-19}$$

As a result of the interactions of different molecules in bulk fluid and at the interface, surface tension is present. Farn (2008) reported that in bulk liquid, the molecules are accumulated of attractive forces in all directions and the resultant force is null; if the gas side is considered, the molecules at the interface are diffused and there are interactions among surface molecules and subsurface liquid molecules. As a consequence, in the last case the resultant force is not equal to zero and the molecules on the surface are characterized by the presence of free energy in excess, that is surface tension.

On the contrary, between two immiscible phases (i.e., A and B) it is possible to define the interfacial tension (γ_{AB}) as the sum of the two separate surface tensions γ_A and γ_B, but minus the interaction energy between them per unit area ψ_{AB}.

$$\gamma_{AB} = \gamma_A + \gamma_B - \psi_{AB} \tag{3-20}$$

Different situations can happen. For example, in the case of similar molecules (water and ethanol) the interfacial tension is very low and the interaction energy is high; in the case of liquid – gas interface, the interfacial tension is equal to the condensed phase (A), due to the fact that the interaction in the gas phase (B) and among A and B is not relevant.

$$\gamma_{AB} = \gamma_A \tag{3-21}$$

Another important feature of the behaviour of the surface tension is its non-linearity trend with surfactant bulk concentration. There is limit concentration value called "Critical Micelle Concentration" (CMC) and when it is overcome the surfactant molecules begin to form aggregates, namely micelles.

3.4.3. EFFECTS OF SURFACTANT IN THE FOAM

Bubbles in foam are present in dispersed mode (image a) in Figure 3-6) and a thin films of liquid, namely lamellae, act as a separation between them. The intersection lines of lamellae make capillaries, known as plateau borders (image b) in Figure 3-6), that all together create a network in the foam. The pressure inside the plateau borders is lower than that in the adjoining lamella and, as a result, the fluid goes through the borders and there is a thinning of the film. The increasing of the thinning determines the increase of the pressure in the lamella. It is owing to the electrostatic and steric repulsion forces among the adsorption layers on the surfaces. This pressure is called disjoining pressure and it increases until the equilibrium and the end of the drainage phase. Image c) in Figure 3-6 shows micelles and other molecules moving in the bulk (in the case of concentration higher than CMC limit value) and surfactant molecules moving in the interface between gas and liquid (in the case of concentration not too low).

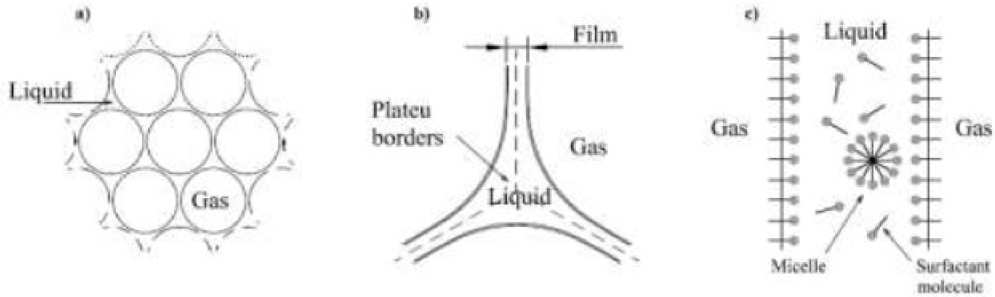

Figure 3-6. Representation of a) bubbles in foam, b) plateau borders, c) foam lamella (De Sarno, 2019).

The phenomenon of liquid drainage from film to the borders causes the stretch of lamella and the diminution of surfactant molecules concentration in the thinner zone. As a consequence, the surface tension in this zone increases a lot with the surface gradient tension along the surface. As reported by Ekserova and Krugliakov (1998) and Farn (2008), thanks to this gradient there is a surfactant mass transfer together to a diffusion of fluid from the bulk to the film surface and, also, a surface flow in the concentration gradient direction. This effect is known as Marangoni effect and it has a stabilising power on the foams. But it is worth to know that it is an advantageous effect in case of compensation via the surface flow and not in the case of molecules diffusion from the bulk.

3.4.4. INTERNAL COLLAPSE AND FOAM DRAINAGE

The stability of foam is governed by two distinct phenomena: foam drainage and internal collapse. The first one is concerned with the losing of liquid volume (ΔV_L) during the time, to re-establish the hydrostatic equilibrium. Foam drainage starts when the foam is created and the liquid begins to move in plateau borders and through them in layers of foam, due to the gravity force. Several equations have been formulated to describe this phenomenon, one example of them is reported by Ekserova and Krugli͡akov (1998) in (3-22).

$$\Delta V_L = \frac{V_{L,0}\tau}{\frac{V_{L,0}}{w_0} + \tau} \tag{3-22}$$

where $V_{L,0}$ and w_0 mean the initial liquid volume in foam and the initial volumetric flow rate in relation to a unit cross-sectional foam area, respectively. There is the dependency of the foam drainage to many parameters, such as FER, viscosity, concentration and type of surfactant etc. When all other parameters being constant, w_0 is inversely proportional to the foam viscosity. Moreover, w_0 is proportional to the square of FER and when the latter increases, at constant dispersity, w_0 decreases due to the thinner radius of plateau borders. In addition, an increase in the concentration of the surfactant provokes a decrease in foam drainage rate, and finally, also the foam dispersity has an effect on the w_0 because of its proportionality to the square of the average radius.

It is possible to define the internal collapse as the separation of liquid and gas that occurs in foam. The internal collapse is due to the diffusion bubble expansion and to the bubble coalescence. In the last case, the coalescence means the fusion of two bubbles because of the breakage of the unstable film that separates them. Instead, the phenomenon of diffusion bubble expansion takes place in polydisperse foams, owing to the different pressure presents between the bubbles of different dimension. What happens is a movement of gas from the smaller bubbles to the bigger ones. In both of the phenomena (i.e., coalescence and diffusion bubble expansion) the specific foam area diminishes.

It is important to underline that the drainage and the internal collapse of the foam have an effect on the general stability of the foam and its lifetime. The natural cause is the intrinsic thermodynamic instability of the system but also external actions could affect the stability of the foam. For example, in lightweight cemented soils technology during the mixing and vibration phases further foam instability may occur.

3.4.5. FOAM BULK PROPERTIES

It is possible to define the weight of foam as follows, considering the weight of gas in bubbles and of residual solid in foam negligible:

$$W_f = W_f^s + W_f^g + W_f^l \cong W_f^l \tag{3-23}$$

In addition, the volume of foam can be expressed as the contribution of the volume of solution V_f^l and the volume of air in bubbles $V_{air,foam}$:

$$V_f = V_f^l + V_{air,foam} = V_f^l + V_f^g \tag{3-24}$$

And from equation (3-24), the expression of volume of air in foam V_f^g can be derived, assuming the density of solution equal to the one of water:

$$V_f^g = V_{air,foam} = V_f - V_f^l = W_f\left(\frac{1}{\gamma_f} - \frac{1}{\rho_{solution}}\right) \approx W_f\left(\frac{1}{\gamma_f} - \frac{1}{\rho_w}\right) \tag{3-25}$$

References

ACI Committee 238, 2008. Report on Measurements of Workability and Rheology of Fresh Concrete.

A.G.I., 1963. Nomenclatura geotecnica e classifica delle terre.

Alarcon-Ruiz, L., Platret, G., Massieu, E., Ehrlacher, A., 2005. The use of thermal analysis in assessing the effect of temperature on a cement paste. Cem. Concr. Res. 35, 609–613. https://doi.org/10.1016/j.cemconres.2004.06.015.

Andrade, F.A., Al-Qureshi, H.A., Hotza, D., 2011. Measuring the plasticity of clays: A review. Appl. Clay Sci. 51, 1-7. https://doi.org/10.1016/j.clay.2010.10.028.

ASTM, C., 2008. 191-08. Standard test methods for time of setting of hydraulic cement by Vicat needle, American Society for Testing and Materials, Annual Book of ASTM Standards. https://doi.org/10.1520/C0191-18.2.

Banfill, P.F.G., 1991. Rheology of Fresh Cement and Concrete. https://doi.org/10.4324/9780203473290.

Barton, C.D., Karathanasis, A.D., 2002. Clay Minerals. Encycl. Soil Sci. 187-192. https://doi.org/10.1081/E-ESS-120001688.

Bergado, D.T., 1996. Soft ground improvement in lowland and other environments. ASCE Press, New York, N.Y.

Chougnet, A., Palermo, T., Audibert, A., Moan, M., 2008. Rheological behaviour of cement and silica suspensions: Particle aggregation modelling. Cem. Concr. Res. 38, 1297–1301. https://doi.org/10.1016/j.cemconres.2008.07.001.

Ekserova, D.R., Kruglia kov, P.M., 1998. Foam and foam films: theory, experiment, application, Studies in interface science. https://doi.org/10.1016/S1383-7303(98)80004-5.

Farn, R.J., 2008. Chemistry and Technology of Surfactants. Wiley

Grim, R.E., 1968. Clay mineralogy, International series in the earth and planetary sciences. McGraw-Hill.

Johnston, C.T., 2018. Clay mineral water interactions. Clay Science, Vol. 9. https://doi.org/10.1016/B978-0-08-102432-4.00004-4.

Martin, R.T., Bailey, S.W., Eberl, D.D., Fanning, D.S., Guggenheim, S., Kodama, H., Pevear, D.R., Środoń, J., Wicks, F.J., 1991. Report of the clay minerals society nomenclature committee: Revised classification of clay materials, Clays and Clay Minerals. https://doi.org/10.1346/CCMN.1991.0390315.

Neville, A.M., 2011. Properties of concrete, 5th ed. Pearson Education Limited.

Paunovic, M., Schlesinger, M., 2006. Fundamentals of Electrochemical Deposition, The ECS Series of Texts and Monographs. Wiley.

Struble, L., Sun, G.K., 1995. Viscosity of Portland cement paste as a function of concentration. Adv. Cem. Based Mater. 2, 62–69. https://doi.org/10.1016/1065-7355(95)90026-8.

Taylor, H.F.W., 1950. Hydrated calcium silicates. Part I. Compound formation at ordinary temperatures. J. Chem. Soc. 3682–3690. https://doi.org/10.1039/JR9500003682.

van Olphen, H., 1977. An introduction to clay colloid chemistry : for clay technologists, geologists, and soil scientists. New York.

4. MATERIALS AND METHODS

In this chapter a description of utilized materials and applied methods is reported. For an extended explanation about the relations between the different components (i.e., amount of soil, cement and foam) of the lightweight cemented soils mixture refer to De Sarno (2019). In fact, the author derived the equations that can be applied to design the mixture, in order to have particular properties that can be correlated to the mechanical strength of the lightweight material. Moreover, from the derived relations, it is possible to fix the precise quantities of soil, cement and foam that are necessary to produce the material, used in construction site. In the following paragraphs, a description of the adopted mix design technique, materials and methods used in this experimental work is presented.

4.1. TREATMENT PARAMETERS DESIGN

The lightweight cemented soil method is characterized by treatment parameters design. The first state parameter defined is water content of slurry, w_s. It indicates the water content for which to prepare the soil slurry. It is strictly related to the liquid limit of the soil w_L; generally it is 1.5 and 3 times w_L.

The amount of water for the grout is called water to cement ratio w_c/c by weight and it is correlated to the cement/soil ratio c/s, also known as cement factor.

In literature, Tsuchida and Egashira (2004) presented an approach characterized by three different mix design parameters: w_s, $m_{c,a}$ (unit amount of cement) and γ (unit weight of material). It is not necessary to determine w_c/c parameter, as stated by the approach, and w_s is fixed taking into account the rheological properties of the soil, by means of a flow test.

$$m_S^S + m_{ws} + m_{c,a} + m_{wc} + m_f = \gamma \tag{4-1}$$

$$\frac{m_S^S}{\rho_S} + \frac{m_{ws}}{\rho_w} + \frac{m_{c,a}}{\rho_{c,a}} + \frac{m_{wc}}{\rho_w} + \frac{m_f}{\gamma_f} = 1 \tag{4-2}$$

Regard to the previous two equations, it is possible to note that the sum of unit amounts (soil, water for slurry, cement, water for cement and foam) is equal to the unit weight of produced material and, in addition, the sum of volumetric amounts is 1. For the authors the range of variations for $m_{c,a}$ is around 90 and 300 kg/m^3; on the contrary, the addition of foam has its effects on the material density and so, as the quantity of foam increases as the density of material decreases.

In this experimental work, two parameters are set at the beginning of the procedure and they are w_s and w_c/c. Then, the other two parameters to fix are the c/s cement factor and n_f, the artificial porosity of the samples thanks to the addition of foam, that corresponds to volume of foam over the volume of material produced:

$$n_f = \frac{V_f}{V} = \frac{W_f}{V\gamma_f} = \frac{m_f}{\gamma_f} \tag{4-3}$$

n_f is only a theoretical value of artificial porosity inside the material. In fact, due to the breakage of the bubbles inside the material due to mixing procedure of foam with soil slurry and grout, the resulting volume of foam will be different and, in particular, lower than the theoretical value.

The actual volume of foam, n_f^* can be calculated as follows:

$$n_f^* = \frac{\gamma_{act} n_f - \Delta_\gamma}{\gamma_{th}} \tag{4-4}$$

where γ_{act} is the actual bulk unit weight, γ_{th} theorical bulk unit weight and $\Delta\gamma$ is the difference between γ_{act} and γ_{th}.

4.2. MATERIALS

The experimental study was carried out on two different types of soil, namely Speswhite Kaolin and Caposele soil. The former is a fine grained soil of industrial production, the latter is natural fine grained soil taken from tunnel excavation in Caposele (Avellino, Italy). Following is reported on the grain size distribution and physical features of both of the soils in Figure 4-1 and Table 4-1.

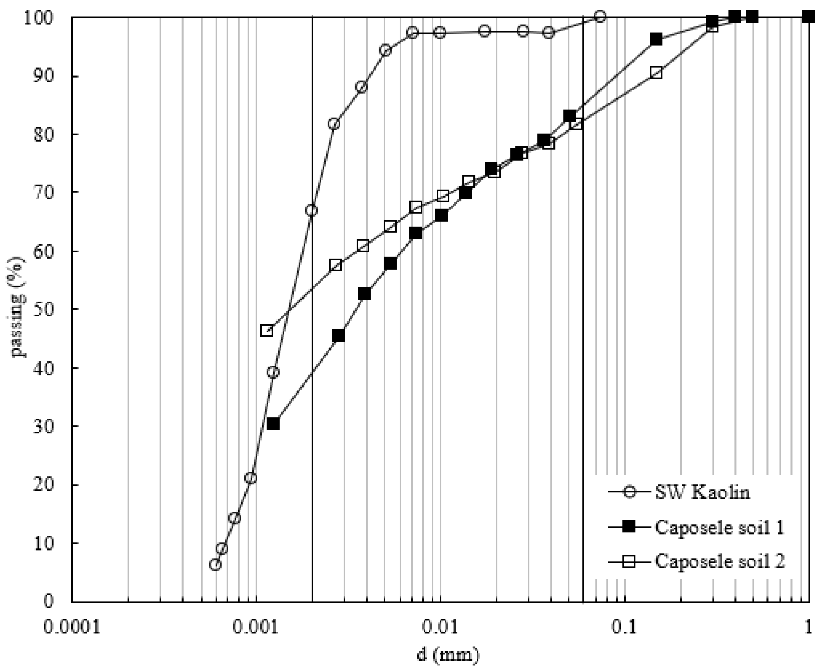

Figure 4-1. Grain size distribution of Speswhite Kaolin, Caposele soil$_1$ and Caposele soil$_2$

Soil	γ_s (kN/m^3)	w_L (%)	w_P(%)	I_P (%)
SW Kaolin	25.9	70	32	38
Caposele soil$_1$	27.5	62	30	32
Caposele soil$_2$	27	73	40	33

Table 4-1. Physical properties of Speswhite Kaolin, Caposele soil$_1$ and Caposele soil$_2$.

The first is Speswhite Kaolin, an artificial clayey silt produced from deposits in the southwest of England by *Imerys Minerals Ltd (UK)*, consisting of kaolinite and muscovite with small amount of quartz, as it can be seen in Figure 4-2 taken from the XRD analysis carried out by De Sarno (2019). The majority part of minerals present in this soil are silica and alumina, in fact they are the characteristic mineral groups of kaolinite and muscovite; in addition, it is possible to find a presence of potassium oxide (K_2O) in muscovite structure. The percentages of the different mineral group are reported in Table 4-2.

The second is Caposele soil and it is a natural clay with silt. In Table 4-1, there is a distinction between Caposele soil$_1$ and Caposele soil$_2$. This is because two different types of Caposele soil from the same excavation site were used during the experimental work. Caposele soil$_1$ refers to the same type of soil also used by De Sarno (2019), while Caposele soil$_2$ refers to the other type used for the preparation of the samples involved in the part of the experimental work on material durability. In both cases (i.e., Caposele soil$_1$ and Caposele soil$_2$), there is presence of quartz and muscovite but, instead of kaolinite, there is calcite. Figure 4-3 reported the XRD analysis results carried out on Caposele soil$_1$ and Caposele soil$_2$.

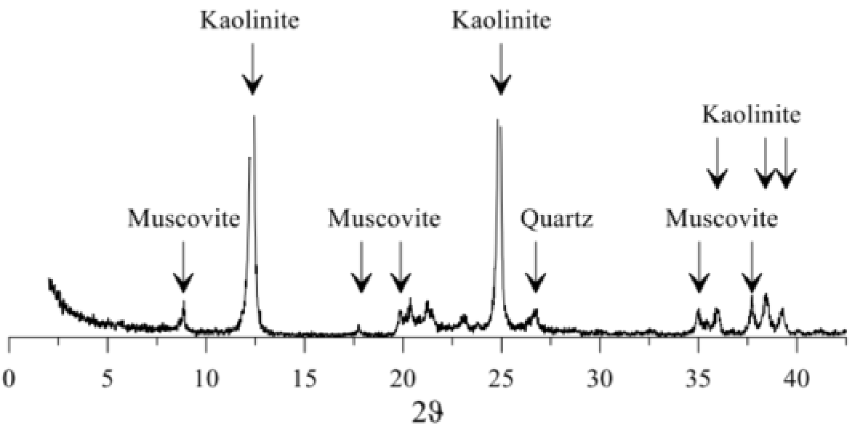

Figure 4-2. Speswhite Kaolin XRD analyses results (De Sarno, 2019).

Group	SiO_2	Al_2O_3	K_2O	Na_2O	TiO_2	CaO
Percentage	53.8	43.75	1.45	0.92	0.05	0.02

Table 4-2. Mineral groups of Speswhite Kaolin (De Sarno, 2019).

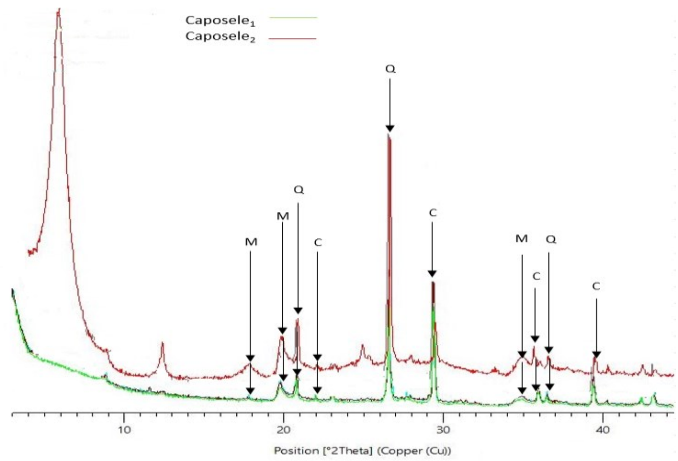

Figure 4-3. Caposele soil$_1$ and Caposele soil$_2$ XRD analyses results M: muscovite, Q: quartz, C: calcite.

4.2.1. SOIL SLURRY

Speswhite Kaolin and Caposele soil slurries were prepared at different water contents of 140%, 124% and 80%, respectively for SW Kaolin, Caposele $soil_1$ and Caposele $soil_2$. In this way, water content for Speswhite Kaolin and Caposele $soil_1$ is 2 times the liquid limit w_L and for Caposele $soil_2$ is 1.1 times it. In the first case (i.e. Speswhite Kaolin and Caposele $soil_1$) the water content value for soil slurry is comprised in the range proposed in literature by other authors (i.e., 1.5 and 3 times w_L); for Caposele $soil_2$ the value of water content for slurry is a bit lower than the range of suggested values in literature, in order to reach the right consistency of slurry, that was impossible to obtain adopting a higher water content.

The viscosity values for the types of slurry were calculated by the following equation:

$$\eta = \left(\frac{9.27}{I_L}\right)^{3.33} \tag{4-5}$$

where I_L is the liquidity index equal to $(w-w_P)/I_P$. The resulting viscosity values are 0.051 Pl for the Speswhite Kaolin, 0.046 Pl for Caposele $soil_1$ and 0.875 Pl for Caposele $soil_2$; they are in agreement with the range of values for the grout reported in paragraph 3.3.4.

4.2.2. CEMENT

The typology of binding agent used for the preparation of all the samples used in the test is Portland cement; in particular, a commercial rapid hardening limestone Portland cement. The exact name with which it is classified is CEM II/A LL 42.5R and it was produced by BUZZI UNICEM spa. The percentages of Calcium Carbonate ($CaCO_3$), Sulphates (SO_3) and Chlorites (Cl^-) are between 6-20%, below 3.5% and 0.08% (standard values are 4% and 0.1% for the last two), respectively. The industrial indications about the unconfined compressive strength are above 25 and 47 MPa after 2 and 28 days (standard values are 20 and 42.5 MPa), respectively. Finally, the initial setting time is more than 2 hours (standard time is at least 60 minutes).

The grout was prepared at a water content to cement ratio (w_c/c) equal to 0.5. Both of the soils were treated at a cement factor (c/s) equal to 0.4.

4.2.3. FOAM

An industrial foam generator, namely GN – 100 AC Bunker (Figure 4-4), was used to prepare the foam to lightweight the samples. It is characterized by a proportional dosing pump to select the requested concentration for the surfactant solution and a foam generator by means of a pump and a compressor to inject air pressure in solution.

For the surfactant, an industrial one called ISOCEM S/L by Isoltech srl was used. Its characteristics are that is liquid, brown, with a specific weight of 10.015 g/l and pH value of 7. It is a mix of anionic and non-ionic surfactants. The requested concentration was 2.5% and the surfactant was diluted with tap water. The density of foam was equal to 75 ± 5 g/l with corresponding FER of 13 ± 1, by means of an air pressure of 3.2 bar.

Figure 4-4. Foam generator GN – 100 AC Bunker (De Sarno, 2019).

Two different values of n_f were fixed for the preparation of the samples, 0.2 and 0.4. The effect of foam was studied by comparing the test results of the samples at those two n_f values with samples only cemented (i.e., n_f equal to 0).

4.2.4. MIX DESIGN PROPORTIONS

In Table 4-3 it is reported a list of the different types of mix prepared for the two kind of soils in this experimental study. The identification of the samples is characterized by a first letter that is K (for the Speswhite Kaolin) and C (for Caposele soil), the second part is CX (where X is the cement factor percentage) and the third part is n_fY (where Y is the n_f percentage). An example of this identification is K_C40%_nf20%, in which Speswhite Kaolin is treated with 40% of cement and lightened with 20% of foam.

Soil	w_s (%)	w_c/c (%)	c/s (%)	n_f (%)	Identification
Speswhite Kaolin	140	50	40	0	K_C40
				20	K_C40_nf20
				40	K_C40_nf40
Caposele soil$_1$	124	50	40	0	C_C40
				20	C_C40_nf20
				40	C_C40_nf40
Caposele soil$_2$	80	50	40	0	C_C40
				20	C_C40_nf20
				40	C_C40_nf40

Table 4-3. Mix design proportions.

4.2.5. SPECIMENS PREPARATION PHASES

The fresh paste was directly poured into the moulds, due to its high workability. To help the procedures of extrusion of the hardened samples, a thin layer of silicone grease was applied on the later walls of the moulds in order to minimize the friction. A schematic diagram of the lightweight cemented soil method is reported in Figure 4-5.

For mechanical tests and non-destructive tests the samples were prepared directly in moulds with the requested dimensions for the specific test, as a result the disturbance on the samples was negligible.

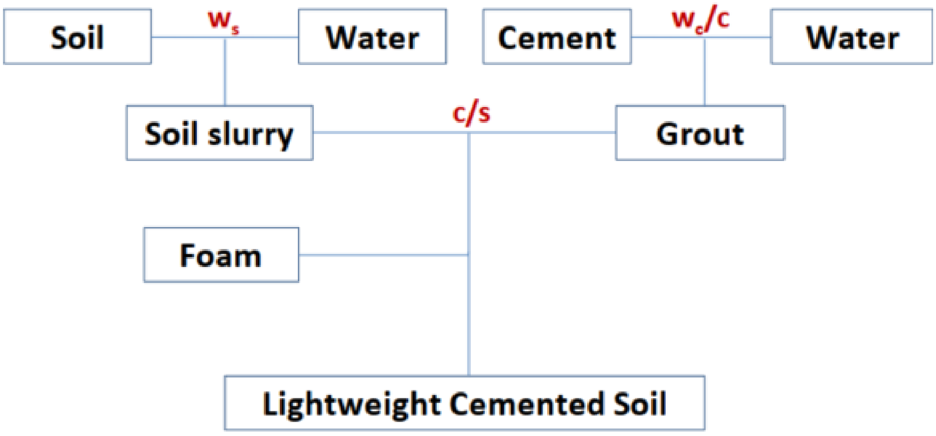

Figure 4-5. Schematic diagram of lightweight cemented soil method (De Sarno, 2019).

The preparation of a lightweight cemented soil sample generally takes place in four distinct phases. In the first phase, the dry soil (W_s) is mixed with water (w_s) in order to obtain the slurry. In the second phase the grout is prepared by mixing anhydrous cement (c/s) with water (w_c/c). In the third phase the grout is added to the slurry and mixed with it until a homogeneous mix is obtained. This procedure is followed in order to obtain a more satisfactory hydration of the cement, which would be more difficult to achieve by directly adding anhydrous cement to the slurry. The fourth phase involves the preparation of the foam and its addition to the previously produced soil-cement-water mixture. The foam is prepared by blowing pressurised air into a solution of water and surfactant. The addition of a suitable quantity of foam makes it possible to regulate the porosity and to obtain a very light material. The phenomenon of setting and hardening of the cement ensures that the air bubbles are fixed in the structure of the material and result in additional voids.

4.3. METHODS

In this section a description of methodology utilized during this experimental study is presented. Different kinds of tests were carried out: mechanical tests (i.e., unconfined compression tests, triaxial tests, torsional shear tests), non-destructive tests (i.e., ultrasonic P-waves and electrical resistivity measurements); as well as wetting-drying cycles procedures and suction measurements. Non-destructive tests were performed at *Laboratorio di Caratterizzazione Lapidei (Stone Characterisation Laboratory), Laboratorio di Geofisica Applicata (Applied Geophysics Laboratory) - Department of Earth, Environmental and Resource Sciences (DiSTAR)* and part of mechanical tests at *Laboratorio di Ingegneria Geotecnica (Geotechnical Engineering Laboratory) – Department of Civil, Building and Environmental Engineering (University of Naples "Federico II").* The other part of mechanical tests, together with wetting-drying cycles procedures and suction measurements, were executed at *Laboratoire Énergies & Mécanique Théorique et Appliquée (LEMTA - University of Lorraine, Nancy-France).*

4.3.1. MECHANICAL TESTS

In this experimental study, unconfined compression tests, triaxial tests and torsional shear tests were executed.

These kinds of tests were carried out for the characterization of the mechanical behaviour of Lightweight cemented soils and for the study of their durability performances.

Unconfined compressive tests were carried out both for the mechanical characterisation of LWCS and during the durability study. For this reason, two different apparatus were used for the tests at *University of Naples "Federico II"* and at *LEMTA (University of Lorraine in Nancy-France)*, respectively. The *Low Pressure Passive Triaxial Cells (GDS Instruments, UK)* and the *2/M – 10 kN MTS ReNew Systems (Materials Testing System* and *MTS Systems Corp, Minneapolis, MN)*, respectively in dotation at *Laboratorio di Ingegneria Geotecnica (Geotechnical Engineering Laboratory, University of Naples "Federico II")* and at *LEMTA (University of Lorraine in Nancy-France)*. The first ones are characterized by a max sample diameter and height of 200 and 400 mm, respectively. The max axial load was 50 kN and by a max pressure ≤ 4 MPa. They are known as passive due to the fact that they are used with an external actuator such as a load frame to apply axial loads. They are shown in Figure 4-6.

Figure 4-6. Low Pressure Passive Triaxial Cells (GDS Instruments, UK), (University of Naples Federico II).

The second one is a compression machine up to an imposed limit load of 10 kN. It is shown in Figure 4-7.

Figure 4-7. 2/M – 10 kN MTS ReNew Systems (Materials Testing System and MTS Systems Corp, Minneapolis, MN), (LEMTA).

The unconfined compression tests at a rate of 1.05 mm/min were carried out according to ASTM D2166. The axial strain and axial normal compressive stress are given by the following relations:

$$\sigma = P/A \tag{4-6}$$

$$\varepsilon = \Delta L/L_0 \tag{4-7}$$

$$A = A_0/(1-\varepsilon) \tag{4-8}$$

where A is the corresponding cross-sectional area (mm^2), A_0 is the initial cross-sectional area of the sample (mm^2), L_0 is the initial length of the test sample (mm), P is the corresponding force (kN), ΔL is the length change of sample (mm), σ is the compressive stress (kPa), ε is the axial strain for the given load. Experimental programmes of unconfined compression tests on both of the two apparatus used are reported in Table 4-4 and Table 4-5.

Soil	c/s (%)	nf (%)	Identification	Curing time (days)	Sample size (mm)	N° of tests
Speswhite Kaolin	40	0	K_C40	3, 7, 14, 28	36x72	12
		20	K_C40_nf 20			12
		40	K_C40_nf 40			12
Caposele Soil	40	0	C_C40	3, 7, 14, 28	36x72	12
		20	C_C40_nf 20			12
		40	C_C40_nf 40			12

Table 4-4. Experimental programme of unconfined compression tests on GDS triaxial cells (University of Naples Federico II).

Soil	c/s (%)	nf (%)	Identification	Environmental load conditions	Sample size (mm)	N° of tests
Speswhite Kaolin	40	0	K_C40	0 w-d 50% RH	36x72	6
		20	K_C40_nf 20	3 w-d 50% RH		6
		40	K_C40_nf 40	3 w-d 90% RH		6
Caposele Soil	40	0	C_C40	0 w-d 50% RH	36x72	4
		20	C_C40_nf 20	3 w-d 90% RH		4
		40	C_C40_nf 40			4

Table 4-5. Experimental programme of unconfined compression tests on 2/M – 10 kN MTS ReNew Systems (LEMTA).

The triaxial tests were carried out in *a Wille Geotechnik stress/path triaxial testing system*, that used a servo-pneumatic loading system for automatic static and cyclic requested loading for different applications. An image of the apparatus is given in Figure 4-8. The maximum axial load is 10 kN, the maximum confining pressure is 2 MPa and for the sample size up to 150 mm. It is equipped with two internal sensors for measuring local deformations. A detailed illustration of circumferential and axial deformation measuring devices is given in Figure 4-9. The triaxial apparatus is also equipped with a single automatic pressure/volume controller (VPC), characterized by fully automatic closed-loop regulation of pressure by an internal high-pressure transducer.

Consolidated drained triaxial tests were carried out at three different confining stresses equal to 50, 100, 150 kPa with a stress rate of 10 kPa/min, adopted for the consolidation phase. The strain rate for the shearing phase was set at 0.1 mm/min. The maximum strain is 20% (for the local axial deformation device is 10%).

Figure 4-8. Wille Geotechnik stress/path triaxial testing system, (LEMTA).

Figure 4-9. Detailed illustration of circumferential and axial deformation measuring devices (Wille Geotechnik web site).

The adopted experimental programme for triaxial tests performed on *Wille Geotechnik stress/path triaxial testing system* is showed in Table 4-6.

In addition, triaxial tests were carried out in a *TXJ*, triaxial compression apparatus coming from *Institute of Industrial Science of University of Tokyo*, supplied by *Laboratorio di Ingegneria Geotecnica (University of Naples, Federico II).*

During the experimental activities, the TXJ was modified by the introduction of a new system to measure the radial strain. In fact, it was not possible to saturate the specimens as it is usual to do during the execution of triaxial tests, due to the presence of the artificial porosity inside the specimens with no linked bubbles. To avoid this problem, an inner cell was introduced coaxial to the specimens and filled with water. When the level of water in the inner cell changes, it can be related to the deformation of the specimens. The differential pressure transducer was employed to measure the difference between the pressure in the inner cell and the one in the reference burette.

To increase the resolution of the radial strain measurements, two different diameters characterized the inner cell: in the upper part the diameter was equal to 60 mm and in the lower part was equal to 90 mm. The part where the water was able to oscillate was equal to 86 mm. The total height of the inner cell was 245 mm.

Moreover, the loading cap and the pedestal were modified. The former became longer (h=120 mm) and the latter lower than the original (h=55 mm). The inner cell and loading cap were realized in aluminium, to avoid water adsorption. The pedestal was done in stainless steel, with a gap along its entire circumference to be able to insert an O-ring to ensure the hydraulic seal. In addition, the inner cell was made up of two separate parts in order to make assembly easier; therefore, external metal ties were also inserted to have even more hydraulic seal.

The average radial strain can be calculated as a function of the total water level variation in the inner cell ΔI_r, as expressed in the following equation by (Aversa and Nicotera, 2002):

$$\varepsilon_r \cong -\frac{1}{2} \cdot \frac{A_b - A_{s0}}{V_{s0}} \cdot \Delta I_r \tag{4-9}$$

where A_b is the cross sectional area of the inner cell of the triaxial apparatus in correspondence with the measuring segment (mm^2), A_{s0} is the initial sample cross section (mm^2), V_{s0} is the initial volume of the sample (mm^3).

Figure 4-10 presents the images of the inner cell open and closed, during the assembly of a test.

Figure 4-10. Details of the inner cell system. On the left, open with specimen inside; on the right, closed.

To calibrate the system a direct way was used by means of the introduction of a precise amounts of water into the inner cell with very precise pipette. That procedure had the aim to directly relate the variation of volume ΔV in equation 4-9 to the output values of the differential pressure transducer. To determine the calibration constant 26 readings were taken. In Figure 4-11 it is reported the graph of the calibration of radial strain system.

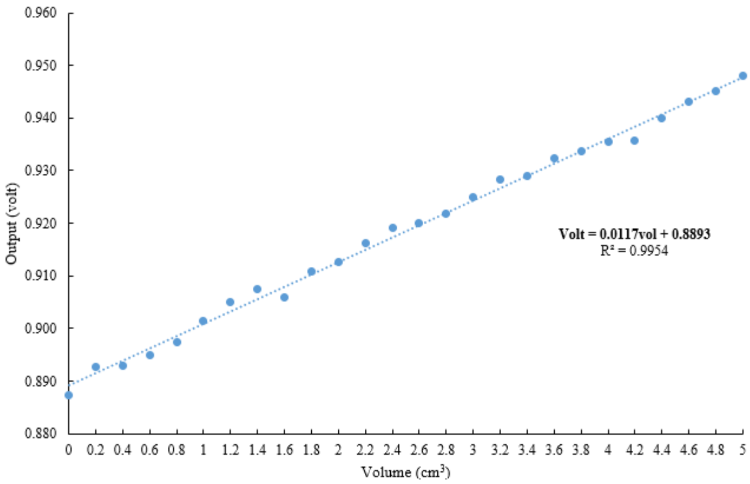

Figure 4-11. Calibration of radial strain measurements system.

Consolidated drained triaxial tests were carried out at three different confining stresses equal to 50, 100, 150 kPa with a stress rate of 10 kPa/min, adopted for the consolidation phase. The strain rate for the shearing phase was set at 6 mm/hr and the maximum strain was 20%.

The adopted experimental programme for triaxial tests performed on TXJ apparatus is shown in Table 4-7.

Soil	c/s (%)	nf (%)	Identification	Confining pressure (kPa)	Environmental load conditions	Sample size (mm)	N° of tests
Speswhite Kaolin	40	20 40	K_C40_nf20 K_C40_nf40	50, 100, 150	3 w-d 50% RH 3 w-d 90% RH	50x100	6 6
Caposele Soil	40	0 20	C_C40 C_C40_nf20	50, 100, 150	3 w-d 90% RH	50x100	3 3

Table 4-6. Experimental programme of triaxial tests on Wille Geotechnik stress/path triaxial testing system (LEMTA).

Soil	c/s (%)	nf (%)	Identification	Confining pressure (kPa)	Sample size (mm)	N° of tests
Speswhite Kaolin	40	0 20 40	K_C40 K_C40_nf 20 K_C40_nf 40	50, 100, 150	50x100	3 3 3
Caposele Soil	40	0 20 40	C_C40 C_C40_nf 20 C_C40_nf 40	50, 100, 150	50x100	3 3 3

Table 4-7. Experimental programme of triaxial tests on TXJ apparatus (University of Naples Federico II).

Finally, torsional shear tests were executed on *THOR cell (Torsional High Output Rig)* provided in *Laboratorio di Ingegneria Geotecnica – University of Naples Federico II* (Figure 4-12). The confinement chamber consists of an aluminium cylinder designed to withstand an operating pressure of 1.5 MPa; moreover, the cell has been equipped with interchangeable pedestals and loading caps to allow tests on specimens of 36, 70 and 100 mm diameter (H/D=2).

The most innovative features of this apparatus are the electromagnetic motor and the amplification system. The former is characterized by eight coils and four magnets that make the motor capable of applying a maximum torque of 5 Nm. The number of coils per coil is 200 and they are capable of withstanding a maximum load of 25 V. The torque application device is powered by a function generator. In addition, there is an amplifier whose task is to convert the voltage signal, sent by the generator, into a high current with the same waveform, which is applied to the coils. It is capable of applying a maximum power of 480 W peak or 320 W continuous, on the load consisting of the 8 coils.

The monitoring system involves the measurement of axial deformations through an LVDT, volumetric deformations with a volume gage, tangential accelerations with a piezoelectric accelerometer, rotations with two pairs of proximity transducers and a torsional load cell. Finally, the instrumental chain consists of programmable function generator, digital voltmeter, digital counter, digital oscilloscope. All these equipment are connected to the switching unit and a personal computer (Figure 4-13).

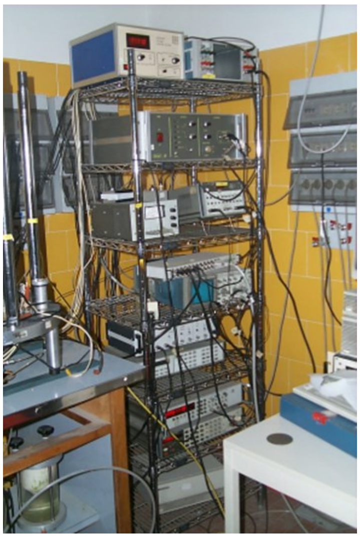

Figure 4-12. THOR apparatus (University of Naples Federico II).

Torsional shear tests were carried out at 100 kPa of confining pressure, frequency of 0.5 Hz and number of cycles equal to 10. The adopted experimental programme for torsional shear tests performed on THOR apparatus is showed in Table 4-8.

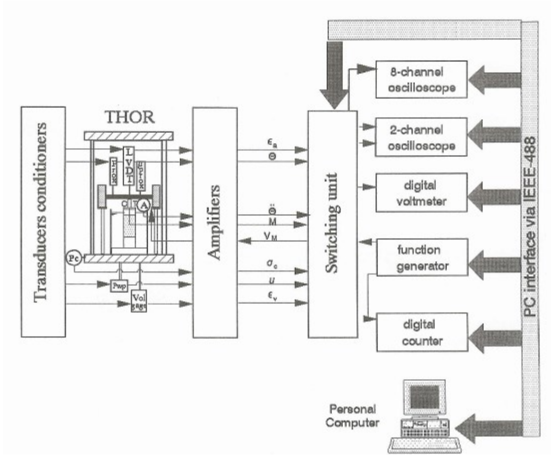

Figure 4-13. THOR equipment scheme (University of Naples Federico II).

Soil	c/s (%)	nf (%)	Identification	Confining pressure (kPa)	Sample size (mm)	N° of tests
Speswhite Kaolin	40	0	K_C40	100	36x72	1
		20	K_C40_nf 20			1
		40	K_C40_nf 40			1

Table 4-8. Experimental programme of torsional shear tests on THOR apparatus (University of Naples Federico II).

4.3.2. NON DESTRUCTIVE TESTS

The experimental activities were carried out at *Laboratorio di Caratterizzazione Lapidei (Stone Characterisation Laboratory)* and at *Laboratorio di Geofisica Applicata (Applied Geophysics Laboratory) - Department of Earth, Environmental and Resource Sciences (DiSTAR), University of Naples Federico II*, respectively for the ultrasonic P-waves velocities and the electrical resistivity measurements.

4.3.2.1. ULTRASONIC TESTS METHOD

Ultrasonic P-wave velocities were recorded using *a BOVIAR DSP UTD 1004 Ultrasonic device* (BOVIAR srl, Naples, Italy), as shown in Figure 4-14. The ultrasonic equipment is capable of measuring the propagation time of compression waves (P-waves) in materials with great accuracy, whether for laboratory measurements on soil, concrete, rock, plastics, fibreglass, wood specimens or for on-site investigations. For the latter, the use of an oscilloscope is necessary in order to avoid in cases of deteriorated materials, poor mechanical quality, and large thicknesses the loss of the signal due to automatic thresholds, set to the intensity level of the signal itself.

The equipment consists of an acquisition control unit equipped with a two-line display, an alpha-numeric keypad, two connectors for connecting the probes and two connectors for the analogue output to allow connection to an oscilloscope (optional) for signal display. The signal is digitised by a bit converter controlled and oversampled by the DSP to achieve resolutions of 0.05 μsec with accuracies of +/- 0.1 μsec.

The instrument has an internal memory for storing the measurement ID and the time read. The probes have their own frequency of 55 kHz and are connected to the control unit via BNC cables. The management software allows automatic calibration of the instrument on the sample provided. The power is provided by four 2300 mAh Ni-Mh 1.2 rechargeable batteries. The transmitter power is adjustable in percentages to avoid signal saturation. The reference standard is UNI-EN 125.

It is equipped with two probes, one of which acts as a P-wave emitter and the other as a receiver. The measurement consists of determining the time it takes for the wave to travel through the material under investigation over the distance between the two probes.

Figure 4-14. The instrument and accessories supplied (BOVIAR Catalogue).

The P-waves velocity (V_P) can be computed by the following equation:

$$V_P = \frac{L}{t_P} \tag{4-10}$$

where L is the travel path length between the two probes and t_P is the travel time of P-waves.

This type of measurement is called direct transmission, in which the direction of propagation of the wave is orthogonal to the faces of the samples on which the probes are positioned, after applying a layer of Propylene Glycol Gel that favours wave transmission at the probe-sample interface and it neutralises the resistance that the air opposes to their propagation.

In the following, it is reported a detailed images sequence of the steps to perform a P-waves velocity measure. Figure 4-15 represents the three stages of probes calibration: a) application of layer Propylene Glycol Gel on one of the probes; b) the distribution of Propylene Glycol Gel on the other one; c) automatic calibration of the instrument on the sample provided by applying a cubic sample to ensure the same pressure on both probes during the measurement phase; in d) the performance of P-waves velocity measurement on a sample, always by applying a cubic sample to ensure the same pressure on both probes during the measurement phase.

Figure 4-15. Calibration of the probes (a,b,c) and measurements of P-waves velocity (d), (University of Naples Federico II).

The P-waves velocity measurements were performed on SW Kaolin and Caposele Soil for both the three types of mix. The curing time was taken in account, since the measurements were made at three, seven, fourteen and twenty-eight days of curing, as it is illustrated in the Table 4-9.

Soil	c/s (%)	nf (%)	Identification	Curing time (days)	Sample size (mm)	N° of tests
Speswhite Kaolin	40	0	K_C40	3, 7, 14, 28	36x72	4
		20	K_C40_nf 20			4
		40	K_C40_nf 40			4
Caposele Soil	40	0	C_C40	3, 7, 14, 28	36x72	4
		20	C_C40_nf 20			4
		40	C_C40_nf 40			4

Table 4-9. Experimental programme of P-waves velocity measurements on Speswhite Kaolin and Caposele Soil.

4.3.2.2. ELECTRICAL RESISTIVITY MEASUREMENTS

Electrical resistivity measurements were carried out using a *Syscal Pro* georesistivity meter from *IRIS Instruments*, available at the *Applied Geophysics Laboratory* of the *Department of Earth Sciences, Environment and Resources - University of Naples Federico II*. The equipment consists of an all-in-one multi-electrode system for electrical resistivity and induced polarisation measurements. The *Syscal Pro* gathers a 10 channel receiver and a 250 W internal transmitter which make it the most powerful system of the Syscal range. It measures both resistivity and chargeability. With a maximal output voltage of $2000V_{pp}$, the *Syscal Pro* is very adapted to detect deep fault in fractured aquifers or to characterize the depths and thickness of the groundwater aquifers. Moreover, for the internal transmitter the current range is between 0 and 2500 mA; for the receiver the resolution/accuracy are: 1μV/0.2%. It is ideal for environmental and civil engineering applications such as monitoring pollution, detecting leaks and monitoring degradation in waste disposal, locating and imaging buried structures and also detecting and characterizing cavities, assessing landslide extension and volume, detecting and locating clayey layers for geotechnical application.

To realise the measurement of electrical resistivity measurement, the georesistivity meter is powered by an external battery. Then, the experimental apparatus is completed by the sample sealed in the orange PVC mold and a balance to monitor its weight, as shown in Figure 4-16.

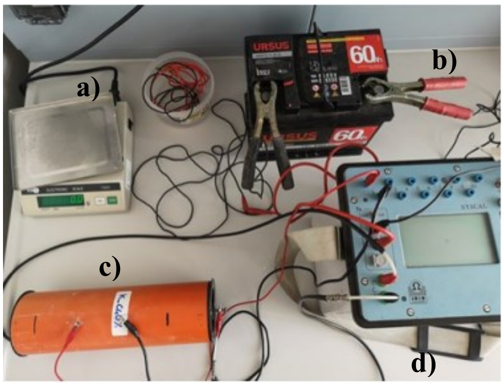

Figure 4-16. Instrumentation for performing electrical resistivity measurement: a) balance; b) battery; c) sample; d) georesistivity meter (University of Naples Federico II).

Four electrodes arranged according to the *Wenner* array are embedded in the soil sample, which involves placing the electrodes in line and equidistant from each other. The two outer electrodes C_1-C_2 are current electrodes, the inner ones P_1-P_2 are potential electrodes, as depicted in the diagram in Figure 4-18.

The instrumentation for performing the electrical resistivity measurement comprises two sections, as illustrated in Figure 4-18: the first one is named *energising* and it is necessary to feed current through electrodes C_1-C_2; the second one is named *receiving* and it serves to measure of the potential difference existing at the voltage electrodes P_1-P_2. The current intensity (I) circulating in the energising system is, by Ohm's law, dependent on the voltage (V) supplied by the georesistivity meter (fixed at 50V) and the resistance R_t of the circuit. The ammeter is connected in series with the energising circuit, and it measures the current intensity circulating in the system. On the other hand, the cables are of the flexible unipolar type with a low ohmic resistance, high insulation and high tensile strength.

The current electrodes used are 10 cm long metal nails, inserted into the sample by penetrating the hermetically sealed plugs at the top and the base of the sample. On the other hand, the voltage electrodes are metal nails 5 cm long. The length of the sample is 20 cm. In Figure 4-17 an image of the samples for electrical resistivity measurements and one of the nails used as current electrode are shown. The measurement of the potential difference at the voltage electrodes depends on the intensity of the current injected, the electrical characteristics of the medium and the distance between the electrodes. In addition, the contact resistance between the potential electrodes and the medium has a big relevance, since a high contact resistance results in a lower measured potential difference value than the actual one.

Figure 4-17. On the left, SW kaolin cemented samples at increasing foam addition. On the right, 10 cm long nail used as a current electrode.

For both types of treated soil (i.e., SW Kaolin and Caposele Soil), three samples were prepared, each of them at a different percentage of added foam (nf=0%, 20% and 40%). For each sample, three measurements were made, and the resistivity measurements were taken over a period of four months. The electrical resistivity measurements were acquired from 24 hours after sample preparation. The details of the experimental programme are reported in Table 4-10.

Soil	**c/s (%)**	**nf (%)**	**Identification**	**Curing time (months)**	**Sample size (mm)**	**Measurements**
SW Kaolin	40	0 20 40	K_C40 K_C40_nf 20 K_C40_nf 40	3	98x200	3 per days
Caposele Soil	40	0 20 40	C_C40 C_C40_nf 20 C_C40_nf 40	3	98x200	3 per days

Table 4-10. Experimental programme of electrical resistivity measurements on SW Kaolin and Caposele Soil.

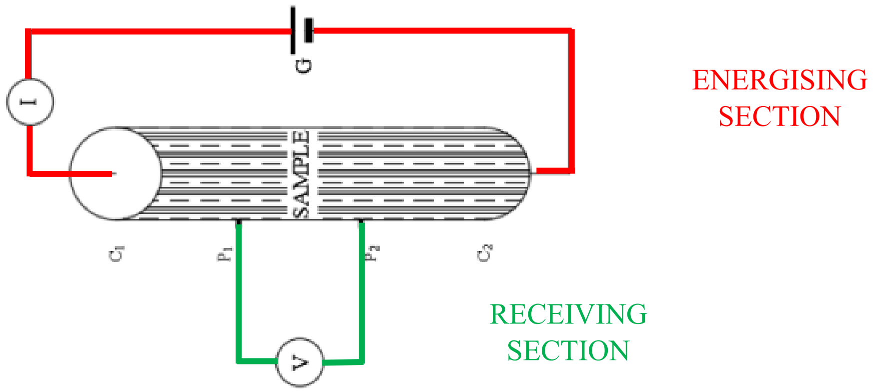

Figure 4-18. Schematic diagram for resistivity measurement.

4.3.3. WETTING AND DRYING CYCLES

The experimental activities were carried out at *Laboratoire Énergies & Mécanique Théorique et Appliquée (LEMTA)*, University of Lorraine in Nancy-France. They were divided into three distinct phases. In the first phase, an initial condition was imposed on all the specimens through a drying phase. In the second phase, the specimens were subjected to wetting and drying cycles. Finally, in the third and final phase, the mechanical tests (i.e., unconfined compression tests and triaxial tests) were performed. Moreover, suction measurements were executed at the end of the mechanical tests to determine the level of suction for the different climatic conditions applied to the samples. It was decided to carry out the suction measurements at the end of the mechanical tests because of the way they were carried out, using the above-mentioned instrument.

In fact, they are performed on part of the soil sample, due to the size of the cup that can be inserted into the instrument for measurement. In order to perform the mechanical test on the sample subject to the wetting-drying cycles, it was not possible to use a part of it to perform the suction measurements before the test was carried out. Nevertheless, the possibility of carrying out the suction measurements before performing the mechanical tests cannot be ruled out, by having a set of samples to be subjected to the same number of w-d cycles, but to be used exclusively for the suction measurements.

The initial phase of drying was carried out completely in the climatic chamber. The equipment used for performing the drying phase was the *Weiss WKL 100/+10 climatic chamber*, with a capacity of 100 litres, temperature range from +10°C to +180°C and relative humidity from 10% to 98%, allowing to simulate various climatic conditions with those temperature and humidity ranges. An image of the climatic chamber is shown in Figure 4-19.

Figure 4-19. Weiss WKL 100/+10 climatic chamber, (LEMTA).

The treated soil samples, after being extruded from their molds, were weighed and measured in terms of height and diameter. Then, they were placed in the climatic chamber and the parameters for the first drying phase were set: a temperature of 20°C and a relative humidity of 50%. The duration of the initial drying was five days: at the end of that phase the samples were weighed again to quantify the loss in weight in terms of water.

The second phase consisted of the execution of wetting-drying cycles. In detail, the wetting-drying cycles were carried out according to two steps. The first one concerned the wetting phase, which was carried out by completely immersing the samples in tap water at a temperature of 20°C for a duration of two days. The second one was the drying phase, which was done in the climatic chamber for a duration of five days, by setting the relative humidity and temperature parameters, as shown in Table 4-11. The duration of a complete cycle was one week.

In particular, two different types of wetting-drying cycles were performed. The first one was characterized by the wetting phase, as previously described, and the drying phase with relative humidity parameter equal to 50% and temperature at 20°C; the number of cycles was three. The second one was equal to the former in terms of wetting phase, temperature value and number of cycles, but it had a relative humidity of 90%.

	Temperature (°C)	RH (%)	Duration (days)	Modality
Wetting	20	-	2	Water immersion
Drying	20	50 90	5	Climatic chamber

Table 4-11. Wetting-drying cycles parameters.

It was decided to carry out the w-d cycles by fixing their number and temperature value, varying the relative humidity parameter between a minimum and a maximum value of 50% and 90%, in order to simulate two different environmental loading conditions.

This made it possible to assess the effect of the application of w-d cycles on the one hand, and the effect of the measured suction value on the mechanical response of the treated material on the other.

The choice of a relative humidity value of 50%, for the first type of w-d cycles, made it possible to compare the results obtained on the tested samples subjected only to the initial condition with the same relative humidity (i.e., 0 w-d_50% RH).

The second type of w-d cycles allowed comparison with the samples subjected to the first type of w-d cycles but varying the relative humidity from 50% to 90%.

With regard to the duration in days of the wetting and drying steps, these were set according to the time it takes for the material to reach an equilibrium condition.

In addition, the water retention curves for LWCS developed by Vitale et al., (2020) were used to verify in which suction range there is a significant change in water content.

4.3.4. SUCTION MEASUREMENTS

The suction measurements were executed by the means of the *WP4C Dewpoint PotentiaMeter*, as shown in Figure 4-20. This instrument uses the chilled-mirror dewpoint technique to measure the water potential of a sample.

In this type of instrument, the sample is equilibrated with the headspace of a sealed chamber that contains a mirror and a means of detecting condensation on the mirror. At equilibrium, the water potential of the air in the chamber is the same as water potential of the sample. In the WP4C, the mirror temperature is precisely controlled by a thermoelectric (Peltier) cooler. Detection of the exact point at which condensation first appears on the mirror is observed with a photoelectric cell. A beam of light is directed onto the mirror and reflected into a photodetector. The photodetector senses the change in reflectance when condensation occurs on the mirror. A thermocouple attached to the mirror then records the temperature at which condensation occurs. Values begin to be displayed indicating that initial measurements are being taken. WP4C then signals by flashing a green LED and/or beeping when final values are reached. The final water potential and temperature of the sample is displayed.

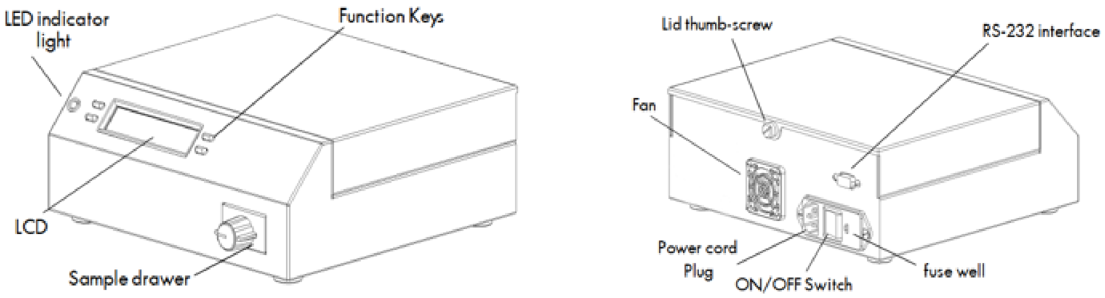

Figure 4-20. Front and back view of WP4C (WP4C Dewpoint PotentiaMeter, Operator's Manual Version 1 2010).

In addition to the technique described above, WP4C uses an internal fan that circulates the air within the samples chamber to reduce time to equilibrium. Since both dewpoint and sample surface temperatures are simultaneously measured, the need for complete thermal equilibrium is eliminated.

The WP4C controls the sample temperature by means of an internal thermo-electrical module that monitors and stabilizes the sample block temperature according to how it is set.

Large temperature differences, between sample and block will cause longer reading times, since a complete and accurate reading will not be made until the difference between the sample temperature and the block temperature is less than 1.0 degree. Before starting a reading, it is important to have cool sample to a temperature slightly below chamber temperature. Owing to this fact, sample is cooled to a set point temperature of 19 °C by using a temperature equilibrium plate instrument.

Stainless-steel cups are used to prepare the samples for suction measurements. In addition, it is possible to oven dry soil samples directly in the stainless-steel cups to determine water content gravimetrically.

The water potential of a solid or liquid sample can be found by relating the sample water potential reading to the vapor pressure of air in equilibrium with the sample. The relationship between the sample's water potential (Ψ) and the vapor pressure of air is in the following equation:

$$\Psi = \frac{RT}{M} \cdot ln \frac{p}{p_0} \tag{4-11}$$

where p is the vapor pressure of the air, p_0 is the saturation vapor pressure at sample temperature, R is the gas constant (8.31 J/mol K), T is the Kelvin temperature of the sample, and M is the molecular mass of water. The vapor pressure of the air can be measured using a chilled mirror, and p_0 is computed from sample temperature.

The WP4C measures water potential by equilibrating the liquid phase water of the samples with the vapor phase water in the headspace of a closed chamber, then measuring the vapor pressure of that headspace. In the WP4C, a sample is placed in a sample cup, which is sealed against a sensor block. Inside the sensor block is a fan, a dew point sensor, and an infrared thermometer. The dew point sensor measures the sample temperature. The purpose of the fan is to speed equilibrium and to control the boundary layer conductance of the dew point sensor.

From these measurements, the vapor pressure of the air in the headspace is computed as the saturation vapor pressure at the dewpoint temperature. When the water potential of the sample and the headspace air are in equilibrium, the measurement of the headspace vapor pressure and samples temperature (from which saturation vapor pressure is calculated) gives the water potential of the sample.

In addition to equilibrium between the liquid phase water in the sample and vapor phase, the internal equilibrium of the sample itself is important. If the sample is not at internal equilibrium, one might measure a steady vapor (over the period of measurement) which is not the true water potential of the sample.

The reading modality used in the suction measurements is the precise mode. In this mode, measurements on a sample are repeated until successive readings agree within a pre-set tolerance (0.03 MPa for Ψ>-40 MPa; otherwise, 0.3 MPa). The reading time is typically 10-15 minutes.

At the end of each mechanical tests, for the three climatic conditions (i.e., drying at 50% of relative humidity, three wetting-drying cycles at 50% of relative humidity and three wetting-drying cycles at 90% of relative humidity) suction measurements were carried out.

References

ASTM D 2166-00. Standard Test Method for Unconfined Compressive Strength of Cohesive Soil. https://doi.org/10.1520/D2166-06.

Aversa, S., Nicotera, M.V., 2002. A Triaxial and Oedometer Apparatus for Testing Unsaturated Soils. Geotechnical Testing Journal, GTJODJ, Vol. 25, No. 1, pp. 3-15. https://doi.org/10.1520/GTJ11075J.

De Sarno, D., 2019. Microstructure and mechanical behaviour of cemented soils lightened by foam. Ph. D. Thesis. University of Naples, Federico II.

WP4C Dewpoint PotentiaMeter, 2010. Operator's Manual Version.

Tsuchida, T., Egashira, K., 2004. The Lightweight Treated Soil Method: New Geomaterials for Soft Ground Engineering in Coastal Areas. CRC Press - Taylor & Francis Group, London.

Vitale, E., Cuisinier, O., Russo, G., Deneele, D., De Sarno, D., Nicotera M.V., Papa, R., Urciuoli, G., 2020. Water retention curves of lightweight cemented soils. E3S Web Conf. Volume 195. https://doi.org/10.1051/e3sconf/202019506004.

5. PHYSICAL AND MECHANICAL PROPERTIES OF LIGHTWEIGHT CEMENTED SOILS

5.1. DESCRIPTION OF THE EXPERIMENTATION PERFORMED

It was stated in the first chapter that this research work is characterized by a first part in which it is proposed a further insight into the chemo-physical and mechanical characterization of the LWCS. In particular, traditional mechanical tests (i.e., unconfined compression tests and torsional shear tests) and the adoption of non-destructive testing methods (i.e., ultrasonic tests and electrical resistivity measurements) made possible to find some correlation relationships in order to assess the properties of the LWCS and to estimate geotechnical parameters, starting from measured quantities. Moreover, these techniques offer the possibility of a quick and non-invasive quality control of the treatment (LWCS method) executed on the soil.

Mechanical and non-destructive tests were executed on lightweight cemented soils and cemented soils (i.e., without the addition of foam) specimens at different curing times, in order to have a more detailed view of the physical characterization and mechanical behaviour, following the works of De Sarno et al., (2019) and Vitale et al., (2020). A description of the tests and the devices is given in Chapter 4 (sections 4.3.1., 4.3.2.1. and 4.3.2.2). Mechanical tests were carried out at *Laboratorio di Ingegneria Geotecnica* (*Geotechnical Engineering Laboratory) – Department of Civil, Building and Environmental Engineering (DICEA), University of Naples Federico II*. The ultrasonic tests and the electrical resistivity measurements were performed at *Stone Characterisation Laboratory* and *Applied Geophysics Laboratory - Department of Earth, Environmental and Resource Sciences (DiSTAR), University of Naples Federico II.*

In what follows, the experimental programme completed is briefly described, while the next sections detail the most significant results obtained for each type of test performed. The interpretation of the results is deferred to the final section of this chapter (section 5.6.).

The experimental investigation was organised as follows:

- **Unconfined compression tests**: they were carried out on both SW Kaolin and Caposele Soil specimens (sections 5.2.1. and 5.4.1.), without foam and at the two different percentages set (i.e., nf 20% and 40%, respectively). They made possible to investigate the effects of the curing time (i.e., 3, 7, 14 and 28 days) and the addition of foam on the unconfined compression strength and stiffness. Table 4-4 (section 4.3.1.) gave an overview of unconfined compression test. For SW Kaolin and Caposele Soil, the characteristics of the samples used in terms of the treatment parameters, the identification of the samples, their dimensions, together with the curing time and the number of tests performed for each type of mixture tested were given.

- **Torsional shear tests**: they were conducted on SW Kaolin specimens (section 5.2.2.), for all of the three mixtures (i.e., nf 20%, 40% and without the addition of foam). Table 4-8 (section 4.3.1) showed the adopted experimental programme about the performed tests. The confining pressure was set at 100 kPa. The tests revealed the evolution of shear modulus G, varying the percentage of foam added to the cemented soil. Moreover, it was possible to examine the effects of foam addition on the linearity threshold in transition from cemented soil to lightweight cemented one (i.e., from K_C40 to K_C40_nf40).

- **P-waves velocity measurements**: they were executed on SW Kaolin and Caposele soil cemented and lightweight cemented specimens (sections 5.3.1. and 5.5.1.). The tests performed at increasing curing time (i.e., 3, 7, 14 and 28 days) put in evidence the development of cement hydration reactions and P-waves velocity values, as function of artificial porosity, highlighted the good treatment performance. Relationships between unconfined compressive strength with P-waves velocity were found, for both the types of soil. Table 4-9 (section 4.3.2.1) reported the experimental programme followed for P-waves velocity measurements.

- **Electrical resistivity measurements**: they were performed on SW Kaolin and Caposele Soil specimens, during a period of three months of acquisition (sections 5.3.2. and 5.5.2.). In both cases, it was possible to see the effect of artificial porosity on the electrical resistivity measurements. Together to P-waves velocity measurements, also this kind of non-destructive tests allowed to assess the properties and the successful treatment of LWCS, due to the effects of the addition of foam and the development of cement hydration reactions on the electrical resistivity trends. Finally, a correlation was found between the unconfined compressive strength and electrical resistivity values. The experimental programme for electrical resistivity measurements was reported in Table 4-10 (section 4.3.2.2.).

5.2. SPESWHITE KAOLIN – MECHANICAL TESTS

5.2.1. UNCONFINED COMPRESSION TESTS

In this section, results of unconfined compression tests are reported. These tests were carried out on cemented SW Kaolin specimens and lightweight cemented SW Kaolin specimens (i.e., nf=20%, 40%).

In Figures 5-1, 5-2 and 5-3 results of the tests performed at increasing curing time are presented for cemented SW Kaolin specimens (i.e., K_C40) and lightweight cemented SW Kaolin specimens (i.e., K_C40_nf20, K_C40_nf40). Tests were conducted at different curing times: 3, 7, 14 and 28 days, comparing the condition of only cemented specimens and the one with the addition of foam, at increasing percentage.

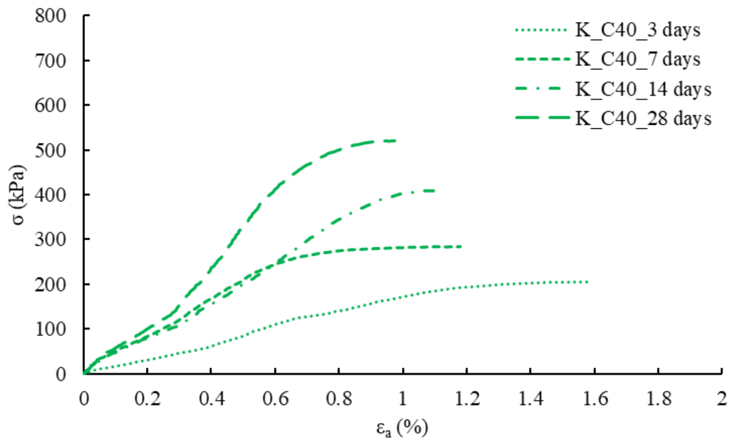

Figure 5-1. Unconfined compression test results on cemented SW Kaolin at increasing curing time.

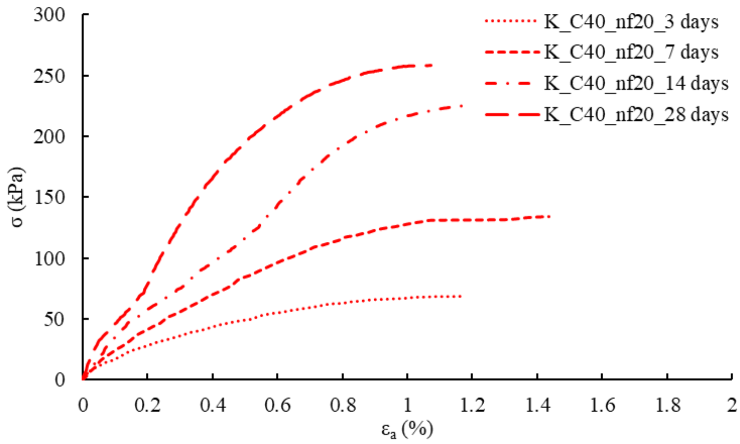

Figure 5-2. Unconfined compression test results on lightweight cemented SW Kaolin with 20% of foam, at increasing curing time.

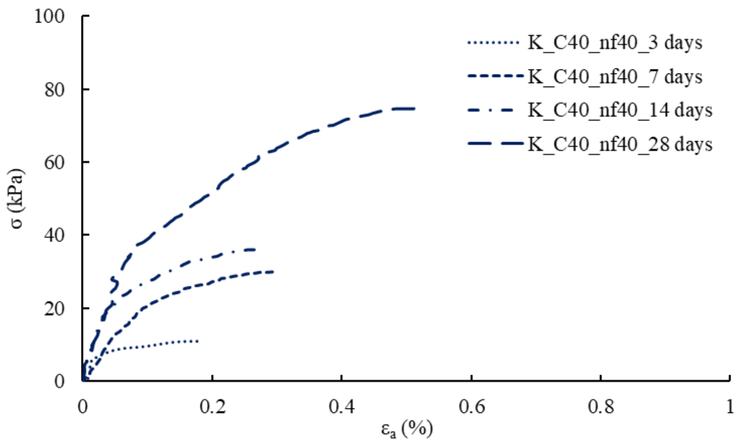

Figure 5-3. Unconfined compression test results on lightweight cemented SW Kaolin with 40% of foam, at increasing curing time.

It has been found that the overall behaviour for the three tested mixtures (i.e., K_C40, K_C40_nf20 and K_C40_nf40) is characterized by an increase in strength and stiffness with increasing curing time. Moreover, it is possible to note that cemented SW Kaolin has a higher strength than the lightweight cemented SW Kaolin, due to the addition of foam.

Considering the stress-strain curves in Figure 5-1 for the cemented SW Kaolin, at increasing curing time the peak strength is achieved at lower deformations. On the contrary, in Figure 5-3 the stress-strain curve for K_C40_nf40 at 28 days of curing time reaches its peak strength at higher deformations than the other curves at lower curing time.

However, the general behaviour shown by the three mixtures during the tests is distinguished by the achievement of the peak strength for cemented SW kaolin in a range of deformations higher than the one for lightweight cemented SW kaolin, at increasing percentage of artificial porosity.

In Figure 5-4 the evolution of the unconfined compressive strength is summarized for the three mixtures tested. It is interesting to see that K_C40 and K_C40_nf20 have the same increasing rate for the UCS from three to fourteen day of curing time; in transition from fourteen to twenty eight days the UCS increasing rate for K_C40 is higher than that one for K_C40_nf20. On the other hand, K_C40_nf40 shows an increment in UCS from three to seven days at a rate higher than that from seven to fourteen days and then increasing again in the transition from fourteen to twenty eight days.

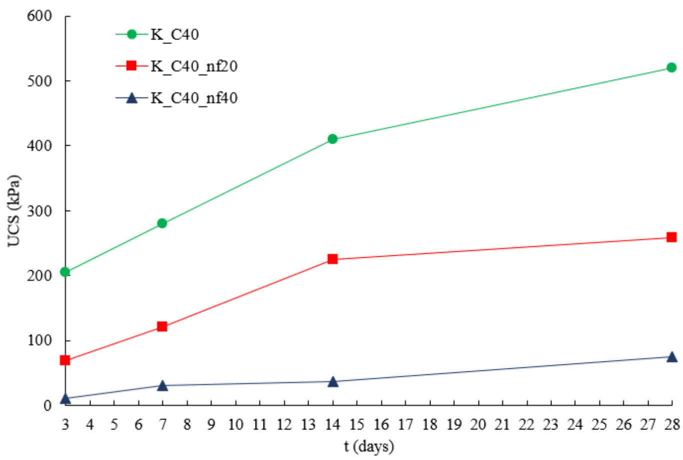

Figure 5-4. Unconfined compressive strength values as function of curing time for K_C40, K_C40_nf20 and K_C40_nf40.

5.2.2. TORSIONAL SHEAR TESTS

In this section, torsional shear test results on cemented SW kaolin and on lightweight cemented SW kaolin are reported. Torsional shear tests were carried out at a confining pressure equal to 100 kPa.

In Figure 5-5 shear modulus-shear strain curves of cemented SW Kaolin and of lightweight cemented SW Kaolin are represented. It is possible to note a decrease in the stiffness of the tested materials in the transition from the cemented soil (i.e., K_C40) to the lightweight cemented soil (i.e., K_C40_nf20, K_C40_nf40).

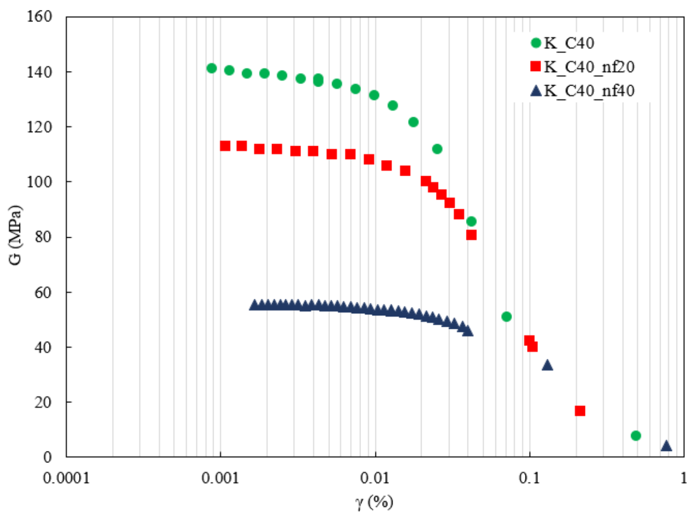

Figure 5-5. Shear modulus - shear strain curves of K_C40, K_C40_nf20, K_C40_nf40, at 100 kPa of confining pressure.

It is interesting to note that the shear moduli G measured from the three tests decrease with increase in shear strain. The rate of decrease is much more pronounced for the cemented SW kaolin mixture (i.e., K_C40) than for the lightweight cemented SW kaolin mixtures (i.e., K_C40_nf20, K_C40_nf40). The maximum values of shear modulus occur at very small shear-strain amplitude, around $\gamma = 0.001\%$. Moreover, an overlap of the shear modulus-shear strain curves is observed for the three tested mixtures at around 0.07% of shear strain.

For the analytical representation of the results the Ramberg-Osgood model was adopted, due to the adherence found with the experimental results. It allows the shear strain to be expressed as a function of the normalised modulus according to the following expression:

$$\gamma = \left(\frac{1 - \frac{G}{G_0}}{C\left(\frac{G}{G_0}\right)^R} \right)^{\frac{1}{R-1}} \tag{5-1}$$

C and R have no physical meaning but identify the position and slope of the decay curve in the plane (G/G_0, γ).

In Figures 5-6 and 5-7, G/G_0 decay curves and damping ratio-strain curves are reported of K_C40, K_C40_nf20 and K_C40_nf40, respectively. In both cases, cemented SW kaolin (i.e., K_C40) and lightweight cemented SW kaolin (i.e., K_C40_nf20, K_C40_nf40), the damping ratio increases with increasing the shear strain.

Starting from the representation of the shear stiffness modulus attenuation curves in normalised form (Figure 5-6), two levels of deformation corresponding to two progressive levels of shear modulus decay were analysed.

A first significant level of deformation is the one that identifies the beginning of non-linearity γ_l. Among the various quantitative methods proposed in the literature for the determination of the non-linearity threshold, the definition suggested by Silvestri (1991) was chosen. He refers to a conventional value of the percentage decrease of G/G_0 (i.e., 5%), which allows for a reliable comparison with other results in the literature and, on the other hand, by locating the threshold at a 5% decay, does not overestimate the non-linearity and, at the same time, allows for a clear appreciation of the attenuation of the curve.

In order to analyse the evolution of non-linearity in more detail as the level of deformation increases, it is useful to refer to a second deformability parameter, representative of the change in modulus as the shear phase progresses from minimum deformations towards failure. In this experimental study, it was chosen to refer to a second level of deformation at a modulus decay of 50%. The reference deformation γ_r was determined and it can be considered significative for the ductility of the material. Then, the ratio γ_r/γ_l was evaluated in order to have a direct measure of the slope of the attenuation curve.

A concise way of analysing the curvature of the function $G/G_0(\gamma)$ is the Ramberg-Osgood parameter R. d'Onofrio et al. (1995) proposed to express R as a function of the ratio γ_r/γ_l:

$$R = \frac{1 + log\frac{\gamma_r}{\gamma_l}}{log\frac{\gamma_r}{\gamma_l} - log\frac{0.95}{0.5}} \tag{5-2}$$

In Table 5-1 the values of initial stiffness (G_0), linearity threshold (γ_l) and reference deformation (γ_r) for the three tested mixtures are reported. Moreover, the ratio γ_r/γ_l and R of Ramber-Osgood are presented.

Mixtures	**G_0 (MPa)**	**γ_l (%)**	**γ_r (%)**	**γ_r/γ_l**	**R**
K_C40	141.2	0.0063	0.1604	25.54	2.13
K_C40_nf20	112.8	0.0091	0.1663	18.22	2.30
K_C40_nf40	55.5	0.0154	0.1587	10.27	2.74

Table 5-1. G_0, γ_l, γ_r, γ_r/γ_l and R values for K_C40, K_C40_nf20 and K_C40_nf40.

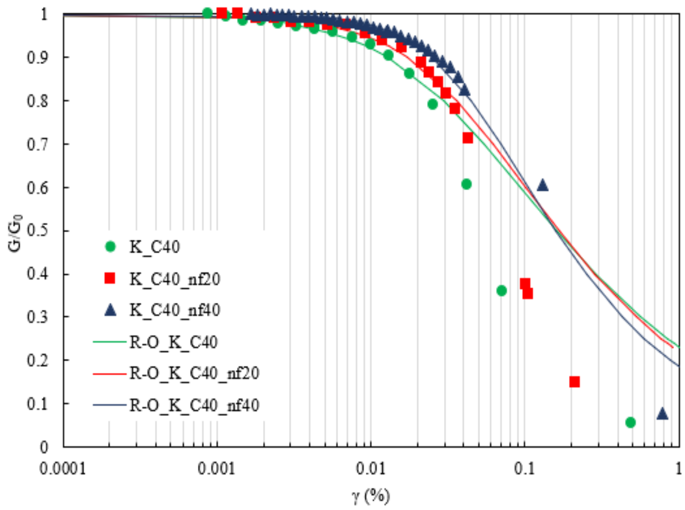

Figure 5-6. Normalised shear modulus curves of K_C40, K_C40_nf20 and K_C40_nf40 at 100 kPa of confining pressure.

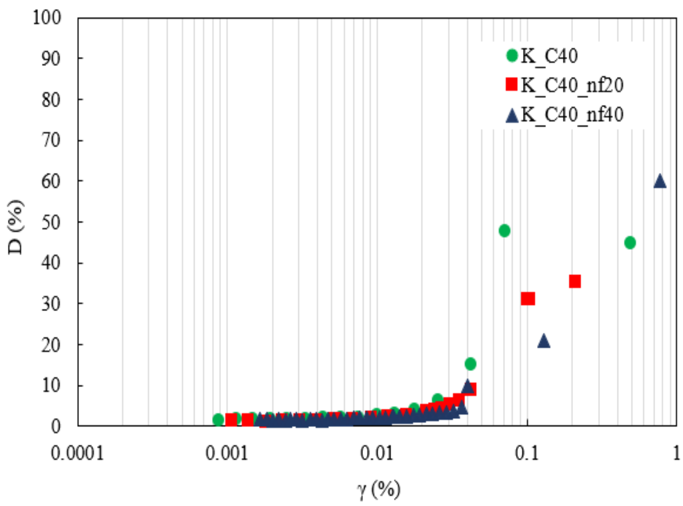

Figure 5-7. Damping ratio- strain curves of K_C40, K_C40_nf20 and K_C40_nf40 at 100 kPa of confining pressure.

From the values reported in Table 5-1 it is possible to observe a decrease in the initial stiffness (G_0) in the passage from K_C40 to K_C40_nf40. It is more evident when the percentage of foam added to the soil-cement-foam goes from nf = 20% to nf =40%. On the contrary, the linearity threshold (γ_l) exhibits an opposite trend, in fact it tends to increase at increasing artificial porosity percentage. The ratio γ_r/γ_l seems to decrease in the transition from a cemented soil to a lightweight cemented soil, while the trend of R parameter is perfectly mirror-image of that obtained for the ratio γ_r/γ_l, as it can be seen in Figure 5-8.

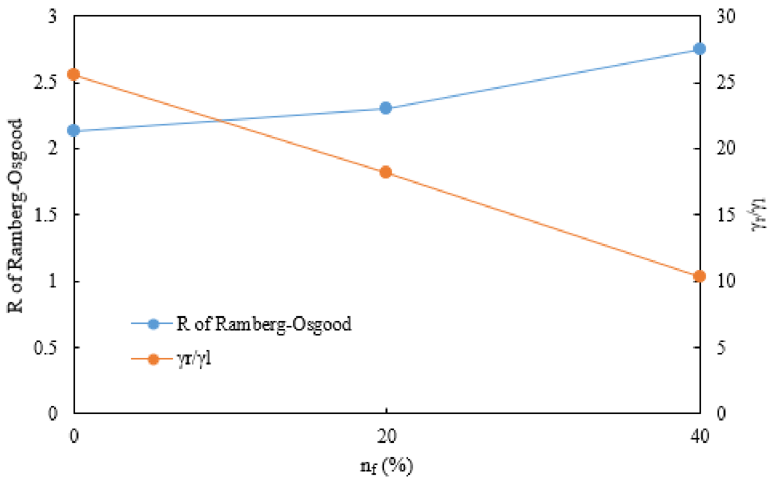

Figure 5-8. Variation of γ_r/γ_l ratio and Ramberg-Osgood parameter R as a function of artificial porosity n_f.

5.3. SPESWHITE KAOLIN – NON DESTRUCTIVE TESTS

5.3.1. COMPRESSION P-WAVES VELOCITY

The trend in P-wave velocity measurements, as the curing time varies and for the different mixtures tested, is shown in Figure 5-9. It can be seen that the measured velocities increase in the transition from 3 to 7 days of curing for all three mixtures considered. Then as time progresses, after 14, 21 and 28 days of curing, the P-wave velocities decrease in the case of the mixture prepared without foam (i.e., K_C40).

The measured velocities continue to increase, even if to a lesser extent than between 3 and 7 days, and tend towards a value which, for longer curing times, is likely to remain unchanged in the case of the two mixtures prepared with foam. The measured P-wave velocities highlight the different nature of the materials tested, in the absence and presence of foam, according to the different values shown in Figure 5-9.

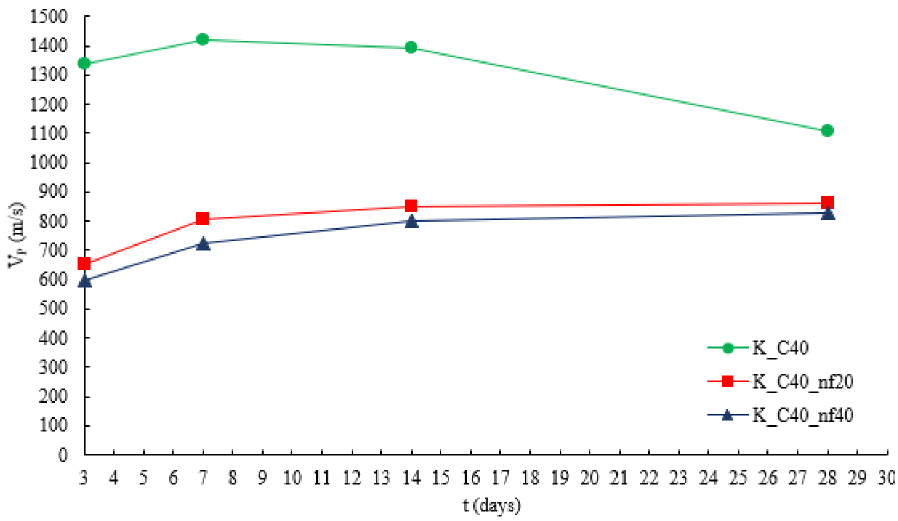

Figure 5-9. P-waves velocity as function of curing time for K_C40,K_C40_nf20, K_C40_nf40.

P-wave velocity values are greater for the cemented soil specimens than those found for the lightweight cemented soil specimens, which is more evident when a greater the amount of foam added. Table 5-2 summarizes the P-wave velocity values as a function of the density of the specimens at different curing times. The velocity of the compression waves is higher in a denser medium, while it decreases in a medium with lower density and increasing artificial porosity .

t (days)	n_f (%)	V_P (m/s)	ρ (kg/m^3)
3	0	1338.6	1372.6
	20	655.0	1109.5
	40	599.7	1025.7
7	0	1417.7	1372.6
	20	807.8	1109.5
	40	725.0	1025.7
14	0	1389.5	1354.6
	20	850.7	1089.2
	40	801.2	1009.7
28	0	1108.4	1332.3
	20	859.2	1069.1
	40	825.3	987.0

Table 5-2. P-waves velocity values as function of density at increasing curing time.

Figure 5-10 plots the P-waves velocity values versus the artificial porosity present in the system. It is possible to observe the decrease in the velocity of compression waves as the percentage of foam added in the specimens increases. There is a good match between the trend of P-waves velocity in Figure 5-10 and the values reported in Table 5-2. In fact, the addition of foam has the aim to lightweight the material with a decrease in its density; as a consequence, it can be seen a decrease in P-waves velocity.

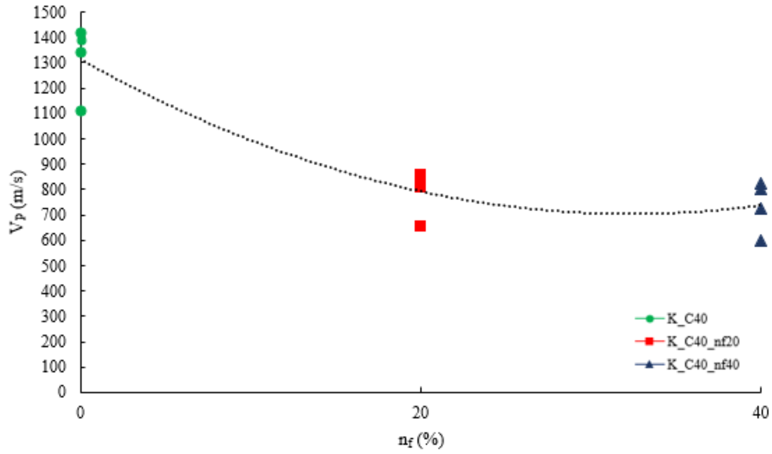

Figure 5-10. P-waves velocity as function of artificial porosity n_f.

However, the ultrasonic velocity tests do not have the chance to acquire information on the strength of the specimens, on which the measurements are carried out. For this reason, it is important to establish a relationship between the P-waves velocity value and the compressive strength, as a results of destructive tests (Hasanzadeh and Shooshpasha, 2019).

As shown in Figure 5-11, the graph suggests that there is a correlation between the compressive strength and the velocity of P-waves. Unconfined compressive strength (UCS) values increase with an increase in the P-waves velocity (V_P). The relationship between UCS and V_P is exponential and its shape is as the following equation:

$$UCS = Ae^{(BV)} \tag{5-3}$$

where UCS is the unconfined compressive strength, A and B are two empirical constants and V stands for the P-waves velocity. In these experimental results, the exponential relationship is as follows in equation 5-4:

$$UCS = 6.5448e^{0.003V_P} \tag{5-4}$$

where A is equal to 6.5448 and B to 0.003.

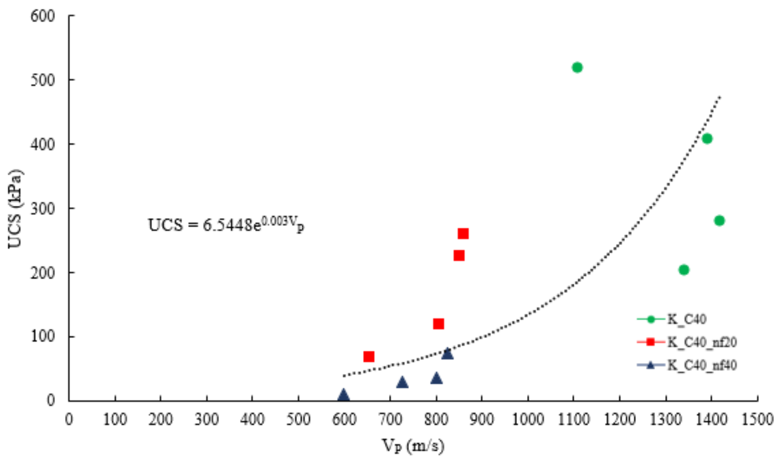

Figure 5-11. Relationship between the P-waves velocity and compressive strength for K_C40, K_C40_nf20, K_C40_nf40.

Moreover, another important feature of non-destructive tests is the possibility to determine average and not punctual values of geotechnical parameters of geomaterials (Lai et al., 2000). Geophysical surveys carried out during geotechnical campaigns are means to have direct information about geotechnical parameters and soil properties (Adewoyin et al., 2017).

5.3.2. ELECTRICAL RESISTIVITY MEASUREMENTS

The trends in electrical resistivity measurements, varying the acquisition time and as a function of the mixtures assessed, are reported in Figure 5-12. It can be seen that the resistivity values increase in the transition from a cemented soil (i.e., K_C40) to a lightweight cemented soil (K_C40_nf20, K_C40_nf40), the more clearly the higher the percentage of foam added to the system.

As shown in the graphs in Figure 5-12, the electrical resistivity curves present a minimum point in the first hours of acquisition to gradually increase as time passes. In the graph SW kaolin exhibits trends characterised by a first linear section up to 6 days of acquisition time, then moving to a second section also linear but with a lower slope up to 33 days and then settling on a constant trend, barring some fluctuations.

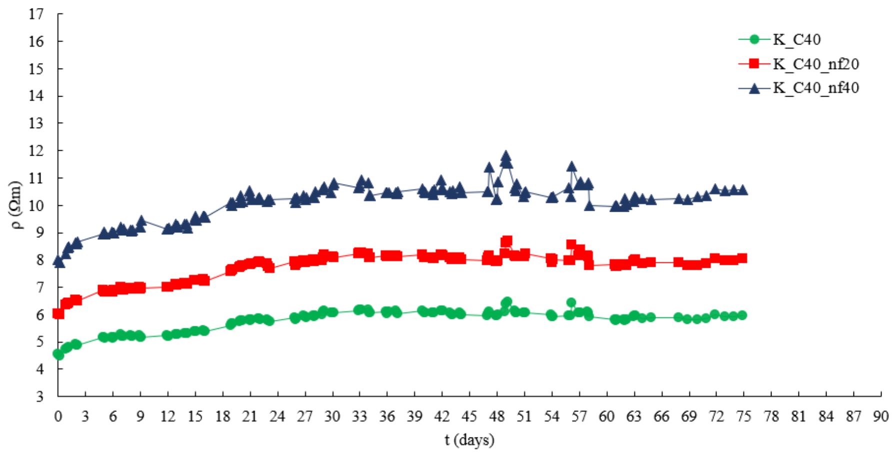

Figure 5-12. Electrical resistivity measurements as function of acquisition time for K_C40, K_C40_nf20 and K_C40_nf40.

It is interesting to correlate the results of unconfined compression tests to the electrical resistivity showed in Figures 5-1, 5-2, 5-3 and 5-12. For a visual representation of the relationship between UCS and ρ, it is possible to refer to Figure 5-13. It can be observed that, given the curing time of the tested mixture, as the artificial porosity increases in terms of percentage of foam added, there is an increase in the electrical resistivity values and in contrast a decrease in the unconfined compressive strength values.

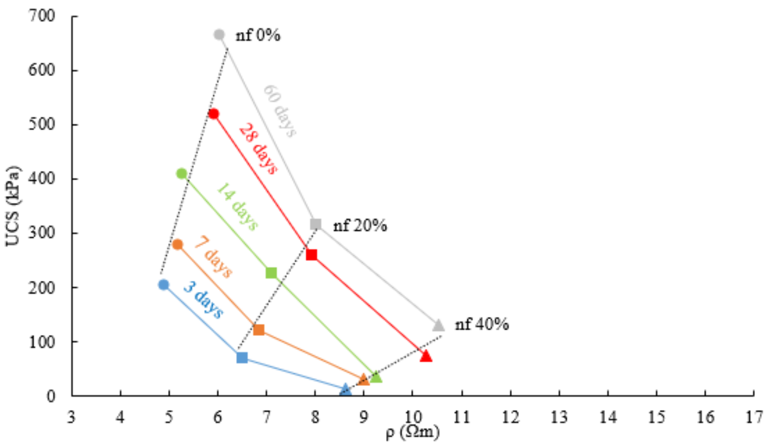

Figure 5-13. Unconfined compressive strength and electrical resistivity measurements correlation for K_C40, K_C40_nf20 and K_C40_nf40.

5.4. CAPOSELE SOIL-MECHANICAL TESTS

5.4.1. UNCONFINED COMPRESSION TESTS

In this section, results of unconfined compression tests are reported, as shown for SW Kaolin. These tests were conducted on cemented Caposele soil specimens and lightweight cemented Caposele soil specimens (i.e., nf=20%, 40%).

In Figures 5-14, 5-15 and 5-16 results of tests performed at increasing curing time are presented for cemented Caposele soil specimens without foam (i.e., K_C40) and with the addition of foam (i.e., K_C40_nf20, K_C40_nf40). Tests were conducted at different curing times: 3, 7, 14 and 28 days, comparing the condition of only cemented specimens and that one of lightweight cemented specimens, at increasing percentage of foam (i.e., 20% and 40%).

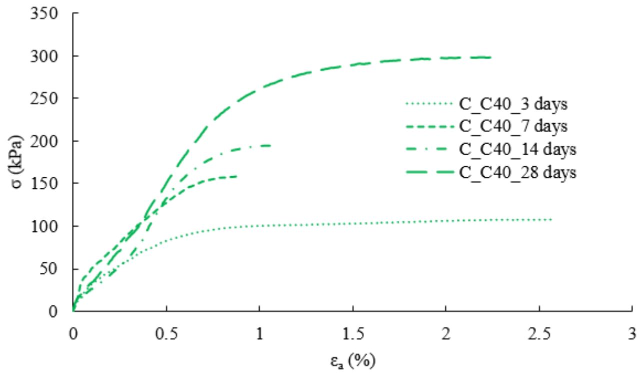

Figure 5-14. Unconfined compression test results on cemented Caposele soil at increasing curing time.

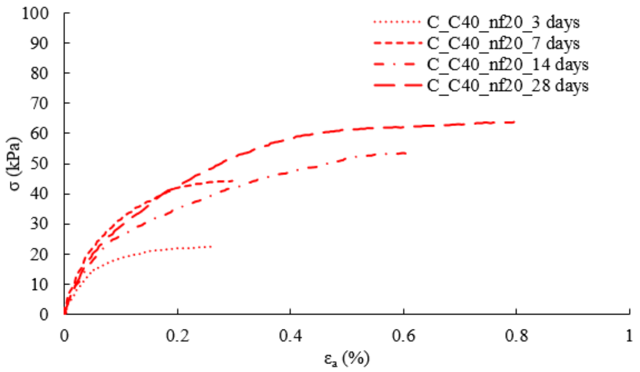

Figure 5-15. Unconfined compression test results on lightweight cemented Caposele soil with 20% of foam at increasing curing time.

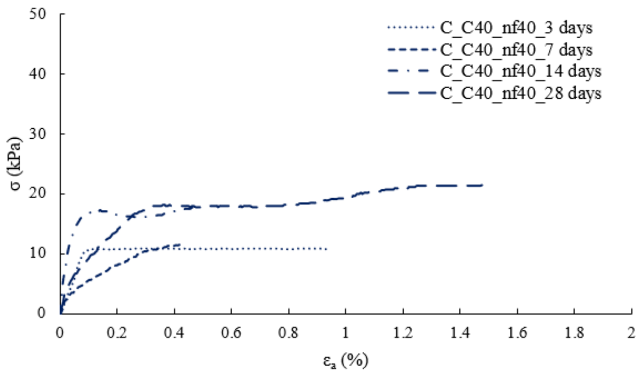

Figure 5-16. Unconfined compression test results on lightweight cemented Caposele soil with 40% of foam, at increasing curing time.

The three tested mixtures (i.e., C_C40, C_C40_nf20 and C_C40_nf40) show a general behaviour characterized by an increase in strength and stiffness at increasing curing time. It is possible to note that cemented Caposele soil has a higher strength than the lightweight cemented Caposele soil, owing to the addition of foam.

In Figure 5-17 the evolution of the unconfined compressive strength is summarized for the three mixtures assessed. Cemented Caposele soil shows an always increasing rate of UCS and it is higher than the ones exhibited by the two mixtures with 20 and 40% of added foam in the system.

It is interesting to see that C_C40 in the transition from three to seven and from fourteen to twenty eight days has the same increasing rate of UCS; on the contrary, it is lower from seven to fourteen days. With regard to C_C40_nf20, in the first seven days of curing the mixtures shows a rate of increase in UCS higher than what it is possible to see in the following days, where the rate is lower. Finally, for C_C40_nf40 the UCS increasing rate is even lower than C_C40_nf20, seeming from 14 to 28 days almost constant trend.

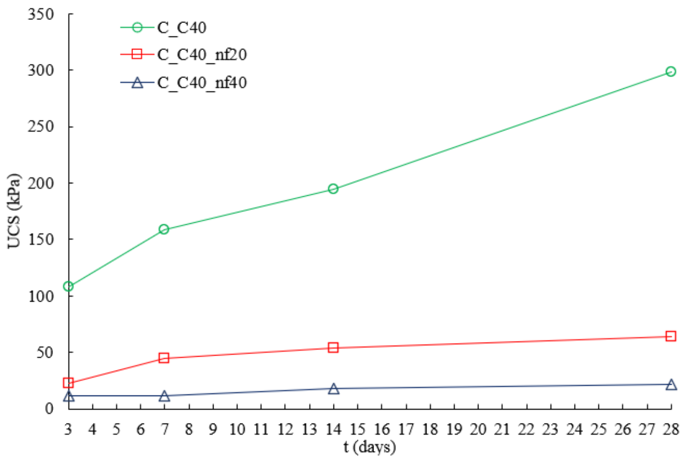

Figure 5-17. Unconfined compressive strength as function of curing time for C_C40, C_C40_nf20 and C_C40_nf40.

5.5. CAPOSELE SOIL – NON-DESTRUCTIVE TESTS

5.5.1. COMPRESSION P-WAVES VELOCITY

The trend in P-wave velocity measurements, as the curing time varies and for the different mixtures assessed, is shown in the graph in Figure 5-18. It can be seen that the measured velocities increase in the transition from 3 to 7 days of curing for all three mixtures considered, even if at a decreasing rate in the transition from cemented Caposele soil to the mixtures at increasing percentage of added foam. After 7 days and until 28 days of curing time, P-waves velocity values tends to increase but at a lower rate than before. This expressed behaviour is almost similar for the three tested mixture.

Nevertheless, it is quite different from the K_C40, K_C40_nf20 and K_C40_nf40 trends shown in Figure 5-9. In fact, after 7 days of curing time in Caposele soil case, the P-waves velocity values tend to increase; whereas for K_C40, the velocity values tend to a progressive decrement and for K_C40_nf20 and K_C40_nf 40 to reach a constant value.

The measured P-wave velocities highlight the different nature of the materials tested, in the absence and presence of foam, according to the different values shown in Figure 5-18, also in the case of Caposele soil.

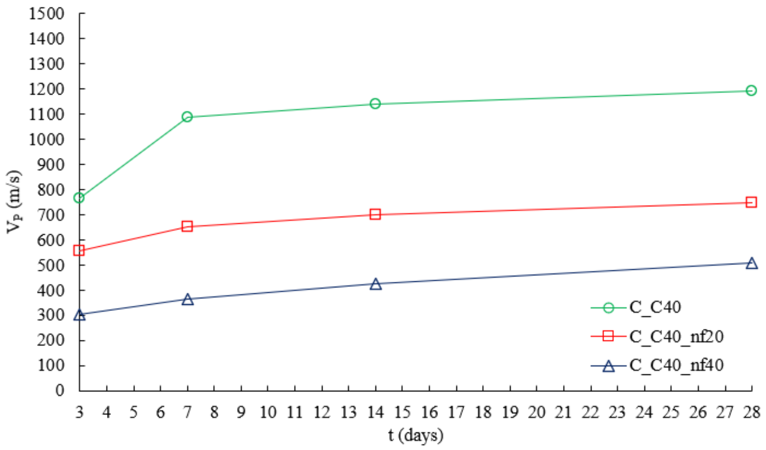

Figure 5-18. P-waves velocity as function of curing time for C_C40, C_C40_nf20 and C_C40_nf40.

P-wave velocity values confirm what was observed in the case of SW Kaolin. In fact, the greater the amount of foam added to cemented soil the lower the P-waves velocity values measured. Table 5-3 reports the P-wave velocity values as a function of the density of the specimens at different curing times. The velocity of the compression waves is higher in a denser medium, while it decreases in a medium with lower density and increasing artificial porosity .

t (days)	n_f (%)	V_P (m/s)	ρ (kg/m³)
3	0	765.83	1433.92
	20	557.09	1315.62
	40	303.03	1112.68
7	0	1088.75	1434.46
	20	650.26	1318.99
	40	364.71	982.79
14	0	1016.36	1435.78
	20	567.46	1321.57
	40	426.28	984.02
28	0	1190.50	1423.76
	20	748.62	1308.77
	40	508.93	958.21

Table 5-3. P-waves velocity as function of density for C_C40, C_C40_nf20 and C_C40_nf40.

Another way to visualize the dependency of P-waves velocity to the density of specimens is to put in relation the compression P-waves velocity to the parameter n_f, which express the percentage of foam added to the soil and hence the artificial porosity introduced to the system, as it can be seen in Figure 5-19. Values reported in Table 5-3 are in good agreement with the trend of P-waves velocity in Figure 5-19. In fact, the addition of foam lighted the cemented soil with a decrease in its density; as a consequence, it can be seen a decrease in P-waves velocity.

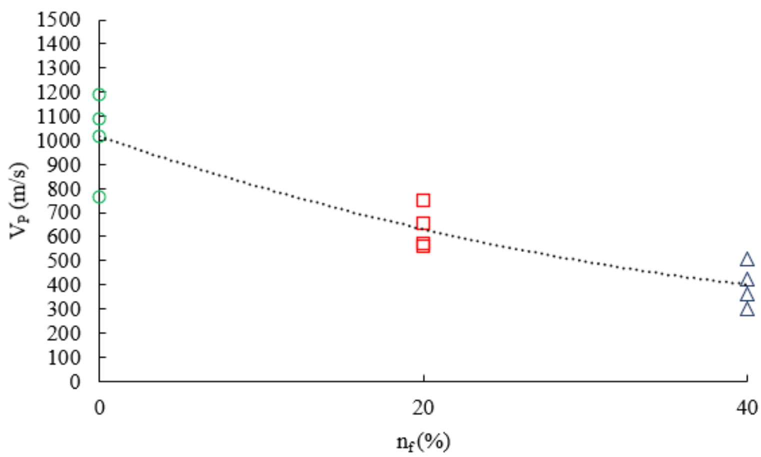

Figure 5-19. P-waves velocity as function of artificial porosity n_f.

Also for Caposele soil, it is established a relationship between the P-waves velocity value and the compressive strength, as results of destructive and non-destructive tests.

In Figure 5-20, the diagram suggests that there is a correlation between the compressive strength and the velocity of P-waves. Unconfined compressive strength (UCS) values increase with an increase in the P-waves velocity (V_P). The relationship between UCS and V_P is exponential and its equation is as follow:

$$UCS = 3.6999e^{0.0038V_P} \tag{5-5}$$

where the two empirical constants are A equal to 3.6999 and B to 0.0038. Compared to the results obtained for SW Kaolin mixtures, it seems that for Caposele soil mixtures there is lower data scattering in the correlation between UCS and V_P. In fact, the coefficient of determination R^2 in case of SW Kaolin is equal to 0.3637, whereas for Caposele soil is 0.9337.

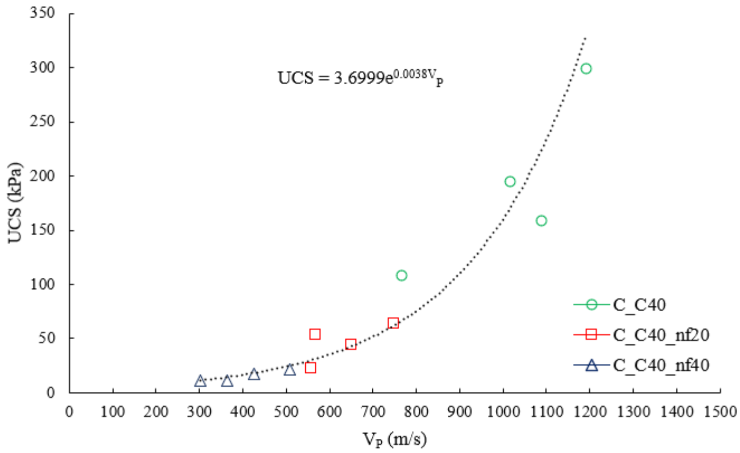

Figure 5-20. Relationship between compressive strength and P-waves velocity values for C_C40, C_C40_nf20 and C_C40_nf40.

5.5.2. ELECTRICAL RESISTIVITY MEASUREMENTS

Electrical resistivity measurements were also performed on Caposele soil mixtures (i.e., C_C40, C_C40_nf20 and C_C40_nf40). Trends of resistivity values during the period of acquisition are shown in Figure 5-21.

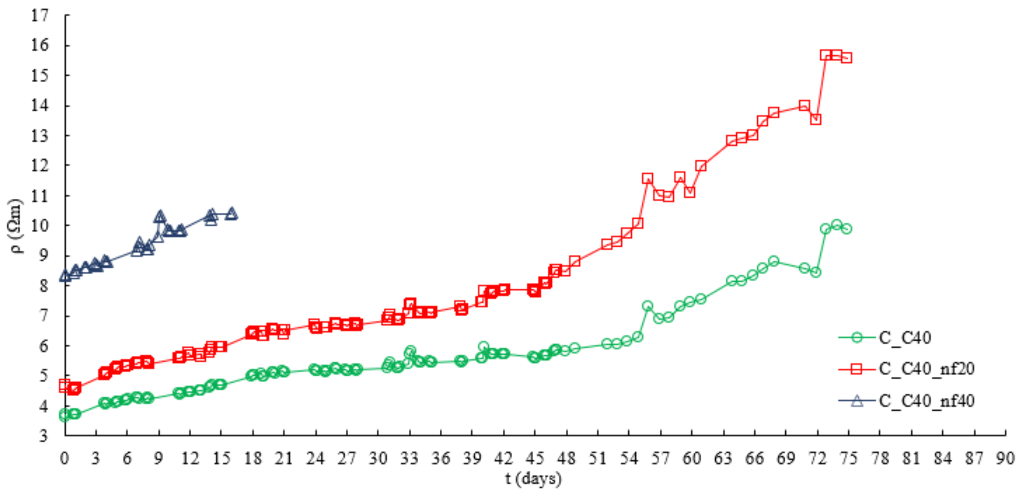

Figure 5-21. Electrical resistivity measurements as function of the acquisition time for C_C40, C_C40_nf20 and C_C40_nf40.

It is possible to note an initial linear but less steeply sloping section compared to the SW Kaolin up to 45 days, and then a significant increase in electrical resistivity values.

The results of Caposele soil are in agreement with those of SW Kaolin. From the results the effect of foam addition in the system soil-cement-water is clear: the higher the percentage of foam, the higher the electrical resistivity values.

Moreover, in Figure 5-22 there is a comparison between the values of electrical resistivity and uniaxial compressive strength, varying the curing time and the artificial porosity introduced in the soil-cement-water system. It is possible to observe how, given the curing time of the tested mixture, as the artificial porosity increases in terms of percentage of added foam, there is an increase in the electrical resistivity values and, on the other hand, a decrease in the unconfined compressive strength values. It is in agreement with SW Kaolin UCS-ρ correlation showed in Figure 5-13.

For C_C40_nf40 mixture the electrical resistivity measurements ends at 18 days of acquisition due to an electrical problem in electrodes-soil coupling.

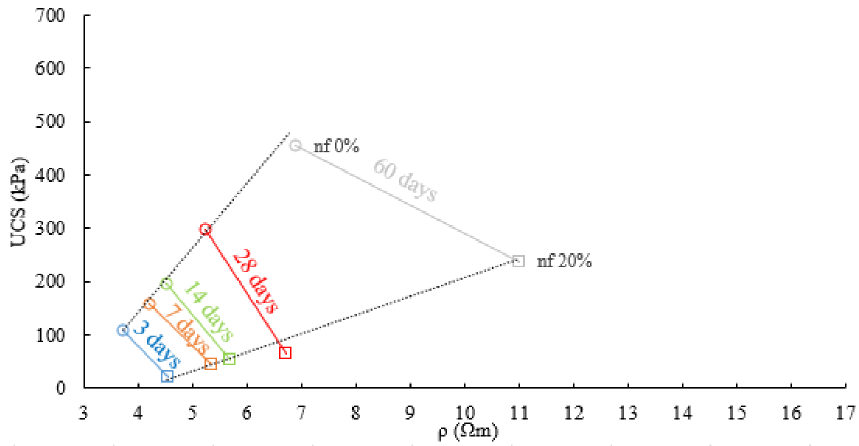

Figure 5-22. Unconfined compressive strength and electrical resistivity measurements correlation for C_C40 and C_C40_nf20.

5.6. DISCUSSIONS

The effects of curing time and addition of foam on SW Kaolin and Caposele soil were investigated by means of mechanical tests and non-destructive tests.

In particular, unconfined compression tests made possible to investigate the unconfined compressive strength for each type of mixture, without the addition of foam and with it. At increasing curing time, for both SW Kaolin and Caposele Soil mixtures, it is observed that the unconfined compressive strength increased. It is due to the development of cement hydration reactions and consequently to the formation of hydration products that contribute to the increase in strength and stiffness of the materials.

Comparing only cemented soils with lightweight cemented soils it is possible to see a general reduction in strength and stiffness of the materials. This is owing to the fact that when foam is added to the soil-water-cement system it has an effect on the physical condition of the lightweight materials, which is identify by higher void ratios. The results concur with the studies of De Sarno et al., (2019) and Vitale et al., (2020), which have shown that foam has not influence on the kinetic of hydration reactions and the following development of cementation products.

Moreover, the results of unconfined compressive strength for Caposele soil mixtures for the same curing time and treatment parameters (i.e., percentage of foam). Also in this case, the findings are consistent with De Sarno (2019), who observed a decrease in strength for both cemented and lightweight cemented Caposele soil specimens in direct shear tests.

From the results of torsional shear tests on SW Kaolin, it is possible to see the evolution of shear modulus G curves with increase in the shear strain amplitude (Figure 5-5). The progressive reduction of stiffness with the increase of shear strain level is linked to soil composition, nature and diffusion of interparticle bonds. Shear modulus G decreases at diminution of chemo-physical bonds and number of particles contacts.

Due to the presence of cementation bonds, the attenuation in the curve G/G_0-γ is not slow and gradual, but it is possible to see a change in slope after the linearity threshold (γ_l) has been exceeded. This type of behaviour becomes less and less visible for lightweight cemented soils (i.e. K_C40_nf20 and K_C40_nf40) as the percentage of foam added increases. In particular, the linearity threshold increases in the transition from K_C40 to K_C40_nf40 (Table 5-1).

To analyse the curvature of function $G/G_0(\gamma)$, two different parameters were introduced. In particular, R coefficient of Ramberg-Osgood model and γ_r/γ_l ratio. R values and γ_r/γ_l were put in relation to the artificial porosity n_f in Figure 5-8. γ_r/γ_l ratio is also a direct measure of the slope of the attenuation curve. The increase in n_f results in an increase in the linearity threshold, with a consequent decrease in γ_r/γ_l ratio but, on the other hand, there is an increment in R coefficient (it is expressible as a decreasing function of the ratio γ_r/γ_l in equation 5-2).

The trend of R is a perfect mirror-image of γ_r/γ_l. These findings are in good agreement with other studies (d'Onofrio et al., 1995; d'Onofrio, 1996).

However, it is possible to observe an overlap of the G-γ curves (Figure 5-5) beyond a shear strain γ = 0.1%. It seems that, independent on the type of mixtures after a determined shear strain level, cemented and lightweight cemented soils have the same G modulus degradation.

The most likely explanation of this behaviour is an internal damage within the specimens (i.e., K_C40, K_C40_nf20 and K_C40_nf40) during the performance of torsional shear tests. It may originate from one hand to the breakage of cemented bonds at the interface of the particle aggregates and, on the other hand, from the breakage of the brittle and porous particle aggregates themselves (Gao et al., 2021), due to the artificial porosity introduced by the addition of foam.

The decrease of the cementation can occur when the soil skeleton is strained. There are different kinds of interparticle forces that can cause strains in the soil (e.g. capillary forces, electrical forces linked to the pore fluid chemistry and interparticle skeletal forces). In this case, the cyclic loading (an interparticle skeletal force) is the reason for the decrease of the cementation (Rinaldi & Santamarina, 2008). It seems that the artificial porosity, and as a consequence the higher void ratio of the lightweight cemented specimens, has no impact on the degradation of shear modulus at certain level of shear strain (i.e., $\gamma = 0.1\%$).

Summing up the results, it seems that the addition of foam is responsible for higher values of linearity threshold (higher the percentage of foam, higher the linearity threshold) and, as a consequence, for the lower change in slope in the G modulus decay curves. This is confirmed by the trends of R coefficient and γ_r/γ_l ratio. Moreover, the decrease of decementation is responsible for the degradation of shear modulus at certain level of shear strain (i.e., $\gamma = 0.1\%$), due to the application of the cyclic loading.

Together with the mechanical tests, non-destructive tests were carried out. In particular, for both the types of soil of this experimental study, P-waves velocity and electrical resistivity measurements were performed. The main purpose of non-destructive methods is the possibility of assessing the properties and successful treatment of lightweight cemented soils, owing to the fact that they are simple and non-invasive techniques. Moreover, it was tried to find correlations between P-wave velocity and electrical resistivity with geotechnical parameters (i.e. UCS), with the aim of having direct information about geotechnical properties of geomaterial without performing mechanical tests, or if the latter are not possible to execute.

Trends of P-waves velocity at increasing curing time were shown in Figures 5-9 and 5-18, respectively for SW Kaolin and Caposele soil. In both cases, it is possible to see different rates of increase in P-waves velocity as function of the curing time. In particular, the rate of increase is higher in the transition from 3 to 7 days of curing and then, from 7 to 28 days, it tends to decrease and to be constant (especially for mixture with 20% and 40% of foam, in both types of treated soils). What is more, similar behaviour is possible to observe in the pattern of strength gain in Figures 5-4 and 5-17, respectively for SW Kaolin and Caposele soil.

The most likely explanation of these findings is the development of cement hydration reactions, that causes the increase in gel/space ratio. In fact, the diminution in volume of pores and, as a consequence of the solid matter, determines an increase of P-waves velocity, due to the presence of hydration products. These findings are consistent with other studies (Ikpong, 1993; Hasanzadeh and Shooshpasha, 2019).

P-waves velocity values are also represented as function of density and artificial porosity, respectively in Table 5-2, Figure 5-10 for SW Kaolin mixtures and in Table 5-3 and Figure 5-19 for Caposele Soil mixtures. These representations are consistent with the major trends shown in Figures 5-9, 5-18: P-waves velocity is greater in a denser medium, while it decreases in a medium with lower density and increasing porosity. This result could also be interpreted as evidence of good treatment performance, as a reduction in P-waves velocity is associated with lower specimens density, due to the introduction of foam into the system.

Relationships between the unconfined compressive strength and P-waves velocity were found for both types of soil. In particular, it seems clear that there is a correlation between the increase of UCS associated with the increase in P-waves velocity. It is confirmed by the exponential trends and the correlation coefficients R^2 found, especially in the case of Caposele Soil (Figure 5-20) where it is higher than that of SW Kaolin (Figure 5-11), due to the lower data scattering.

The results obtained are in good agreement with literature works (Yesiller et al. (2000), Hasanzadeh and Shooshpasha (2019), Pu et al. (2019) and Chen et al. (2020)).

In the last section of this chapter electrical resistivity measurements were reported for SW Kaolin and Caposele Soil. In particular, the trends of electrical resistivity measurement as function of the acquisition time were illustrated in Figures 5-12 and 5-21, respectively for SW Kaolin and Caposele Soil mixtures. It can be seen that, for both soil types studied, the resistivity values increase in the transition from a cemented soil (nf 0%) to a lightweight cemented soil (nf 20%, 40%), in a more evident way the higher the percentage of foam added to the system.

This behaviour is justified by the increase in artificial porosity produced by increasing quantities of foam in the soil-water-cement system. The pathways for the passage of electrical current are tortuous, due to the presence of footprints left by the foam bubbles in the soil and which are not filled by the cement products, as a result of the development of pozzolanic reactions.

The electrical resistivity curves show a minimum point in the first four hours of acquisition and gradually increase as time passes. It is possible to explain this behaviour in light of the formation process of the hydration products of the cement present in the analysed mixtures. The decrease in resistivity values in the first four hours is probably attributable to the immediate dissolution of soluble ions from the cement particles. The mobilisation of the ions favours the electrical conductivity, reciprocal of the electrical resistivity. Immediately after this initial period and up to 24 hours, a slight rise in resistivity values is observed due to the formation of the first hydrated phases, a product of pozzolanic reactions. The progressive hydration of the cement reduces the percentage of free water with a reduction in the ionic mobility of the system. The behaviour described is in agreement with that reported in other literature works (Wei et al., 2012), where the electrical resistivity development with time is attributed to the reduction of pore space and, on the other hand, to the augment of solid matrix.

From 24 hours onwards, as shown in Figures 5-12 and 5-21, the increase in resistivity values is observed as the hydration products are formed. The main reason to explain this kind of behaviour is that, at increasing curing time, there is a development of the pozzolanic reactions and, as a result, a decrease in water content of the soil-water-cement and soil-water-cement-foam mixtures (Horpibulsuk et al., 2003). The passage of curing time leads to the formation of cementing products, such as calcium silicate hydrate (CSH) and calcium aluminate hydrate (CAH). Their formation binds the soil particles together, resulting in a denser soil structure. These aspects together result in increasingly tortuous paths for the passage of electric current, justifying the increase in resistivity that is observed. These findings are in good agreement with many other studies in literature (Bergado et al., 1996; Holm, 1999; Liu et al., 2007; Chen et al., 2011; Vincent et al., 2017).

For the SW Kaolin (Figure 5-12), the resistivity values of the three mixtures stabilise around a constant value as the curing time increases. For the Caposele soil (Figure 5-21), a change in the slope of the resistivity curves is observed at a curing time of around 45 days, indicating a trend of more rapid increase in electrical resistivity over time. For the observation time interval (i.e., three months), the curves do not reach a constant resistivity value as observed for SW Kaolin. The described trend is similar for the two specimens treated with cement in the absence of foam and with 20% foam. For the mixture with 40% of foam, the electrical resistivity curve is shown up to the curing time of 16 days, from which point onwards there were problems acquiring the measurement.

The significant increase in the electrical resistivity values is probably due to the formation of a second phase of hydration products following the development of pozzolanic reactions between the Portlandite precipitated after the first hydration reactions and the clay minerals constituting the Caposele Soil (probably montmorillonite, as it can be seen in XRD image in Figure 4-3). It cannot be excluded that this increase in resistivity can also be found in the case of SW Kaolin, but for longer observation times, due to the low reactivity of its clay minerals.

Finally, correlations between the electrical resistivity measurements and unconfined compressive strength values are reported in two graphs in Figures 5-13 and 5-22, respectively for SW Kaolin and Caposele Soil. For both investigated soils, it is possible to observe how, given the curing time of the tested mixture, as the artificial porosity increases in terms of percentage of foam added, there is an increase in the electrical resistivity values and conversely a decrease in the uniaxial compressive strength values. This type of behaviour is consistent with the previous findings in terms of trends for UCS and electrical resistivity and are in agreement with other works (Liu et al. (2007), Wei et al., (2012)).

Moreover, these kinds of correlations could be useful in determination of geotechnical parameters where it is not possible to execute mechanical test (i.e., unconfined compression tests). In addition, geophysical surveys as electrical resistivity measurements can also be applied as a tool with which to carry out quality control in order to verify the success of the treatment.

The electrical resistivity trends obtained highlight the change in resistivity values depending on the treated soil mixture on which the measurement is performed. Furthermore, from the measurements taken, it was possible to see an evolution of the electrical resistivity values from the first hours of the curing time, that is a symptom of the development of the cement hydration reactions and the consequent formation of the cement products.

Thus, on the one hand the different range of electrical resistivity values from the lowest to the highest, is symptomatic of the presence or absence of artificial porosity in the system and, on the other hand, a possible monitoring of the treated soil mixture, can indicate whether the development of pozzolanic reactions is taking place.

References

Adewoyin, O.O., Joshua, E.O., Akinwumi, I.I., Omeje, M., Joel, E.S., 2017. Evaluation of Geotechnical Parameters using Geophysical Data. J. Eng. Technol. Sci., Vol. 49, No. 1, 95-113. https://doi.org/10.5614/j.eng.technol.sci.2017.49.1.6.

Bergado, D.T., Anderson, L.R., Miura, N., Balasubramaniam, A.S., 1996. Soft ground improvement in lowland and other environments. American Society of Civil Engineers, New York.

Chen, L., Du, Y.-J., Liu, S.-Y., M. ASCE, Jin, F., 2011. Evaluation of Cement Hydration Properties of Cement-Stabilized Lead-Contaminated Soils Using Electrical Resistivity Measurement. Journal of Hazardous, Toxic, and Radioactive Waste, Vol. 14, No. 4, October 1, 2011. https://doi.org/ 10.1061/(ASCE)HZ.1944-8376.0000073.

Chen, T.-T., Wang, W.-C., Wang, H.-Y., 2020. Mechanical properties and ultrasonic velocity of lightweight aggregate concrete containing mineral powder materials. Journal of Constr. Build. Mater., 258 (119550). https://doi.org/10.1016/j.conbuildmat.2020.119550.

d'Onofrio, A., 1996. Comportamento meccanico dell'argilla di Vallericca in condizioni lontane dalla rottura. Ph. D. Thesis. University of Naples, "Federico II".

d'Onofrio, A., Santucci de Magistris, F., Silvestri, F., Vinale, F., 1995. Behaviour of compacted sand-bentonite mixtures from small to medium strains. First Earthquake Geotech. Eng. Conf. Tokyo, Vol. 1, 133-138 Balkema.

De Sarno, D., 2019. Microstructure and mechanical behaviour of cemented soils lightened by foam. Ph. D. Thesis. University of Naples, "Federico II".

De Sarno, D., Vitale, E., Deneele, D., Nicotera, M.V., Papa, R., Russo, G., Urciuoli, G., 2019. Effects of cement and foam addition on chemo-mechanical behaviour of lightweight cemented soil (LWCS). E3S Web Conf., 92. https://doi.org/10.1051/e3sconf/20199211006.

Gao, H., Xia, S., Chen, F., Stuedlein A.W., Li, X., Wang, Z., Shen, Z., Chen, X., 2021. Dynamic shear modulus and damping of cemented and uncemented lightweight expanded clay aggregate (LECA) at low strains. Soil Dynamics and Earthquake Engineering. Volume 142, 2021, 106555. https://doi.org/10.1016/j.soildyn.2020.106555.

Hasanzadeh, A., Shooshpasha, I., 2019. Effects of silica fume on cemented sand using ultrasonic pulse velocity. Journal of Adhesion Science and Technology. https://doi.org/10.1080/01694243.2019.1582890.

Holm, G., 1999. Applications of dry mix methods for deep soil stabilization. Paper presented at the international conference on dry mix methods for deep soil stabilization, Stockholm, pp. 3-13.

Horpibulsuk, S., Miura, N., Nagaraj, T.S., (2003). Assessment of strength development in cement admixed high water content clays with Abam's law as a basis. Geotechnique 53(4), pp. 439-444.

Ikpong, AA., 1993. The relationship between the strength and non-destructive parameters of rice husk ash concrete. Cem Concr Res., 23:387–398. https://doi.org/10.1016/0008-8846(93)90104-H.

Lai, C.G., Foti, S., Godio, A., Rix, G., J., Sambuelli, L., Socco, V.L., 2000. Caratterizzazione Geotecnica dei Terreni Mediante l'Uso di Tecniche Geofisiche. Riv. It. Geotecnica, Numero speciale: sviluppi nell'esecuzione e nell'impiego delle indagini geotecniche, 99-118.

Liu, S.Y., Du, Y.J., Han, L.H., Gu, M.F., 2007. Experimental study on the electrical resistivity of soil-cement admixtures. Environ Geol (2008) 54:1227–1233. https://doi.org/10.1007/s00254-007-0905-5.

Pu, S., Hong, B., Liu, X., Xu, F., Shan, H., 2019. Detection Technology of Foamed Mixture Lightweight Soil Embankment Based on Ultrasonic Wave Transmission Method. Advances in

Materials Science and Engineering, vol. 2019, Article ID 9654819, 15 pages. https://doi.org/10.1155/2019/9654819.

Rinaldi, V.A., Santamarina, J.C., 2008. Cemented soils: small strain stiffness. Deformational Characteristics of geomaterial. Vol. 1, edited by S.E. Burns et al., pp. 267-276, IOS, Amsterdam.

Silvestri, F., 1991. Analisi del comportamento dei terreni naturali in prove cicliche e dinamiche di taglio torsionale. Ph. D. Thesis. University of Naples, “Federico II”.

Vincent, N.A., Shivashankar, R., Lokesh, K.N., Jacob, J.M., 2017. Laboratory Electrical Resistivity Studies on Cement Stabilized Soil. Hindawi International Scholarly Research Notices Volume 2017, Article ID 8970153, 15 pages https://doi.org/10.1155/2017/8970153.

Vitale, E., Deneele, D., Russo, G., De Sarno, D., Nicotera, M. V., Papa, R., Urciuoli, G. 2020. Chemo-mechanical behaviour of lightweight cemented soils. Acta Geotech. 15, 933–945. https://doi.org/10.1007/s11440-019-00797-8.

Wei, X., Xiao, L., Li, Z., 2012. Prediction of standard compressive strength of cement by the electrical resistivity measurement. Construct. Build. Mater., 31 (2012), pp. 341-346. https://doi.org/10.1016/j.conbuildmat.2011.12.111.

Yesiller, N., Hanson, J.L., Usmen, M.A., 2000. Ultrasonic Assessment of Stabilized Soils. Soft Ground Technology Conference May 28 - June 2 | Noordwijkerhout, the Netherlands https://doi.org/10.1061/40552(301)14.

6. DURABILITY UNDER ENVIRONMENTAL LOADING CONDITIONS

6.1. DESCRIPTION OF THE EXPERIMENTATION PERFORMED

The second part of this research work is dedicated to the durability issue under environmental loading conditions. Mechanical tests were carried out on lightweight cemented soil and cemented soil (i.e., without the addition of foam) specimens after the execution of wetting-drying cycles on them; suction measurements were executed after the performance of mechanical tests. The final aim is the study the evolution, and eventually degradation, of their mechanical behaviour.

The experimental procedures for performing wetting-drying cycles, suction measurements and a description of the mechanical tests (i.e., unconfined compression tests and triaxial tests) can be found in Chapter 4 (sections 4.3.3., 4.3.4. and 4.3.1. respectively). They were carried out at *Laboratoire Énergies & Mécanique Théorique et Appliquée (LEMTA - University of Lorraine, Nancy-France).*

In what follows, the adopted experimental programme is briefly reported, while the next sections show the most significant results obtained for each type of test performed. The discussion of the results is destinated to the final section of this chapter (section 6.4.).

The experimental investigation was organised as follows:

- **Wetting-drying cycles**: in order to submit SW Kaolin and Caposele Soil specimens to environmental load conditions wetting-drying cycles were performed on them. Table 4-11 (section 4.3.3.) reported wetting-drying parameters in terms of temperature, relative humidity, duration and modality of each phase.

- **Unconfined compression tests**: these first kind of tests were executed with the aim to indagate the effects of wetting-drying cycles on the mechanical behaviour of LWCS (sections 6.2.1. and 6.3.1.). In particular, it was seen the effects on the evolution of unconfined compressive strength and stiffness. They were carried out on both SW Kaolin and Caposele Soil specimens, without foam and at the two different percentages set (i.e., nf 20% and 40%, respectively). Table 4-5 (section 4.3.1.) gave an overview of unconfined compression tests. For SW Kaolin and Caposele Soil, treatment parameters, the identification of the samples and their dimensions, together with the environmental load conditions and the number of tests performed for each type of mixture tested were given.

- **Triaxial tests**: these test were executed on SW Kaolin and Caposele Soil specimens (sections 6.2.2. and 6.3.2.), for the three types of mixtures at different environmental load conditions and three different levels of confining pressure, as reported in Table 4-6 (section 4.3.1.). It was indagated the evolution and degradation of shear strength in relation to environmental load conditions; failure envelopes were determined, together with cohesion and friction angle parameters.

- **Suction measurements:** they were performed on SW Kaolin and Caposele Soil specimens after the execution of the mechanical tests (section 4.3.4.). These suction values were used to interpreter mechanical tests results and, as a consequence, the degradation of mechanical behaviour linked to suction variation according to environmental load conditions applied.

6.2. EVOLUTION OF MECHANICAL BEHAVIOUR

Speswhite Kaolin and Caposele soil specimens, cemented and lightweight cemented, were subjected to wetting-drying cycles, in order to study the evolution of their mechanical behaviour and, as a result, to test their durability performances under environmental loading conditions. In the following, the results for SW Kaolin will be shown in terms of unconfined compression tests and triaxial tests. Then effects of suction and wetting-drying cycles will be described. Finally, a comparison between SW Kaolin and Caposele soil results will be made.

6.2.1. UNCONFINED COMPRESSION TESTS

In this section, results of unconfined compression tests are reported. These tests were carried out on cemented SW Kaolin specimens and lightweight cemented SW Kaolin specimens (i.e., nf=20%, 40%). Three environmental loading conditions were tested. The first one is an initial drying phase at 50% relative humidity; it is common to all the specimens and preliminary to the other two conditions. The second one corresponds to three wetting-drying cycles at a relative humidity equal to 50%. The third one is characterized by three wetting-cycles at a relative humidity of 90%.

In the following, the identification of the mixtures is the same as that one adopted in Chapter 5. For the environmental loading conditions: “0 w-d_50% RH” stands for the first one, “3 w-d_50% RH” for the second one and “3 w-d_90% RH” for the last one.

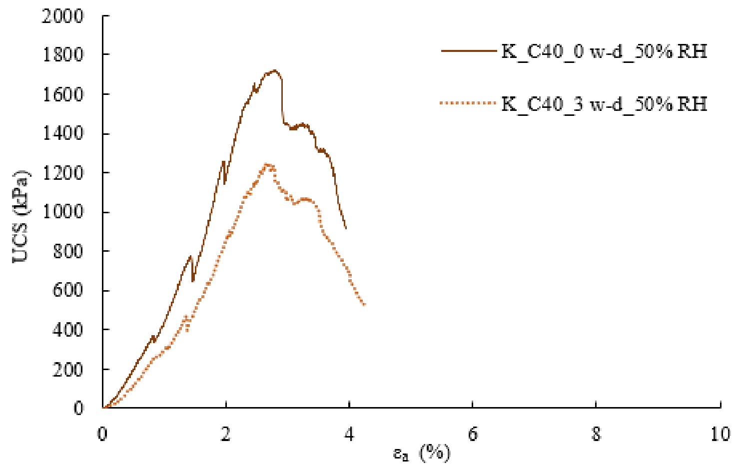

Figure 6-1. Unconfined compression test results on cemented SW Kaolin, comparing the initial condition and three wetting-drying cycles at the same RH = 50%.

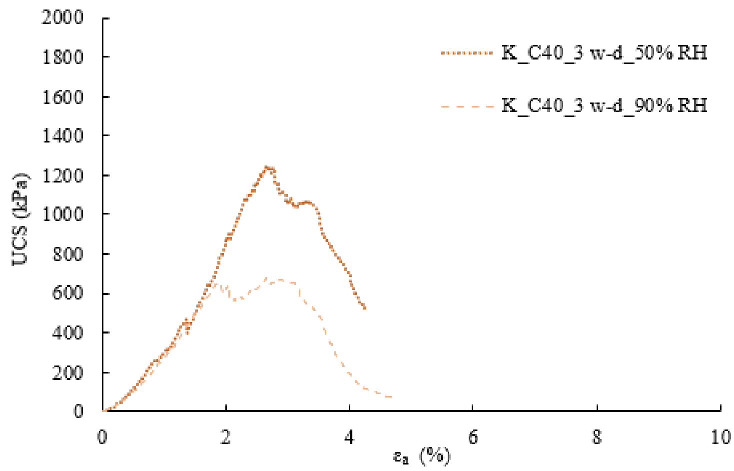

Figure 6-2. Unconfined compression test results on cemented SW Kaolin, comparing three wetting-drying cycles conditions at RH = 50% and 90%.

In Figures 6-1 and 6-2 the results of the tests performed on cemented SW Kaolin specimens without foam (i.e., K_C40), under three environmental loading conditions are presented.

In particular, in Figure 6-1 the initial condition with that at three wetting-drying cycles are compared and both of them are characterized by the same relative humidity equal to 50%. Keeping constant the relative humidity parameter, it is possible to see a decrease in strength and stiffness from the initial condition (i.e., only drying phase) for the one at three wetting-drying cycles. Moreover, in Figure 6-2 there is a comparison between the two conditions at equal number of cycles, but at different levels of relative humidity (i.e., 50% and 90%). Also in this case, a reduction in strength is observed in the transition from one condition to the other, as the relative humidity value increases.

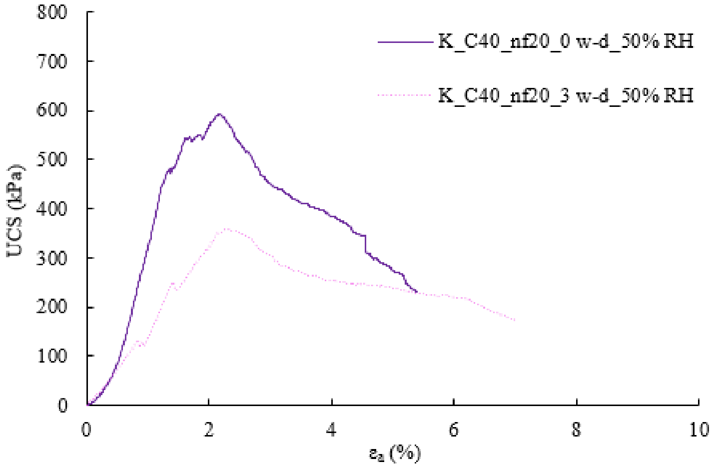

Figure 6-3. Unconfined compression test results on lightweight cemented SW Kaolin with 20% foam, comparing the initial condition and three wetting-drying cycles at the same RH = 50%.

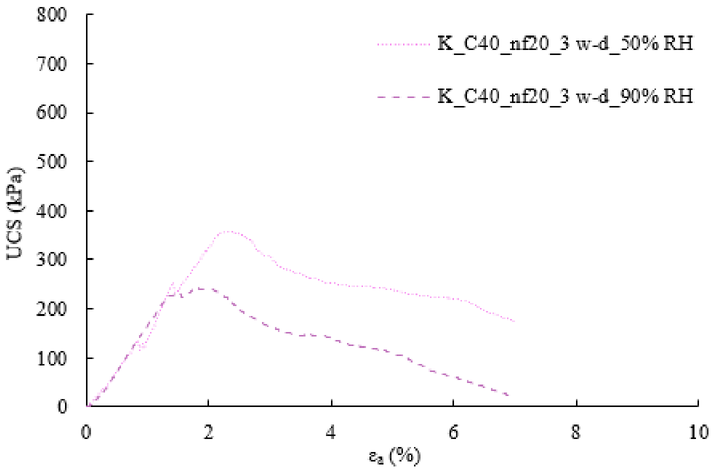

Figure 6-4. Unconfined compression test results on lightweight cemented SW Kaolin with 40% foam, comparing three wetting-drying cycles conditions at RH = 50% and 90%.

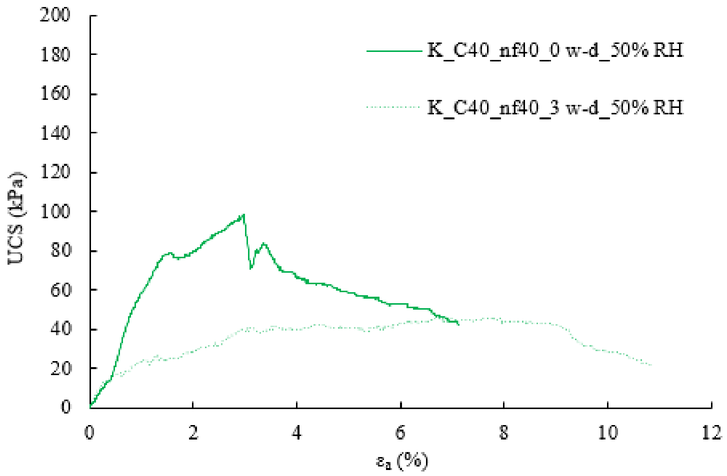

Figure 6-5. Unconfined compression test results on lightweight cemented SW Kaolin with 20% foam, comparing the initial condition and three wetting-drying cycles at the same RH = 50%.

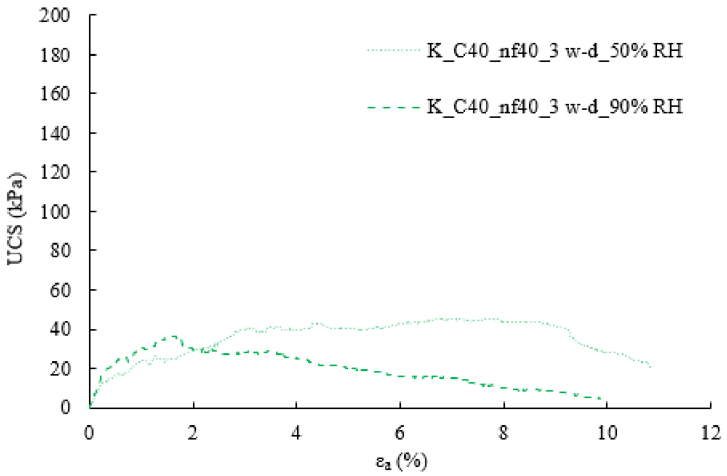

Figure 6-6. Unconfined compression test results on lightweight cemented SW Kaolin with 40% foam, comparing three wetting-drying cycles conditions at RH = 50% and 90%.

The behaviour observed for cemented SW Kaolin is common to the other two tested mixtures (i.e., K_C40_nf20 and K_C40_nf40). In fact, looking at Figures 6-3, 6-4 before and at Figures 6-5, 6-6 after, it is noted the same decrease in strength and stiffness that is observed for cemented SW Kaolin. Moreover, it is important to underline the reduction in strength and stiffness increases as the artificial porosity rises, in terms of percentages of added foam.

6.2.2. TRIAXIAL TESTS

In this section the results of the triaxial tests performed on SW Kaolin specimens mixture (i.e., K_C40_nf20 and K_C40_nf40) are presented. In particular, triaxial tests were carried out on SW Kaolin specimens that were subjected at two different environmental loading conditions: three wetting-drying cycles at 50% of relative humidity and three wetting-drying cycles at 90% relative humidity.

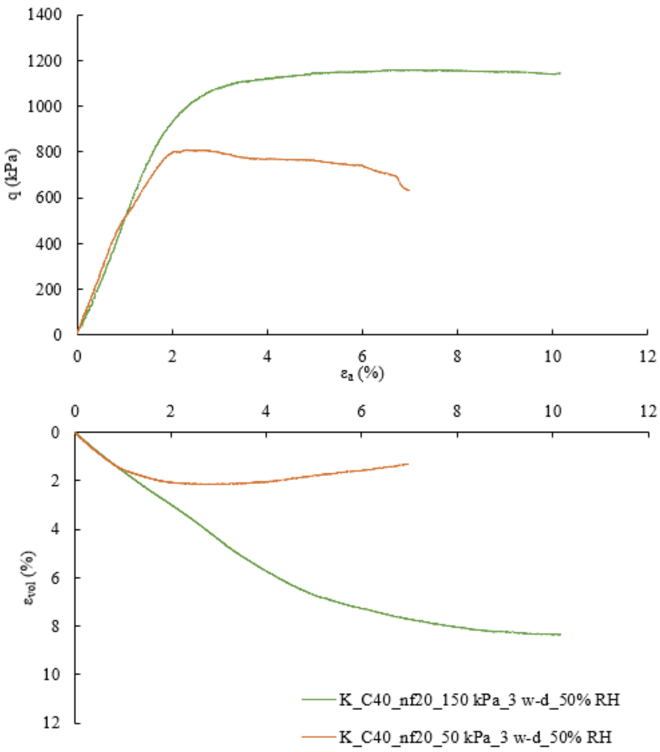

Figure 6-7. Triaxial tests on K_C40_nf20 after three wetting-drying cycles at 50% relative humidity.

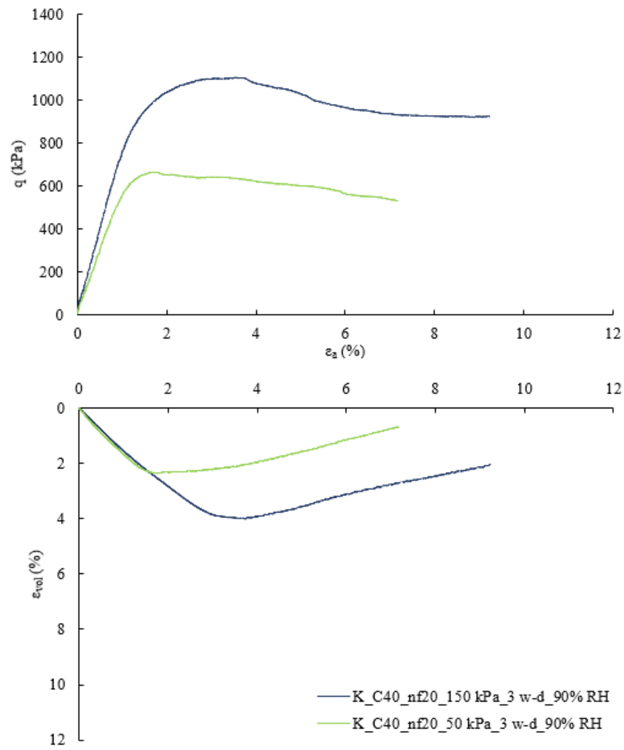

Figure 6-8. Triaxial tests on K_C40_nf20 after three wetting-drying cycles at 90% relative humidity.

Figure 6-7 presents triaxial tests results on lightweight cemented SW Kaolin with 20% foam, subjected to three wetting-drying cycles at 50% relative humidity. First of all, it is possible to note the effect of the confining pressure; in fact, in the transition from 50 kPa to 150 kPa, there is an increase in the strength of the material with a mechanical behaviour ductile and contractive, from the volumetric point of view.

Figure 6-8 shows triaxial tests results on lightweight cemented SW Kaolin with 20% foam, subjected to three wetting-drying cycles at 90% relative humidity. Also in this case, it is possible to note the role of confining pressure. In fact, it is observed that the strength and stiffness increase as the confining pressure grows.

It is interesting to compare the triaxial tests results already shown. Figure 6-9 shows an initial comparison of triaxial sample K_C40_nf20, keeping constant the confining pressure (i.e., 50 kPa) and the number of wetting and drying cycles, by varying the level of relative humidity (i.e.

50% and 90%). Figure 6-10 presents a second comparison of the triaxial tests. The parameters are the same as the previous case, but only the confining pressure changes (i.e. 150 kPa).

In both cases, in the transition from a lower to a higher value of relative humidity (i.e., 50% and 90%, respectively) it can be seen that there is a decrease in the mechanical performance of the material. In particular, it is possible to detect a clear reduction in the strength, in terms of deviatoric stress. From the volumetric point of view, the mechanical behaviour shown in Figure 6-10 seems to be different to the one presented in Figure 6-9. In fact, the volumetric response associated with K_C40_nf20_150 kPa_3 w-d cycles_90% RH is characterized by a higher value of volumetric deformations than the one associated with K_C40_nf20_150 kPa_3 w-d cycles_50% RH. Hence, this observation seems to be in contrast with the volumetric response reported in Figure 6-9.

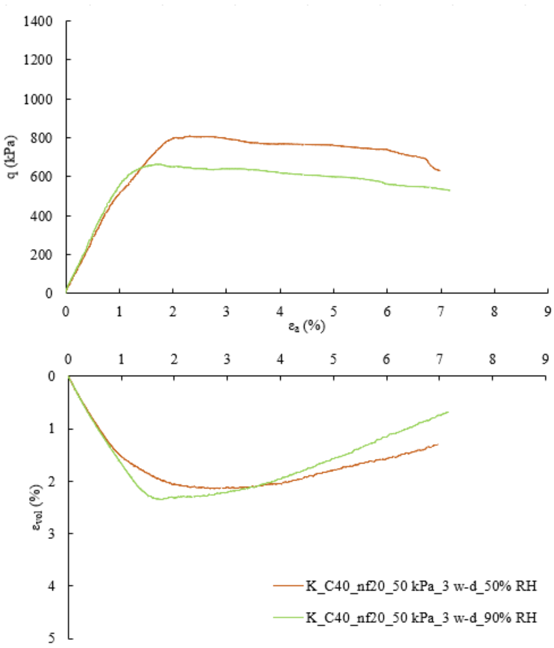

Figure 6-9. Triaxial tests on K_C40_nf20 at 50 kPa of confining pressure, three wetting-drying cycles at 50% and 90% relative humidity.

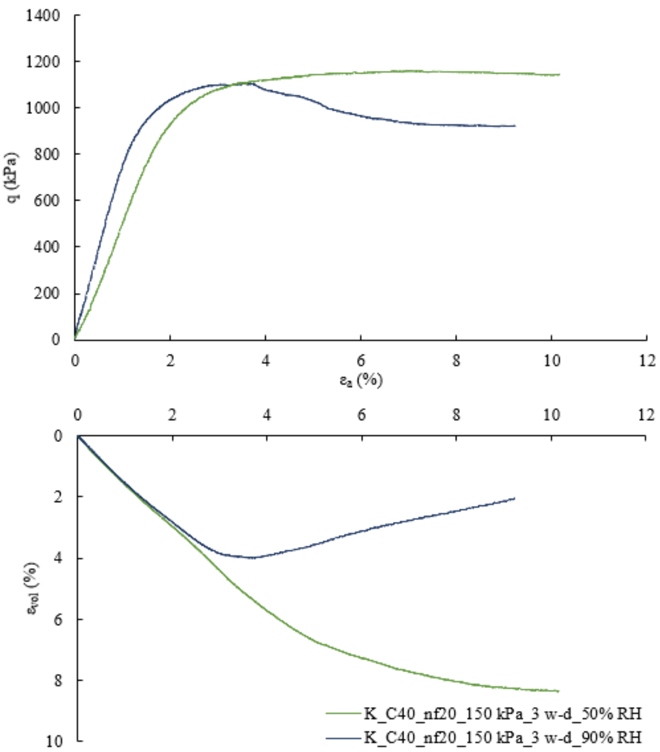

Figure 6-10. Triaxial tests on K_C40_nf20 at 150 kPa of confining pressure, three wetting-drying cycles at 50% and 90% relative humidity.

The same representation of triaxial tests results are reported also for K_C40_nf40.

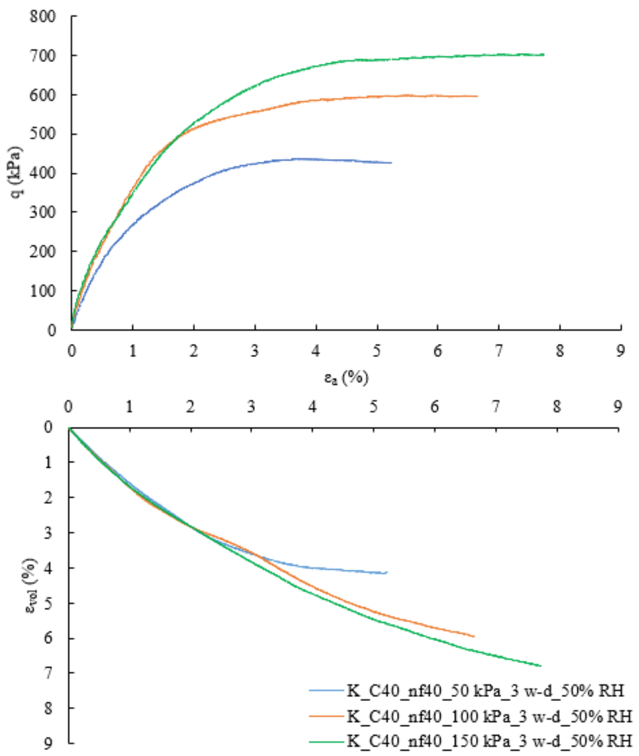

Figure 6-11. Triaxial tests on K_C40_nf40 after three wetting-drying cycles at 50% relative humidity.

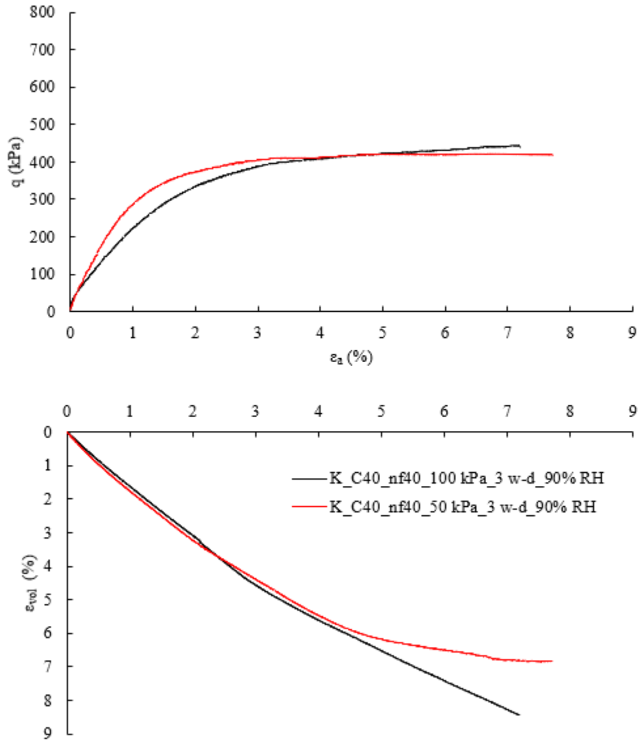

Figure 6-12. Triaxial tests on K_C40_nf40 after three wetting-drying cycles at 90% relative humidity.

In Figure 6-11, the triaxial tests results for the environmental loading conditions of three wetting-drying cycles at 50% relative humidity are presented. Also this time, it is clear the influence of confining pressure in the increase of strength and stiffness, in transition from 50 kPa to 150 kPa. Moreover, at increasing confining pressure, failure occurs at higher levels of deformation. The mechanical behaviour of K_C40_nf40 is ductile and contractive, with a general strength reduction if compared to K_C40_nf20.

In Figure 6-12, the triaxial tests results are reported for the climatic stress conditions of three wetting-drying cycles at 90% relative humidity. They confirmed a ductile and contractive mechanical behaviour of K_C40_nf40, even if the effect of confining pressure is not visible. The stress-strain curves are similar between them in terms of strength in the transition from 50 kPa to 100 kPa.

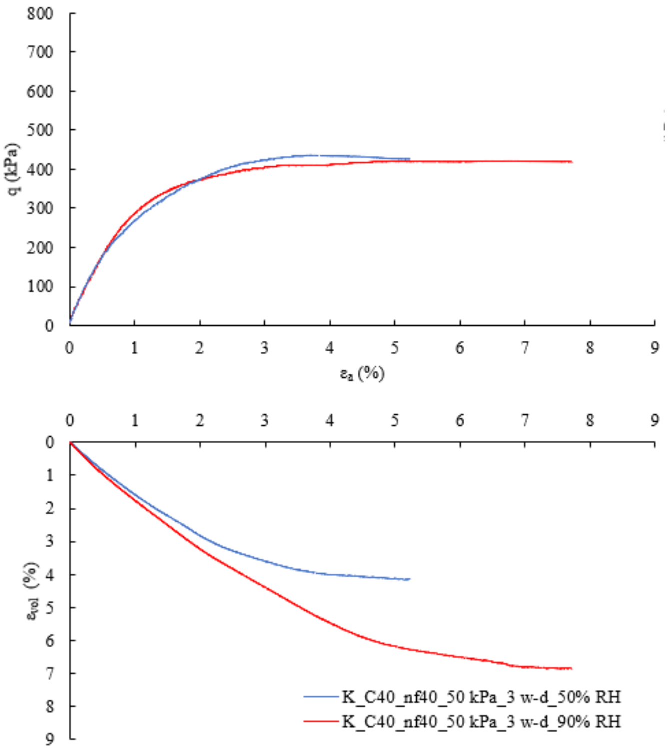

Figure 6-13. Triaxial tests on K_C40_nf40 at 50 kPa of confining pressure, three wetting-drying cycles at 50% and 90% relative humidity.

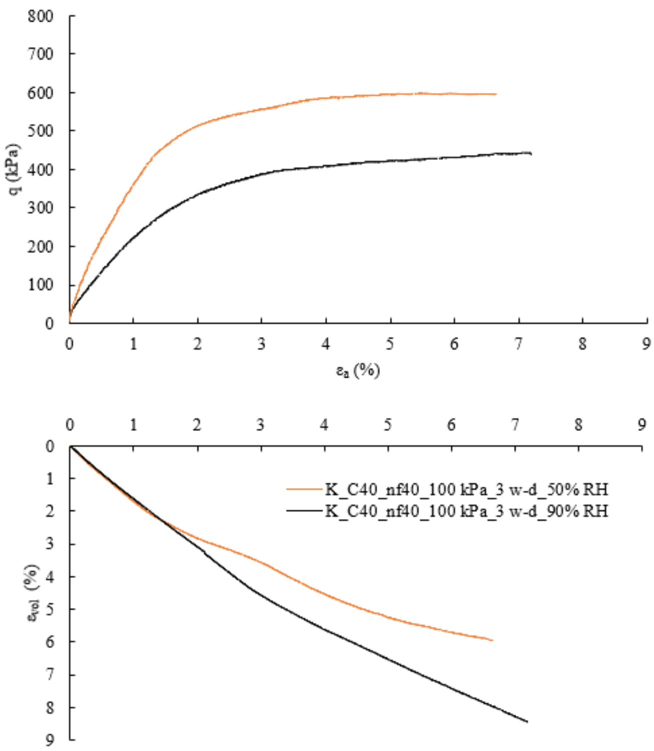

Figure 6-14. Triaxial tests on K_C40_nf40 at 100 kPa of confining pressure, three wetting-drying cycles at 50% and 90% relative humidity.

Also for K_C40_nf40, it is interesting to compare the triaxial tests results presented. In Figure 6-13 and Figure 6-14, two comparisons of triaxial tests on K_C40_nf40, keeping constant the confining pressure value (i.e., 50 kPa and 100 kPa, respectively) and the number of wetting and drying cycles, by varying the relative humidity (i.e. 50% and 90%, respectively).

Both cases confirmed what is observed for K_C40_nf20. In fact, in the transition from a lower to a higher value of relative humidity (i.e., 50% and 90%, respectively) it can be seen that there is a decrease in the mechanical performance of the material. In particular, a clear reduction in the strength, in terms of deviatoric stress is observed. From the volumetric point of view, the mechanical behaviour showed is congruent with the one illustrated for K_C40_nf20, in Figure 6-9.

6.2.3. EFFECTS OF CURRENT VALUE OF SUCTION

To investigate the evolution of mechanical behaviour of lightweight cemented SW Kaolin, suction measurements were performed after the execution of mechanical tests.

Figure 6-15 presents a relationship between the unconfined compressive strength values, previously shown in section 6.1.1., and the suction measurements carried out after the execution of the tests.

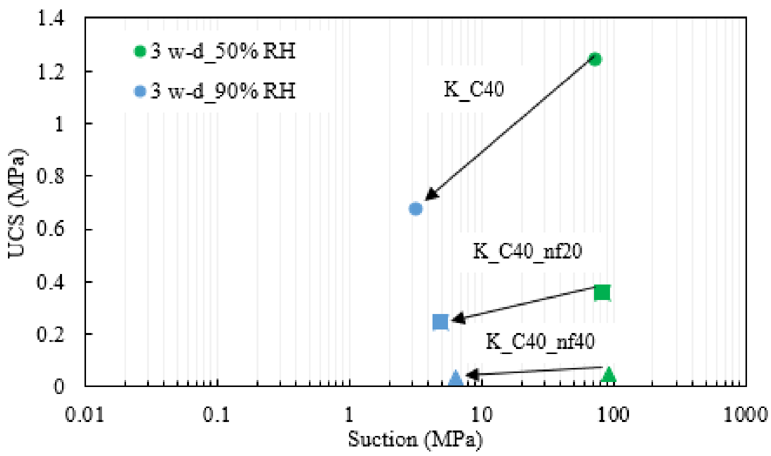

Figure 6-15. Unconfined compressive strength values as function of suction measurements for K_C40, K_C40_nf20 and K_C40_nf40 comparing three wetting-drying cycles conditions at 50% and 90% relative humidity.

Two different environmental loading conditions are analysed: the first one corresponds to three wetting-drying cycles at 50% relative humidity and the second one to three wetting-drying cycles at 90% relative humidity. It is observed that the reduction of UCS values is correlated to a decrease in suction measured on lightweight cemented SW Kaolin specimens, keeping constant the number of wetting-drying cycles applied to the specimens. The black arrows help to visualize that diminution in strength in transition from a lower to higher value of relative humidity (i.e., 50% and 90%), associated with the two assessed conditions.

Moreover, it is interesting to note that the reduction in strength is higher for K_C40 than for the other two mixtures (i.e., K_C40_nf20 and K_C40_nf40); what is more, the decrease in strength is even lower at increasing artificial porosity, in terms of percentage of added foam.

Figure 6-16 confirms the reduction in suction with the representation of the collected data. Suction values are plotted on the water retention curves by Vitale et al., (2020b) for cemented and lightweight cemented SW Kaolin at 90 days of curing time. The disposition of the data on the curves clearly shows the reduction in current values of suction, from 50% to 90% relative humidity.

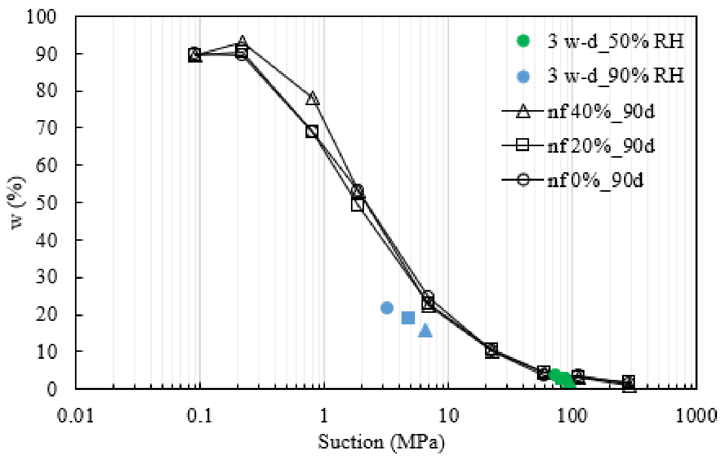

Figure 6-16. Suction measurements values at three wetting-drying cycles conditions at 50% and 90% relative humidity, plotted on water retention curves for K_C40, K_C40_nf20 and K_C40_nf40 (water retention curves from Vitale et al., 2020b).

Failure envelopes obtained from the triaxial tests conducted on K_C40_nf20 and K_C40_nf40 are represented in Figure 6-17. Data are reported in terms of σ_1-σ_3 and are compared two different environmental loading conditions, both of them at three wetting-drying cycles but at two level of relative humidity (i.e., 50% and 90%).

Considering K_C40_nf20 and comparing the two test conditions can be seen that there is a reduction in the strength of the material, that seems to be qualitatively in agreement with the mechanical behaviour observed from the results of unconfined compression tests.

On the other hand, comparing K_C40_nf20 and K_C40_nf40 both of them at 50% relative humidity, increasing the amount of foam it is possible for the reduction in strength of material.

Values of friction angle and cohesion derived from the failure envelopes put in evidence a correlation between them and the values of suction, measured on the specimens after the test.

In Table 6-1, values of suction, cohesion and friction angles are reported. Considering K_C40_nf20, it is noted that higher suction values correspond to lower relative humidity (i.e. 50%) and in transition from 50% to 90% of relative humidity there is a diminution in cohesion values, but not in friction angles that seems to be constant.

Comparing K_C40_nf40 with K_C40_nf20 keeping constant the environmental loads condition, it is possible to see an increase in the suction value, but a decrease in cohesion and friction angle values.

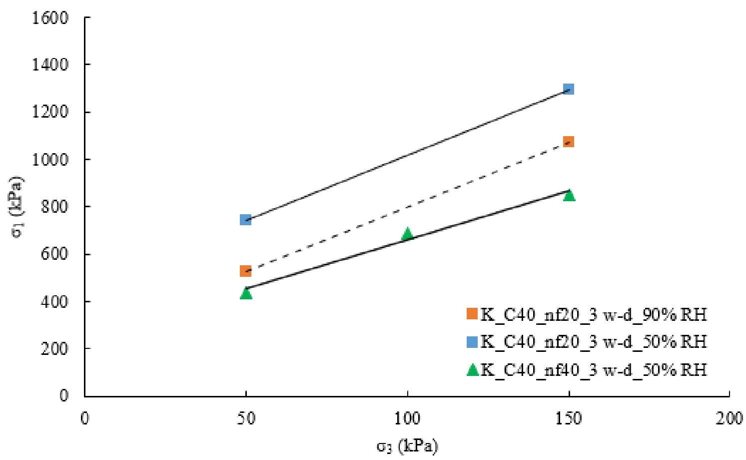

Figure 6-17. Failure envelopes for K_C40_nf20 at three wetting-drying cycles (50% and 90% of relative humidity) and K_C40_nf40 at three wetting-drying cycles (50% of relative humidity).

Identification	N° of w-d cycles	RH (%)	Suction (MPa)	c (kPa)	Φ (°)
K_C40_nf20	3	50	82.9	100.5	43.7
		90	4.9	53.2	43.7
K_C40_nf40	3	50	92.9	59.8	37.8

Table 6-1. Suction, cohesion and friction angle values for the two different mixtures at two relative humidity values.

6.2.4. EFFECTS OF WETTING-DRYING CYCLES

Figure 6-18 shows a comparison of the initial drying phase and three wetting-drying cycles, both at 50% relative humidity. Also in this case, unconfined compressive strength values are represented as function of suction measured values.

It is possible to observe a decrease in UCS values, as previously observed in Figure 6-15. The black arrows help to see the strength reduction from one condition to the other. Even this data representation confirms that the diminution in strength is higher for a cemented specimen and becomes lower for a lightweight cemented specimens, in more evident way at increasing percentage of added foam.

However, these environmental loading conditions tested are characterized by suction values almost similar to them, as shown in Figure 6-19. In fact, suction values plotted on water retention curves are arranged close together in the same range of values.

Keeping constant the level of relative humidity (i.e., 50%), the effect of application of wetting-drying cycles seems to be responsible for the evolution of mechanical performance of Lightweight cemented SW Kaolin specimens.

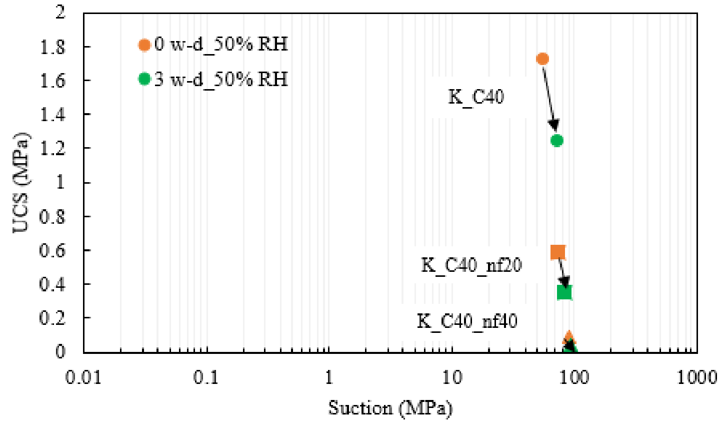

Figure 6-18. Unconfined compressive strength values as function of suction measurements for K_C40, K_C40_nf20 and K_C40_nf40 comparing the initial condition of drying phase with three wetting-drying cycles condition, at equal relative humidity of 50%.

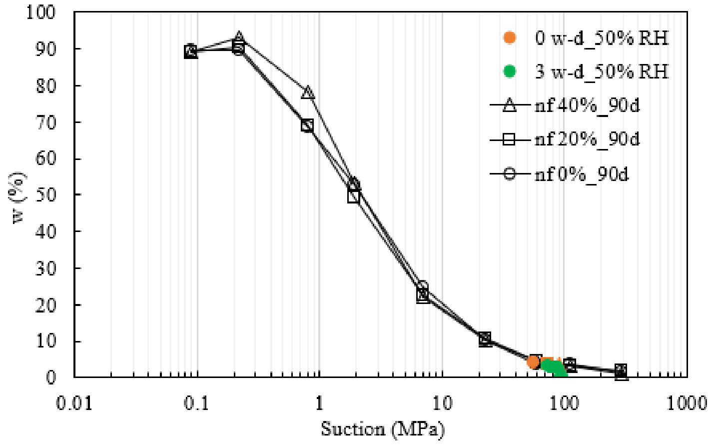

Figure 6-19. Suction measurements values at initial condition of drying phase and three wetting-drying cycles condition at equal relative humidity of 50%, plotted on water retention curves for K_C40, K_C40_nf20 and K_C40_nf40 (water retention curves from Vitale et al., 2020b).

6.3. SPESWHITE KAOLIN AND CAPOSELE SOIL COMPARISONS

As shown for SW Kaolin, also lightweight cemented Caposele soil specimens were subjected to wetting-drying cycles, in order to study the evolution of their mechanical behaviour and to test their durability performances under environmental loads. In the following, some results comparisons between SW Kaolin and Caposele Soil are presented, in order to highlight the differences among an artificial, industrially produced soil (i.e., SW Kaolin) and another one with natural origin (i.e., Caposele soil).

6.3.1. UNCONFINED COMPRESSION TESTS

In Figure 6-20 and Figure 6-21, the results of the unconfined compression tests are compared for the initial condition at RH=50%, between K_C40 and C_C40, K_C40_nf20 and C_C40_nf20.

In Figure 6-22 and Figure 6-23, the results of the unconfined compression tests are compared for the three wetting-drying cycles condition at RH=90%, between K_C40 and C_C40, K_C40_nf20 and C_C40_nf20.

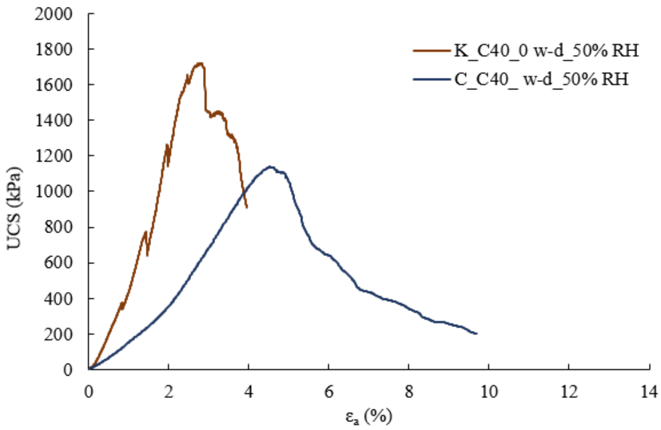

Figure 6-20. Unconfined compression test results on K_C40 and C_C40, at the initial condition with RH=50%.

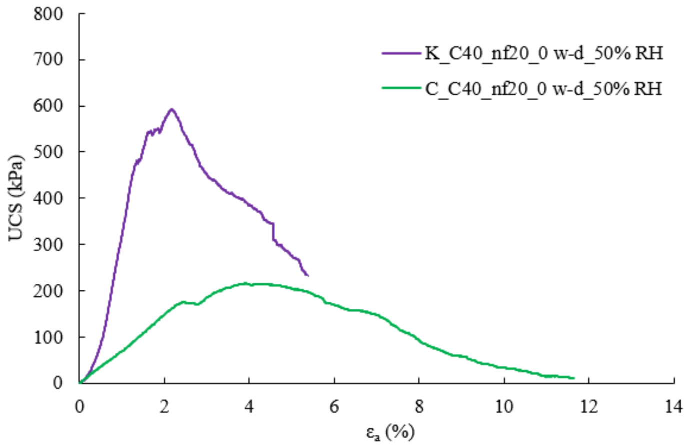

Figure 6-21. Unconfined compression test results on K_C40_nf20 and C_C40_nf20, at three wetting-drying cycles initial condition with RH=50%.

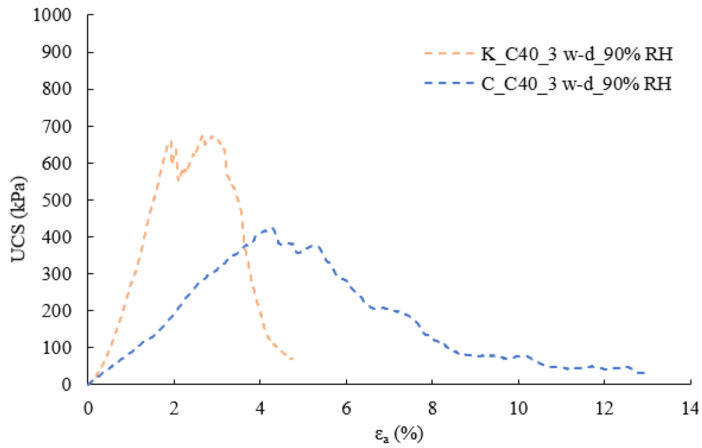

Figure 6-22. Unconfined compression test results on K_C40 and C_C40, at three wetting-drying cycles condition with RH=90%.

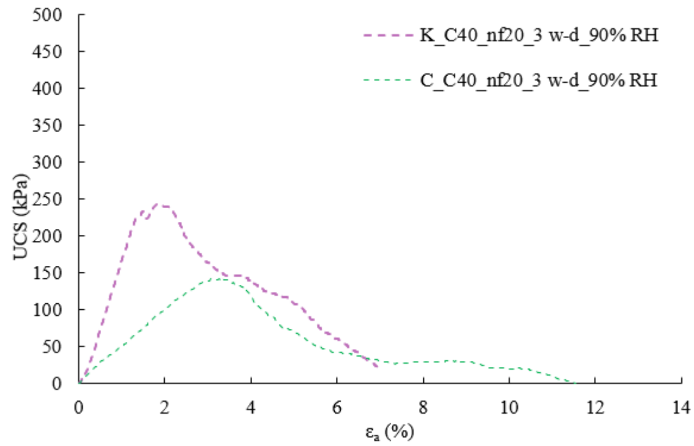

Figure 6-23. Unconfined compression test results on K_C40_nf20 and C_C40_nf20, at three wetting-drying cycles initial condition with RH=90%.

It is interesting to note that, for both the analysed environmental loading conditions, the strength and stiffness of Caposele soil are less than SW Kaolin soil.

Moreover, it is important to find a confirmation in the role of foam on the mechanical behaviour response. In fact, there is a decrease in strength and stiffness for Caposele soil going from C_C40 to C_C40_nf20, in both the two environmental loads conditions examined.

Identification	N° of w-d cycles	RH (%)	Suction (MPa)	w (%)
K_C40	0	50	55.5	4.3
K_C40_nf20			72.9	3.7
C_C40			45.3	10.1
C_C40_nf20			72.6	7.5
K_C40	3	90	3.3	21.7
K_C40_nf20			4.9	18.7
C_C40			10.7	19.1
C_C40_nf20			18.7	16.2

Table 6-2. Suction values for K_C40, K_C40_nf20, C_C40 and C_C40_nf20 at initial condition (50% RH) and at three wetting-drying cycles (90% RH).

In Table 6-2, suction values for K_C40, K_C40_nf20, C_C40 and C_C40_nf20 at initial condition (50% RH) and at three wetting-drying cycles (90% RH) are summarised.

In the case of initial condition, a comparison between SW Kaolin and Caposele soil mixtures shows a moderate reduction in suction in agreement with water content values. In the case of three wetting-drying cycles at 90% relative humidity, the trend is the opposite of the previous case. In fact, Caposele soil is characterized by a lower suction value than SW Kaolin, once again in accordance with water content levels.

6.3.2. TRIAXIAL TESTS

Comparisons of triaxial tests results are reported in Figures 6-24 and 6-25. They are equal in terms of compared mixtures and environmental loading condition considered (i.e., K_C40_nf20 and C_C40_nf20, 3 w-d_90% RH respectively), they only differ for the confining pressures (i.e., 50 kPa and 150 kPa).

From the results observation, it is possible to note that C_C40_nf20 is characterized by lower strength and stiffness compared to K_C40_nf20, in particular in Figure 6-25.

Also the effect of confining pressure is confirmed in Figure 6-26: there is an increase in strength and stiffness for Caposele soil from 50 to 150 kPa, as previously observed for SW Kaolin. The volumetric behaviour of Caposele soil becomes less dilatant, associated with a transition from brittle to ductile behaviour at increasing confining pressure (from 50 to 150 kPa, Figure 6-26).

Failure envelopes of K_C40_nf20 and C_C40_nf20 are reported in Figure 6-27. The trends concur with the previous findings and the values, reported in Table 6-3, confirm the difference between SW Kaolin and Caposele soil mixtures. In fact, it is possible to observe a reduction in the level of suction between them. Moreover, C_C40_nf20 is characterized by a higher cohesion value but lower friction angle than K_C40_nf20.

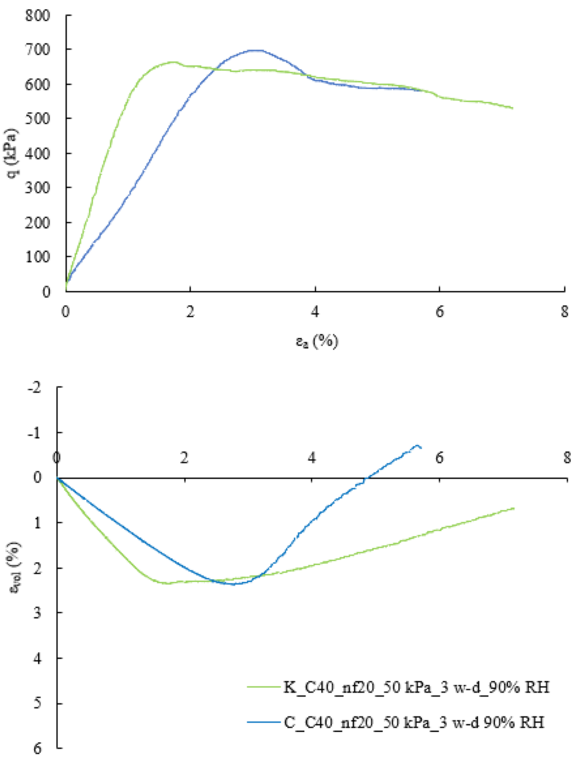

Figure 6-24. Triaxial test results for K_C40_nf20 and C_C40_nf20, at 50 kPa and at three wetting-drying cycles condition (90% RH).

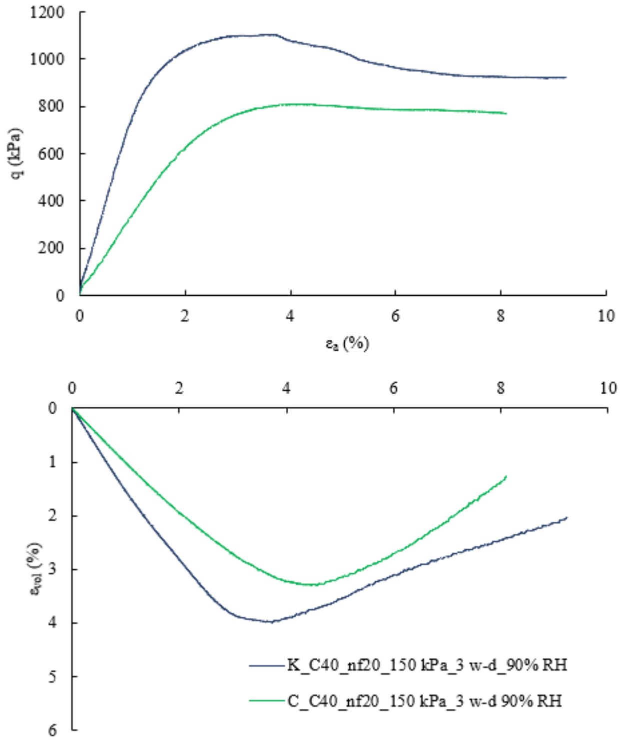

Figure 6-25. Triaxial test results on K_C40_nf20 and C_C40_nf20, at 150 kPa and three wetting-drying cycles conditions (90% RH).

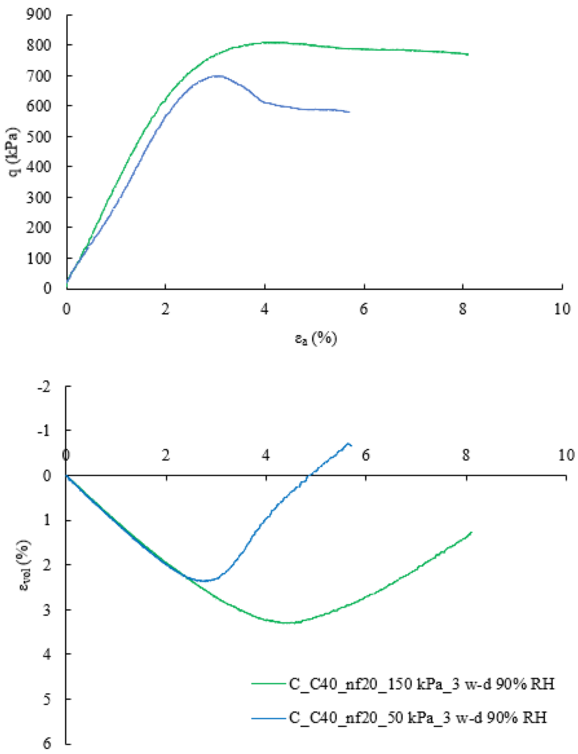

Figure 6-26. Triaxial tests on C_C40_nf20 after three wetting-drying cycles at 90% relative humidity, at 50 kPa and 150 kPa .

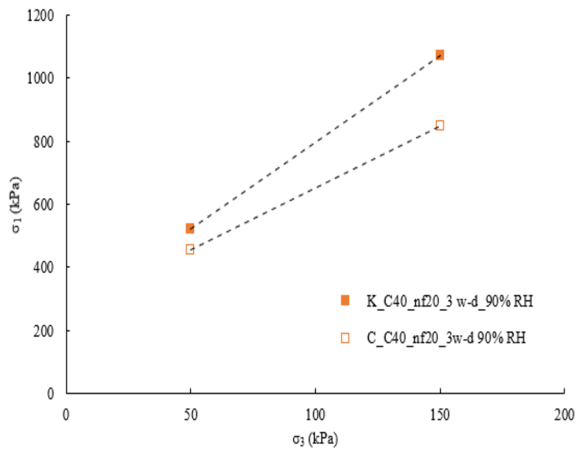

Figure 6-27. Failure envelopes for K_C40_nf20 and C_C40_nf20, at three wetting-drying cycles (90% RH).

Identification	N° of w-d cycles	RH (%)	Suction (MPa)	w (%)	c (kPa)	Φ (°)
K_C40_nf20	3	90	4.9	18.7	53.2	43.7
C_C40_nf20			1.5	25.4	64.9	36.5

Table 6-3. Suction, cohesion and friction angle values for K_C40_nf20 and C_C40_nf20, at three wetting-drying cycles (90% RH).

6.4. DISCUSSION

The effects of current value of suction and wetting-drying cycles were investigated on cemented and lightweight cemented SW Kaolin. By means of mechanical tests (i.e., unconfined compression tests and triaxial tests) it was possible to study the durability of the material and suction measurements made it possible to understand what role suction plays in the evolution of the mechanical response of the material, together with its degradation.

Results of unconfined compression tests on cemented and lightweight cemented SW Kaolin specimens reveal different information about the performance of lightweight cemented material, subjected to wetting-drying cycles. First of all, the comparison between the initial conditions (i.e., 0 w-d_50% RH) and that of three wetting-drying cycles (i.e., 3 w-d_50% RH), at the same level of relative humidity, clearly shows the effect of the application of wetting-drying cycles. In fact, curves in Figures 6-1, 6-3 and 6-5 show a visible reduction in strength and stiffness for K_C40, K_C40_nf20 and K_C40_nf40.

Moreover, in Figure 6-18 it is possible to note that the decrease in strength cannot be ascribed to a change in the current level of suction in the specimens. It is confirmed by the representation of suction values on water retention curves in Figure 6-19. As it can be seen, there is no significative variations in suction values between the two environmental loading conditions. It is owing to the fact that the relative humidity (i.e., 50%) is kept constant among them. These results are consistent with other studies which have shown that strength reduction is attributable to cemented structure degradation during wetting-drying cycles (Neramitkornburi et al., 2014).

On the other hand, considering the other environmental load condition (i.e., 3 w-d_90% RH) and comparing it with the one at equal number of wetting-drying cycles but at different level of relative humidity (i.e., 3 w-d_50% RH), it is possible to see the effect of the current value of suction on the evolution of the mechanical behaviour of lightweight cemented SW Kaolin. Results of unconfined compression tests reported in Figures 6-2, 6-4 and 6-6 show a reduction in strength for K_C40, K_C40_nf20 and K_C40_nf40 in the transition from lower to higher level of relative humidity. Figures 6-15 and 6-16 present the relation between UCS and suction values and the disposition of the latter on water retention curves. It confirmed the decrease in strength observed in the illustration of stress-strain curves (i.e., Figures 6-2, 6-4 and 6-6) and, unlike the previous case, also the different values of current suction are responsible for the observed mechanical response.

In fact, in Figure 6-15 and even more in Figure 6-16, it is possible to see the diminution in level of suction, determined by the passage from lower to higher relative humidity value (i.e., from 50% to 90%).

Results of the triaxial tests conducted on K_C40_nf20 and K_C40_nf40 at 50, 100 and 150 kPa of confining pressure in the two environmental loading conditions corresponding to the 3 w-d_50% RH and 3 w-d_90% RH, are in agreement with the considerations made in the case of unconfined compression tests. In particular, Figure 6-9 for K_C40_nf20 and Figures 6-13 and 6-14 for K_C40_nf40, confirm the reduction in strength accompanied by an increase in volumetric strains, associated with the transition from lower to higher value of relative humidity.

Failure envelopes in Figure 6-17 and values of suction, cohesion and friction angle reported in Table 6-1 seem to be in line with the mechanical behaviour observed from the triaxial test results. In fact, in Figure 6-17 the comparison between failure envelopes for K_C40_nf20 at 3 w-d_50% RH and 3 w-d_90% RH underlines the reduction in strength which is confirmed by the values of the cohesion "c" and friction angle "Φ" parameters obtained from the failure envelopes, in Table 6-1. In particular, suction values are reported for the two analysed environmental loading conditions. It is seen that there is an important reduction in suction when there is transition between the two conditions, associated with the decrease in cohesion values and constant friction angle. The obtained data concur with other literature works, where it was shown that variation in the level of suction has a predominant effect on cohesion parameter instead of friction angle, that remains almost constant (Shen et al., 2009; Elsharief and Abdulaziz, 2013; Pujiastuti et al., 2018).

For K_C40_nf40, even if the measured suction level is higher than that registered for K_C40_nf20 at the same environmental load condition (i.e., 3 w-d_50% RH), cohesion and friction angle values are lower than K_C40_nf20. It is due to the different physical state with higher void ratio that characterizes lightweight cemented soil, at increasing foam content (De Sarno, 2019).

An important implication of these findings is the role of suction in the evolution of mechanical behaviour of lightweight cemented soils. In particular, results suggest that suction contributes to the strength of lightweight cemented soils. In fact, it helps the cementation of the fabric to resist large deformations, sustaining the particles associations together as it was an additional binding agent. The strength of cemented bonds between soil particles governs the shear strength of a cemented soil, as asserted by several authors (Karube and Kato, (1994); Wheeler and Karube, (1995) and Toll et al., (2017)).

Suction provides an additional bonding force at the contacts of soil particles, due to the action of water menisci at particle contacts. The menisci act tensile force at soil particles contacts increasing the intergranular stresses with an overall stabilising effect on the soil skeleton (Gallipoli et al., 2003).

During wetting and drying cycles, the suction variation has an amplitude dependent on the environmental condition imposed; as a consequence, a cyclical variation in the intergranular stresses at particle contact is expected, which can induce mechanical degradation of cement bonds between particle aggregates (fatigue-type mechanisms).

Comparing samples not submitted to wetting and drying cycles (i.e., 0 w-d_50% RH) with samples after three wetting-drying cycles (i.e., 3 w-d_50% RH), the mechanical degradation of cement bonds is responsible for the lower strength of the samples subjected to wetting and drying cycles, even if the current value of suction after the mechanical tests is the same, as observed in Figures 6-1, 6-3, 6-5 and 6-18.

The comparison between the two environmental load conditions (i.e., 3 w-d_50% RH and 3 w-d_90% RH) highlights the influence of the current suction level on the mechanical strength. Low relative humidity (i.e., 50% RH) is related to high suction value (e.g. for nf20%, suction is equal to 82.9 MPa), whereas high relative humidity (i.e., 90% RH) is accompanied by low suction value (e.g. for nf20%, suction is equal to 4.9 MPa). Suction acts as an additional binding agent on the mechanical strength (i.e., the higher the suction, the higher the strength).

Moreover, the mechanical degradation of cement bonds is also linked to the amplitude of suction variation during the wetting and drying cycles. The comparison of two environmental load conditions, with the same number of w-d cycles and at different relative humidity value (i.e., 3 w-d_50% RH and 3 w-d_90% RH), shows the combined effect of the amplitude of suction variation during w-d cycles and the current suction value depending on the environmental load condition applied (Figures 6-2, 6-4, 6-6 and 6-15).

In the last part of this chapter, comparisons were made between SW Kaolin and Caposele soil mechanical responses at environmental loading conditions. Unconfined compression tests reveal a decrease in strength and stiffness for Caposele soil mixtures, both cemented and lightweight cemented. Suction values for Caposele soil mixtures, reported in Table 6-2, are in agreement with the general trends of SW Kaolin mixtures. In fact, values are in the same ranges of SW Kaolin.

Considering separately the two conditions examined (i.e., 0 w-d_50% RH and 3 w-d_90% RH), it is possible to note in the first case that the values of suction are almost similar to those of SW Kaolin; in the second case, suction values of Caposele soil are slightly higher than those of SW Kaolin. It is consistent with water contents values reported (higher the suction, lower the water content and vice versa).

The most likely explanation of this kind of results, referring to suction values, is that Caposele soil mixtures are prepared at lower slurry water content than SW Kaolin mixtures (w_{slurry}=1.1 w_L for Caposele soil$_2$ and w_{slurry}=2 w_L for SW Kaolin, as explained in chapter 4.) That determines a different preparation water content for the mixtures of the two soil types and, in particular, lower for the Caposele soil.

Moreover, also in the case of Caposele soil mixtures, it is possible to see a further decrease in strength and stiffness in transition from a cemented material to a lightweight cemented one. It is due to the addition of foam in soil-water-cement system and it confirms the mechanical behaviour observed for SW Kaolin from Figure 6-1 to Figure 6-6.

The differences observed for SW Kaolin and Caposele soil in unconfined compression tests results are found also in triaxial tests results. In fact, it is clear that there is a decrease in the shear strength and stiffness in transition for Caposele soil with respect to SW Kaolin, keeping constant the foam content and the environmental loading conditions.

In addition, as observed for SW Kaolin, the effect of confining pressure can be seen on Caposele soil (Figure 6-26). At higher confining pressure the mechanical behaviour changes from brittle to ductile and the volumetric behaviour seems to be less dilatant.

Comparison of the failure envelopes is also presented (Figure 6-27), together with related cohesion and friction angle values associated with suction values (Table 6-3). At the same environmental loading condition, Caposele soil is characterized by a lower value of suction than SW Kaolin, with a higher cohesion value and lower friction angle. This finding seems to be in contrast to what was found for SW Kaolin (Table 6-1), where it was shown that the decrease in suction values caused a decrease in the cohesion values; but, in this case a possible explanation is related to the water content values. In fact, Caposele soil is characterized by a higher water content value and, as a result, by a lower suction.

Summing up the results, the decrease in strength between SW Kaolin and Caposele soil can be attributed to the different levels of suction among them, confirm the important role of this parameter in the evolution and degradation of mechanical behaviour.

References

De Sarno, D., 2019. Microstructure and mechanical behaviour of cemented soils lightened by foam. Ph. D. Thesis. University of Naples, Federico II.

Elsharief, M.A., Abdulaziz, O.A., 2015. Effects of Matric Suction on the Shear Strength of Highly Plastic Compacted Clay. Innovative Geotechnics for Africa - Bouassida, Khemakhem & Haffoudhi (Eds.) 2015 ISBN : 978-9938-12-936-6 .

Gallipoli D., Gens, A., Sharma R., Vaunat J., (2003). An elasto-plastic model for unsaturated soil incorporating the effects of suction and degree of saturation on mechanical behaviour. Géotechnique. Volume 53 Issue 1, February 2003, pp. 123-135. https://doi.org/10.1680/geot.2003.53.1.123.

Karube, D., Kato, S., 1994. An ideal unsaturated soil and the Bishop's soil. International conference on soil mechanics and foundation engineering. 1994, pp 43-46.

Neramitkornburi, A., Horpibulsuk, S., Shen, S.L., Chinkulkijniwat, A., Arulrajah, A., Disfani, M.M., 2014. Durability against wetting-drying cycles of sustainable Lightweight Cellular Cemented construction material comprising clay and fly ash wastes. Construct Build Mater, 77 (2015), pp. 41-49. https://doi.org/10.1016/j.conbuildmat.2014.12.025.

Pujiastuti, H., Rifa'i, A., Adi, A.D., Fathani, T.F., 2018. The effect of matric suction on the shear strength of unsaturated sandy clay. International Journal of GEOMATE, Feb. 2018 Vol.14, Issue 42, pp.112-119. Geotec., Const. Mat. & Env., https://doi.org/10.21660/2018.42.72825.

Shen, C.N., Fang, X., Wang., H.W., Sun, S.G., Guo, J.F., 2009. Research on Effects of Suction, Water Content and Dry Density on Shear Strength of Remoulded Unsaturated Soils. Yantu Lixue/Rock and Soil Mechanics, v. 30, (5), 2009, p. 1347-1351.

Toll, D.G., Ali Rahman, Z., 2017. Critical state shear strength of an unsaturated artificially cemented sand. Géotechnique, Volume 67 Issue 3, March 2017, pp. 208-215. https://doi.org/10.1680/jgeot.15.P.042.

Vitale, E., Cuisinier, O., Russo, G., Deneele, D., De Sarno, D., Nicotera M.V., Papa, R., Urciuoli, G., 2020b. Water retention curves of lightweight cemented soils. E3S Web Conf. Volume 195. https://doi.org/10.1051/e3sconf/202019506004.

Wheeler, S.J., Karube, D., (1995). Constitutive modelling. State of the Art Report. Proc. 1st Int. Conf. on Unsaturated Soils, Paris, 3, 1323–1356. ISBN: 90-5410-583-6.

7. CONCLUSIONS

The main objectives of this research work are the chemo-physical and mechanical characterisation of LWCS, together with the study of the durability of the treatment under environmental loads.

The starting points on which the definition of the experimental programme, followed in the course of the study, was based are the recent works of De Sarno et al., (2019) and Vitale et al., (2020). The authors analysed aspects of the microstructure and mechanical behaviour of LWCS, considering the effects of cement and foam addition on the soil during curing time.

The experimental work was carried out on two different types of soil: the former, SW Kaolin is an artificial clay, industrially produced; the latter is Caposele soil, with natural origins. SW Kaolin was selected because of their chemo-physical properties well-known; instead, Caposele soil was chosen for comparison with a natural soil with similar plasticity features to SW Kaolin.

Regard to Caposele soil, there is a distinction between Caposele soil$_1$ and Caposele soil$_2$. This is because two different types of Caposele soil from the same excavation site were used during the experimental work. The tested mixtures are reported in Table 7-1.

Chemo-physical and mechanical characterisation of LWCS, together with the durability study under environmental conditions, were examined via mechanical tests (i.e., unconfined compression tests, torsional shear tests and triaxial tests).

In the first part of the work, dedicated to chemo-physical and mechanical characterization of LWCS, particular attention is paid to the application of non-destructive testing methods (i.e., ultrasonic tests and electrical resistivity measurements) to find some correlation relationship with the aim of determining properties of LWCS and to estimate geotechnical parameters, taking into account the measured quantities. Due to their being non-invasive and fast techniques, they have proven to be a valuable tool to control the correct execution of the treatment (i.e., LWCS method).

Soil	w_s (%)	w_c/c (%)	c/s (%)	n_f (%)	Identification
Speswhite Kaolin	140	50	40	0	K_C40
				20	K_C40_nf20
				40	K_C40_nf40
Caposele soil$_1$	124	50	40	0	C_C40
				20	C_C40_nf20
				40	C_C40_nf40
Caposele soil$_2$	80	50	40	0	C_C40
				20	C_C40_nf20
				40	C_C40_nf40

Table 7-1. Tested mixture and mix design proportions.

Unconfined compression tests executed on both types of soil, considering the effects of foam addition and increasing curing time, showed that strength and stiffness increased, due to the development of cement hydration reactions and consequently to the formation of hydration products. In both types of soil, a decrease in the strength and stiffness was observed in transition from cemented to lightweight cemented soil, at increasing foam content, confirming that foam has no effects on the kinetic of cement hydration reactions but only on the physical state of the specimens, by additional voids.

Torsional shear tests on SW Kaolin mixtures results indicated that the addition of foam is responsible for higher values of linearity threshold (higher the percentage of foam, higher the linearity threshold) and, as a consequence, for the lower change in slope in the G modulus decay curves. Moreover, independent on a type of mixtures after a determined value of shear strain level, cemented and lightweight cemented soils have the same G modulus decay.

SW Kaolin and Caposele soil trends of P-waves velocity, at increasing curing time, confirmed the development of cement hydration reactions. What is more, P-waves velocity as function of density and artificial porosity showed that it is greater in a denser medium than in one with lower density and increasing porosity. It is an evidence of good treatment performance, because of the reduction in P-waves velocity is linked to lower specimens density, owing to the foam introduction in soil-water-cement system.

Correlation relationship between unconfined compressive strength and P-waves velocity were determined for SW Kaolin and Caposele soil. The increase of UCS associated with P-waves velocity were confirmed by the exponential trends and the high correlation coefficient found.

On the other hand, electrical resistivity measurements results showed an increase in electrical resistivity in the transition from cemented soil to lightweight cemented one, in a more evident way the higher the percentage of foam added to the system. An explanation of the observed behaviour stands in the artificial porosity presence. In fact, less dense the sample, higher the measured electrical resistivity value.

The electrical resistivity technique has proved to be a valuable tool for checking in situ the correct execution of the treatment, due to the possibility to see the evolution of cement hydration reactions and, as consequence, of the formation of hydration products from the electrical resistivity curves. Moreover, also the mineralogical composition is responsible for the trends differences between SW Kaolin and Caposele soil mixtures.

Finally, correlation between electrical resistivity measurements and unconfined compressive strength values were found. Fixing the curing time and increasing the percentage of added foam, was observed that the increase in electrical resistivity measurement was accompanied by a decrease in the unconfined compressive strength value. These kinds of correlation relationships are useful in the estimation of geotechnical parameters (for example UCS) when tradition and destructive mechanical tests are not able to perform.

The second part of this experimental work concerned with the study of durability of LWCS under the effects of environmental loads.

Particular attention is paid to the effects of suction and wetting-drying cycles on cemented and lightweight cemented SW Kaolin and then, show the comparison with some results obtained for the Caposele soil.

Comparisons between three different environmental loads conditions made possible to analyse distinctly the effect of role of suction and wetting drying cycles, due to the variation of relative humidity levels. By means of unconfined compression tests and triaxial tests results consideration about the evolution and degradation of mechanical behaviour of lightweight cemented SW Kaolin were made.

First of all, unconfined compression test results highlighted a reduction in strength and stiffness for all the SW Kaolin mixtures tested (i.e., K_C40, K_C40_nf20 and K_C40_nf40). In particular, the comparison between the first two environmental load conditions, keeping constant the relative humidity level (i.e., 50%) made it possible to attribute the degradation of the material mechanical behaviour to the application of wetting and drying cycles.

When the other two conditions are compared to each other, at two different relative humidity levels, a decrease in strength was again found in the tested mixtures. In that case number of cycles was kept constant, but there was a difference in the relative humidity value (i.e., 50% and 90%).

Triaxial test results were in agreement with the observation made in the case of unconfined compression tests. In fact, it was observed a decrease in shear strength and an increase in volumetric strains, in the transition from lower to higher value of relative humidity.

Failure envelopes trends were consistent with the previous findings; reduction in cohesion values was linked to a decrease in suction values, while friction angles remained constant. On the other hand, comparing K_C40_nf20 and K_C40_nf40 at the same environmental load conditions, it was possible to see a decrease in cohesion and friction angle parameters, due to the higher percentage of foam content.

It is evident that suction has an important role in the evolution of the mechanical behaviour of lightweight cemented soils. In fact, it seems to contribute to the strength of LWCS, due to supporting action of particles groups and helping the cementation of the fabric to resist at large deformations.

The mechanical degradation of cement bonds between particle aggregates is induced by a cyclical variation in the intergranular stresses at particle contact, owing to the amplitude of suction variation during wetting and drying cycles, dependent on the environmental condition imposed. As a consequence, the mechanical degradation of cement bonds is responsible of the lower strength and stiffness of the samples subjected to wetting and drying cycles.

Moreover, a further effect of the current value of suction on the LWCS strength is also shown. Suction acts as an additional binding agent on the mechanical strength (i.e., the higher the suction, the higher the strength and vice versa).

Comparisons between SW Kaolin and Caposele soil were made. Similar results were found for both SW Kaolin and Caposele soil.

Hence it seems that the effects of environmental loads conditions on the mechanical behaviour experimentally observed in the case of a commercial kaolin are in agreement with natural Caposele soil.

In conclusion, it is evident that this study on LWCS durability has shown the importance of role of suction in mechanical behaviour, that strongly depends on the environmental load conditions applied.

7.1. FURTHER DEVELOPMENTS

The experimental study was focused on the chemo-physical and mechanical characterization, together with durability study under environmental loads conditions, of LWCS. It has been demonstrated that the results on SW kaolin, industrially produced soil, are consistent with those on Caposele soil, natural excavated soils.

Mechanical tests results gave the possibility to interpreter qualitatively the effects of foam addition on the mechanical behaviour evolution. These results, together with more mechanical investigations, should be applicable to constitutive modelling of the observed behaviour.

The application of non-destructive techniques (i.e., ultrasonic testing and electrical resistivity) highlight the potentialities of this investigation method. In fact, results suggest that, by means of these techniques, relationships with the aim of determining properties of LWCS can be found and geotechnical parameters can be estimated. Due to their being non-invasive and fast techniques, they have proven to be a valuable tool to control the correct execution of the treatment. As a results, the findings are of direct practical relevance and the proposed method can be readily used in practice.

On the basis of the promising findings presented in this thesis, future work will involve the Caposele soil remaining issues in terms of mechanical characterization and durability study.

Future studies of the LWCS durability issue would be of interest. Further research into the effects of environmental loads (for example freeze-thaw cycles and leaching) is necessary to extend the knowledge of durability performances of LWCS. Moreover, the next stage is also linked to the study of LWCS hydraulic properties, that are strongly correlated to durability problems.

References

De Sarno, D., Vitale, E., Deneele, D., Nicotera, M.V., Papa, R., Russo, G., Urciuoli, G., 2019. Effects of cement and foam addition on chemo-mechanical behaviour of lightweight cemented soil (LWCS). E3S Web Conf., 92. https://doi.org/10.1051/e3sconf/20199211006

Vitale, E., Deneele, D., Russo, G., De Sarno, D., Nicotera, M. V., Papa, R., Urciuoli, G. 2020.Chemo-mechanical behaviour of lightweight cemented soils. Acta Geotech. 15, 933–945. https://doi.org/10.1007/s11440-019-00797-8